

UNCLASSIFIED

AD 265 093

*Reproduced
by the*

**ARMED SERVICES TECHNICAL INFORMATION AGENCY
ARLINGTON HALL STATION
ARLINGTON 12, VIRGINIA**



UNCLASSIFIED

NOTICE: When government or other drawings, specifications or other data are used for any purpose other than in connection with a definitely related government procurement operation, the U. S. Government thereby incurs no responsibility, nor any obligation whatsoever; and the fact that the Government may have formulated, furnished, or in any way supplied the said drawings, specifications, or other data is not to be regarded by implication or otherwise as in any manner licensing the holder or any other person or corporation, or conveying any rights or permission to manufacture, use or sell any patented invention that may in any way be related thereto.

309
60509
U. S. A R M Y
TRANSPORTATION RESEARCH COMMAND
FORT EUSTIS, VIRGINIA

TCREC TECHNICAL REPORT 61-108

STATE-OF-THE-ART SUMMARY
• AIR-CUSHION VEHICLES

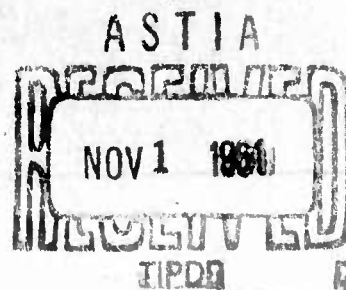
Task 9R99-01-005-14

Contract DA 44-177-TC-724

August 1961

prepared by :

AERONUTRONICS
A DIVISION OF FORD MOTOR COMPANY
Newport Beach, California



3509
265 093
CATA
AS A

U. S. A R M Y
TRANSPORTATION RESEARCH COMMAND
FORT EUSTIS, VIRGINIA

TCREC TECHNICAL REPORT 61-108

STATE-OF-THE-ART SUMMARY
• AIR-CUSHION VEHICLES

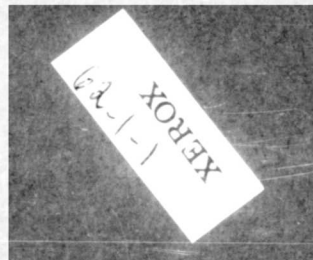
Task 9R99-01-005-14

Contract DA 44-177-TC-724

August 1961

prepared by :

AERONUTRONICS
A DIVISION OF FORD MOTOR COMPANY
Newport Beach, California



DISCLAIMER NOTICE

When Government drawings, specifications, or other data are used for any purpose other than in connection with a definitely related Government procurement operation, the United States Government thereby incurs no responsibility nor any obligation whatsoever; and the fact that the Government may have formulated, furnished, or in any way supplied the said drawings, specifications, or other data is not to be regarded by implication or otherwise as in any manner licensing the holder or any other person or corporation, or conveying any rights or permission, to manufacture, use, or sell any patented invention that may in any way be related thereto.

ASTIA AVAILABILITY NOTICE

Qualified requesters may obtain copies of this report from

Armed Services Technical Information Agency
Arlington Hall Station
Arlington 12, Virginia

This report has been released to the Office of Technical Services, U. S. Department of Commerce, Washington 25, D. C., for sale to the general public.

The information contained herein will not be used for advertising purposes.

The findings and recommendations contained in this report are those of the contractor and do not necessarily reflect the views of the Chief of Transportation or the Department of the Army.

SPECIAL PROGRAMS OPERATIONS

Submitted to:

U. S. Army Transportation
Research Command
Fort Eustis, Virginia

CONTRACT NO. DA 44-177-TC-724

TECHNICAL REPORT

STATE-OF-THE-ART SUMMARY

AIR-CUSHION VEHICLES

REVISION 1

Prepared by:

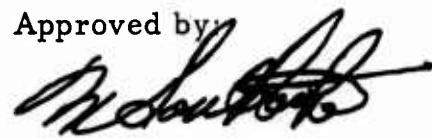


William L. Rawlings



Donald H. Seivens

Approved by:



Murray F. Southcote, Manager
Air-Cushion Vehicles Department

August 1961

AERONUTRONIC

A DIVISION OF *Ford Motor Company*

FORD ROAD / NEWPORT BEACH, CALIFORNIA

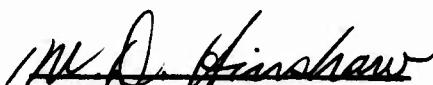
FOREWORD

This report is a current revision of the basic report "State of the Art Summary of Air Cushion Vehicles." Revision is made necessary by the rapidly expanding horizons of the Ground Effect Machine, or GEM. The original purpose--to collate, summarize, and present in unified notation the results of the diversity of research effort being conducted by aeronautical, mechanical, and marine-oriented organizations--is continued unchanged in the present revision.

It is also the purpose of this report to evaluate the various existing theories in comparison with experimental data. Where satisfactory correlation between theory and data is not apparent or where experimental data are lacking, the inference is that emphasis should be placed on additional research effort in these areas.

It is obvious that an effort that encompasses a large scope, such as the state of the art of even a segment of a technology, will result in errors and omissions. Attempts have been made in this revision to correct the errors and omissions found in the basic report. This Command would appreciate notification of any errata or significant omission of theory or experimental data which would invalidate the conclusions contained in either the revision or the basic report.

APPROVED:


WILLIAM D. HINSHAW
PROJECT ENGINEER

APPROVED:


RAPHAEL F. GAROFALO
CWO-4, USA
ASSISTANT ADJUTANT

CONTENTS

Section		Page
	ILLUSTRATIONS	iv
	NOTATION	vii
1.0	SUMMARY	1-1
2.0	ANNULAR JET	2-1
3.0	PLENUM CHAMBER	3-1
4.0	HILLER DIFFUSER	4-1
5.0	LABYRINTH SEAL	5-1
6.0	RAM WING	6-1
7.0	GETOL	7-1
8.0	LEVAPAD	8-1
9.0	RECIRCULATING ANNULAR JET	9-1
10.0	ANNULAR WATER CURTAIN VEHICLE	10-1
11.0	REFERENCES	11-1

ILLUSTRATIONS

Figure		Page
2-1	Theoretical Ratio of Base Pressure to Total Pressure - Stanton-Jones Theory	2-3
2-2	Comparison of Base Pressure Theory (Strand) and Data - Aeronutronic Data (Reference 2)	2-6
2-3	Vortex Region Pressure Ratio - Aeronutronic Data (Reference 2)	2-7
2-4	Inner Wall Pressure Ratio - Aeronutronic Data (Reference 2)	2-10
2-5	Comparison of Base Pressure Theory (Stanton-Jones) and Data - Aeronutronic Data (Reference 2)	2-11
2-6	Jet Reaction Coefficient - Strand Theory Compared to Aeronutronic Data (Reference 2) - $\theta = 0$ Degrees	2-12
2-7	Jet Reaction Coefficient - Strand Theory Compared to Aeronutronic Data (Reference 2) - $\theta = 30$ Degrees	2-13
2-8	Jet Reaction Coefficient - Strand Theory Compared to Aeronutronic Data (Reference 2) - $\theta = 45$ Degrees	2-14
2-9	Jet Velocity Ratio - Strand Theory Compared to Aeronutronic Data (Reference 2) - $\theta = 0$ Degrees	2-17
2-10	Jet Velocity Ratio - Strand Theory Compared to Aeronutronic Data (Reference 2) - $\theta = 30$ Degrees	2-18
2-11	Jet Velocity Ratio - Strand Theory Compared to Aeronutronic Data (Reference 2) - $\theta = 45$ Degrees	2-19
2-12	Base Pressure Ratio Comparison	2-20
2-13	Current and Previous Data Comparison (Reference 2 Data Compared with Data Summarized in Publication U-926 - $\theta = 0$ Degrees)	2-22

ILLUSTRATIONS (Continued)

Figure		Page
2-14	Optimum Thickness to Height Ratio and Jet Inclination Angle (Experimental Optimum Compared with Theoretical Optimum)	2-27
2-15	Minimum Hovering Ground Effect Power Factor - G (Experimental Minimum Compared with Theoretical Minimum	2-28
2-16a	Comparison of Two- and Three-Dimensional Pitch Stability $-\theta = 0$ Degrees - $h/d = 0.03$ - $h/d = 0.05$. .	2-37
2-16b	Comparison of Two- and Three-Dimensional Pitch Stability $-\theta = 0$ Degrees - $h/d = 0.10$	2-38
2-17	Static Longitudinal Hovering Stability (Skirts). . . .	2-40
2-18	Static Longitudinal Hovering Stability (Intravents). .	2-41
2-19	Static Lateral Hovering Stability (Skirts)	2-43
2-20	Static Lateral Hovering Stability (Intravents)	2-44
2-21	Static Heave Stability - Simple Peripheral Jet (Based on Reference 15)	2-46
2-22	Damping in Heave (Reference 15)	2-47
2-23	Effect of Forward Speed on Pitching Moment and Stability (Reference 17)	2-49
2-24	Comparison of Power and Cost of Four Longitudinal Control Schemes	2-51
3-1	Plenum Chamber Hovering Ground Effect Power Factor - Experiment Compared to Theory	3-4
3-2	Plenum Chamber G Compared to Annular Jet Minimum G . .	3-6
4-1	Diffuser-Plenum Fan Ground Effect Hovering Power Factor	4-5

ILLUSTRATIONS (Continued)

Figure		Page
4-2	Diffuser-Plenum Data Point Compared with Theory and Annular Jet	4-7
6-1	Effect of the Ground on Lift and Drag - AR = 1; $\frac{t}{c} = 0.22$	6-4
6-2	Effect of Ground on L/D	6-5
6-3	Effect of Aspect Ratio on $(\frac{L}{D})_{MAX}$ - $\frac{t}{c} = 0.22$	6-6
6-4	Effect of Thickness and Endplates on $(\frac{L}{D})_{MAX}$ - AR = 1.	6-7
10-1a	Effect of Operational and Design Variables on Air Leakage -(Reference 37) Aeronutronic Fairing - C Versus δ	10-6
10-1b	Effect of Operational and Design Variables on Air Leakage - (Reference 37) C Versus θ	10-7
10-2	Hovering Ground Effect Power Factor - $\theta = 33$ Degrees.	10-15
10-3	Minimum Hovering Ground Effect Power Factor - Effect of Jet Thickness and Jet Turning Parameter - $\theta = 33$ Degrees.	10-16
10-4	Minimum Hovering Ground Effect Power Factor - $\theta = 33$ Degrees	10-17

NOTATION

Symbol	Quantity	Dimension
b	Wing span Base length	ft.
c	Circumference of peripheral jet	ft.
C	Discharge coefficient	-
C_D	Drag coefficient = D/qS	-
C_L	Lift coefficient = L/qS	-
\bar{C}_r	Jet reaction coefficient	-
d	Diameter	ft.
D	Drag	lb.
D_{mom}	Momentum drag	lb.
G	Ground effect power factor = $P/P_{i\infty}$	-
h	Altitude or height above ground	ft.
HP	Horsepower = $P/550$	
i	Length of inlet for two-dimensional plenum	ft.
j	Unit momentum flux = $J = \int_0^{t_e} v_j^2 dt_e$ (measured in ground effect)	lb/ft.
J	Momentum flux	lb.
J_d	Momentum flux at diffuser exit	lb.

Symbol	Quantity	Dimension
K	Loss coefficient applied to diffuser dynamic pressure to determine total pressure loss from diffuser exit to plenum chamber = $(p_{t_d} - p_{t_b})/q_d$	-
K_d	In diffuser-plenum theory this accomplishes the same as K in the plenum chamber theory.	-
K_g	Ground friction loss coefficient	-
K_s	Nozzle-gap spanning loss	-
K_{j-2}	$K_d + K_g + K_s$	-
l	Length, circumference	ft.
L	Lift	lb.
m	Mass	lb-sec ² /ft
\dot{m}	Mass flow rate	lb-sec/ft
M	Moment	ft-lb
n	Rotational speed	rev/sec
N_1	$h/l/s$	-
N_2	t_e/h	-
p_e	ambient static pressure, absolute	lb/ft ²
p_b	Base pressure, gage	lb/ft ²
p_d	Duct static pressure, gage	lb/ft ²
p_g	Experimentally measured ground board static pressure, gage	lb/ft ²

Symbol	Quantity	Dimension
p_o	Static pressure at outside edge of jet, gage	lb/ft^2
p_v	Vortex region static pressure, gage	lb/ft^2
p_w	Static pressure on inner wall of jet exit, gage	lb/ft^2
p_{t_b}	Base total pressure, gage	lb/ft^2
p_{t_j}	Jet total pressure, gage	lb/ft^2
\bar{p}_{t_j}	Integrated average jet total pressure, gage (from test data)	lb/ft^2
Δp_{tDL}	Total pressure loss in ducting	lb/ft^2
Δp_{tF}	Total pressure rise across fan	lb/ft^2
Δp_{tFL}	Total pressure loss across fan (associated with blade wake)	lb/ft^2
Δp_{tL}	Combined ducting and fan total pressure loss	lb/ft^2
P	Power, power of air-cushion vehicle	ft-lb/sec
P_{i_∞}	Ideal hovering power = $\frac{L}{2\sqrt{\rho}} \sqrt{\frac{L}{S}}$	ft-lb/sec
P_T	Theoretical hovering power	ft-lb/sec
P_{Ta}	Theoretical hovering power of air pumping system, in water curtain concept	ft-lb/sec

Symbol	Quantity	Dimension
P_{Tj}	Theoretical hovering power of water pumping system, in water curtain concept	ft-lb/sec
q	Dynamic pressure, $\frac{1}{2}\rho V^2$	lb/ft ²
q_i	Dynamic pressure at inlet	lb/ft ²
q_j	Jet dynamic pressure	lb/ft ²
q_z	Dynamic pressure associated with V_z	lb/ft ²
Q	Volume flow rate	ft ³ /sec
r	Radius	ft.
r_o	Radius of base to centerline of jet	ft
R	Radius of plenum chamber vehicle	ft.
R_g	Radius to point of zero ground board pressure	ft.
S	Platform area	ft ²
$S_{b\text{ eff}}$	Effective base area	ft ²
S_d	Diffuser exit area	ft ²
S_j	Jet area	ft ²
S_v	Vortex pressure area	ft ²
S_w	Area on inner wall of jet between base and point where jet starts to turn	ft ²
S_x	Air flow exit area	ft ²

Symbol	Quantity*	Dimension
S_1	Area of station 1 (diffuser throat) in diffuser-plenum concept	ft ²
t	Jet thickness - in water curtain concept	ft.
t_e	Jet thickness at nozzle exit	ft.
t_o	Theoretical jet thickness at point where V_{j_o} exits	ft.
u	Fan tip velocity	ft/sec
v_f	Axial velocity at fan	ft/sec
\bar{V}_j	Integrated average jet velocity	ft/sec
V_{j_o}	Velocity resulting from expansion of total pressure to local static pressure	ft/sec
\bar{V}_{j_o}	Velocity resulting from expansion of integrated average experimental total pressure to local static pressure	ft/sec
V_z	Jet velocity rearward component	ft/sec
V_1	Velocity at station 1 (diffuser throat) in diffuser- plenum concept	ft/sec
α	Angle of pitch - entrance angle of water jet into free water surface (measured from vertical)	deg

Symbol	Quantity	Dimension
β	Rearward inclination of jet exit velocity vector, measured from vertical	deg
Γ	$90-\theta$	deg
γ	$\alpha-\theta$	deg
δ	water curtain jet shape parameter	-
ϵ	$\tan^{-1} \left(\frac{C_D}{C_L} \right)$ fan blade	-
ζ	Duct loss coefficient	-
η_{fa}	Air fan efficiency	-
η_{iw}	Internal efficiency of water system	-
η_{ia}	Internal efficiency of air system	-
η_p	In plenum chamber, ratio of base static pressure to base total pressure	-
η_r	Ram recovery efficiency	-
θ	Jet inclination angle, measured from vertical	deg.
ν	Ratio of fan hub to fan tip diameters	-
ρ	Density of air	lb-sec ² /ft ⁴
ρ_a	Density of air	lb-sec ² /ft ⁴
ρ_w	Density of water	lb-sec ² /ft ⁴

<u>Symbol</u>	<u>Quantity</u>	<u>Dimension</u>
σ	Fan characteristic number	-
ϕ	Ratio of axial velocity through fan to fan tip velocity	-
ψ	Fan total pressure rise coefficient	-
ω	Fan rotation speed	radians/sec.
subscript ∞	Condition far from ground or far from vehicle	-

1.0 SUMMARY

This report is Revision 1 of "State of the Art Summary, Air-Cushion Vehicles," Aeronutronic Publication U-926. It is written primarily for those familiar with Publication U-926, and follows the same general outline and section breakdown as before. When no significant knowledge has been added to a particular subject, the appropriate section is denoted as unchanged. In some cases sections are added to or revised. In other cases the sections are completely rewritten in light of more up-to-date information.

Two air-cushion concepts have been added to those analyzed in Publication U-926. They are the recirculating annular jet and the water-wall concepts. The first of these is applicable to the amphibious mobility role. Insufficient information is available to evaluate this concept. The second is limited in application to overwater use. For low speeds over water, the water-wall vehicle appears to require 25 to 50 percent less power than the annular jet, which requires the least power of the concepts suitable for amphibious roles. At high speeds the water-wall concept suffers a penalty in momentum drag which may limit its utility. The cross-over speed where the water-wall concept ceases to appear attractive depends upon the specific vehicle geometry, size and weight.

As when Publication U-926 was written, much of the recently available information pertains to the annular jet type vehicles. Experimental data summarized here confirm the theoretical power estimates of Publication U-926 to within approximately 10 percent. Therefore, it still appears that the annular jet vehicle requires less power than other concepts for amphibious mobility at clearance heights estimated to be required.

Several studies have been made of particular vehicle models in forward motion. However, these programs have not been of sufficient generality to lend themselves to inclusion in this report.

Annular jet type vehicles can be made stable in pitch and roll up to heights approximating 25 percent of the appropriate vehicle dimension through the use of intraventing jets. No estimates of power required for such fixes are available, but current work should permit such evaluations. Vehicle control by use of differential jet control offers the possibility of providing c.p. shifts of ± 4 percent of vehicle length or width. Such control is estimated to cost between 10 to 30 percent of vehicle lift power.

The problems associated with jet impingement on the ground remain unsolved and, to a large extent, undefined. Recent propeller work has shown that blade damage caused by foreign-object ingestion can be alleviated by nickel plating. Investigations under way in the VTOL field will probably shed light on methods of reducing debris-blowing. However, further work will be required to extend VTOL investigations to include the higher planform loadings and wake velocities inherent with air-cushion vehicles. Debris deflectors appear promising but no new work has been published concerning them.

Publication U-926 stated that the air-cushion vehicle appears to offer considerable promise as a complement to existing transportation systems where off-the-road and amphibious mobility is required. This conclusion is still valid. Further work is required in the following areas before this can be proved conclusively:

- a. Increased height capability
- b. Improved stability, control and maneuvering capabilities
- c. Reduced debris problem.

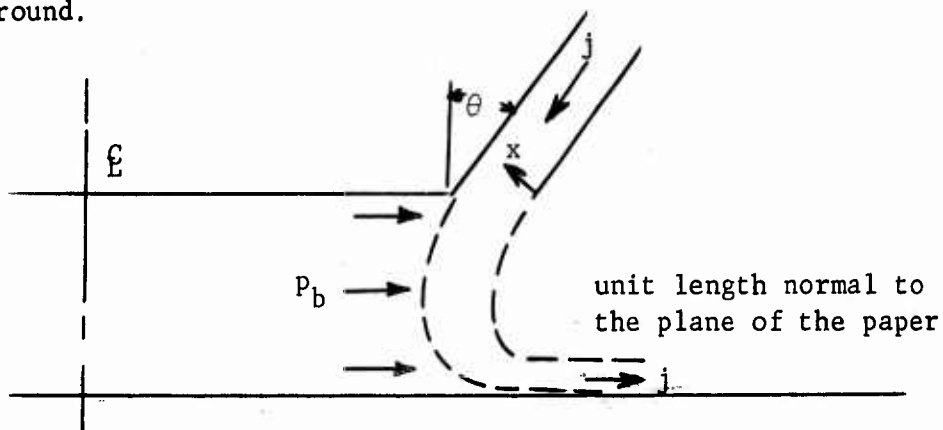
2.0 ANNULAR JET

2.1 THEORETICAL CONSIDERATIONS - HOVERING

2.1.1 Momentum Theory

Since the preparation of Publication U-926, a momentum theory by Stanton-Jones has become available (Reference 1). It was originally an appendix to Stanton-Jones' presentation at the Princeton Symposium, but unfortunately was not included in the compilation of papers.

As in the case of Chaplin's momentum theory, Stanton-Jones' theory is a momentum pressure-force balance. The accompanying sketch shows the jet flow to the ground.



The only assumptions of the Stanton-Jones theory are that constant base pressure is exerted on the inner surface of the jet, constant ambient pressure on the outer surface of the jet and constant jet momentum throughout the turn. Note that previous restrictions of constant thickness and turn radius do not appear here.

Stanton-Jones presents estimations of $\frac{p_b}{p_{tj}}$ as a function of $\frac{t_e}{h}$ and θ

based on evaluation of jet momentum by two separate methods. The first method is to assume that static pressure varies linearly across the jet from ambient to base pressure. This results in the same relation as that derived in Publication U-926 and will be given no further consideration here.

The second method was to consider a pressure momentum-force balance across a small element of the jet and integrate this relation across the jet.

$$dp_j = \frac{\rho V_j^2}{R} dx$$

where $\rho V_j^2 = 2 q_j = 2(p_t - p_j)$

Although it is not expressly stated in Reference 1, it appears that an assumption is required in addition to those previously mentioned; e.g., that each jet streamline follows a circular path with radius equal to that of the innermost streamline.

$$R = \frac{h}{1 + \sin \theta}$$

The result of the integration is then

$$\frac{p_b}{p_{tj}} = 1 - e^{-2 \frac{t}{h} (1 + \sin \theta)}$$

Figure 2-1 shows this variation for $\theta = 0$ degrees, 30 degrees and 45 degrees. Similar relations can be derived for jet reaction and volume flow. These relations could permit a theoretical optimization for power requirements as was done in Publication U-926. However, time and level of effort of this study prevented such optimization*. Available experimental data (see Section 2.2) will be compared to the Strand theory for which the jet geometry has been optimized. The data indicate, however, considerable potential utility for this neat, simple theory. Further analysis of the Stanton-Jones theory is warranted.

2.1.2 Vortex Flow Theory

Unchanged

2.1.3 Convair Conformal Mapping Theory

Unchanged

* A report published too late for inclusion herein contains additional work along these lines. Strand, T., Royce, W.W., Fujita, T., "Performance Theory for High-Speed Ground Effect Machines", Vehicle Research Corporation Report No. 11, June 1, 1961.

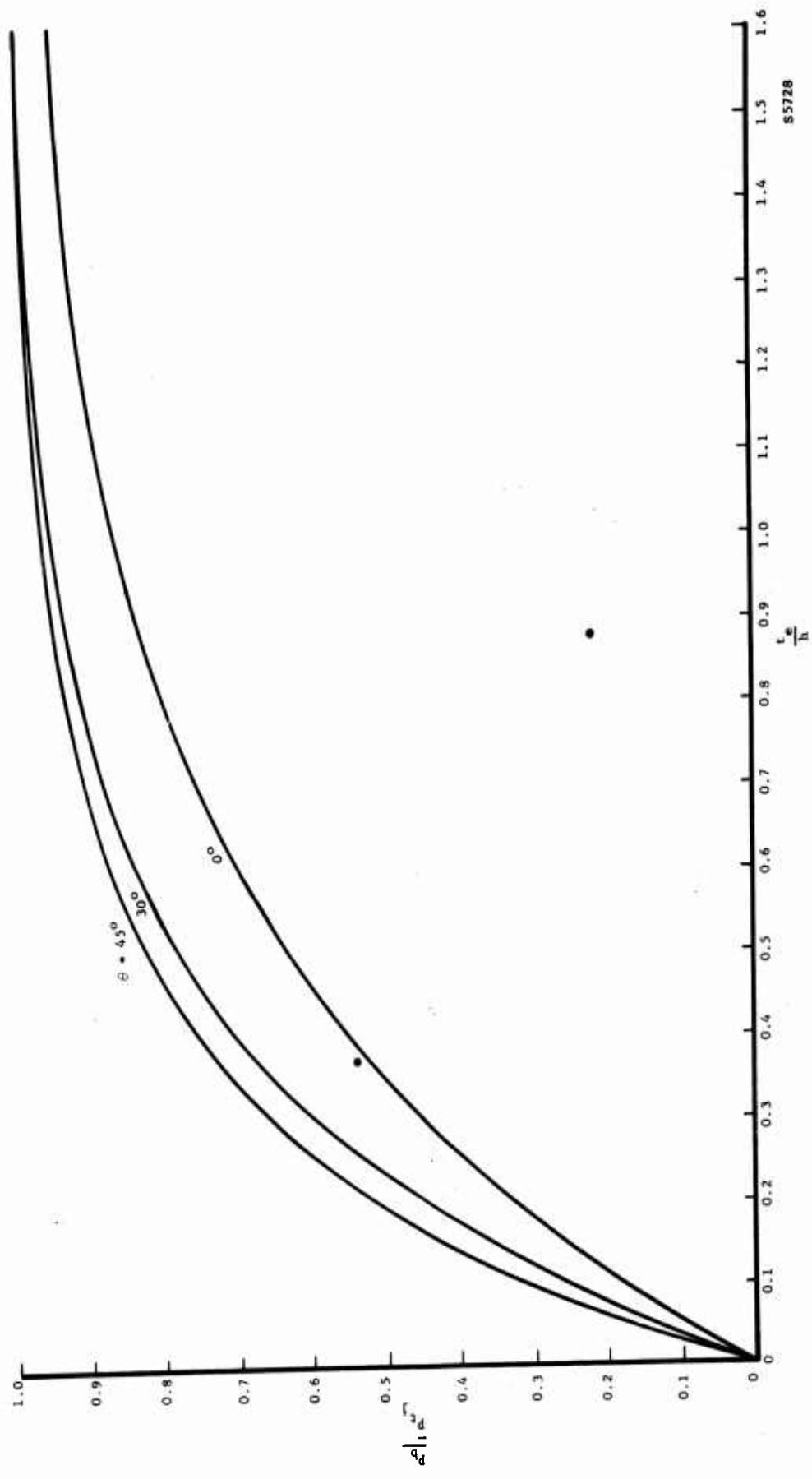


FIGURE 2-1. THEORETICAL RATIO OF BASE PRESSURE TO TOTAL PRESSURE
- STANTON-JONES THEORY

2.2 TEST DATA - HOVERING

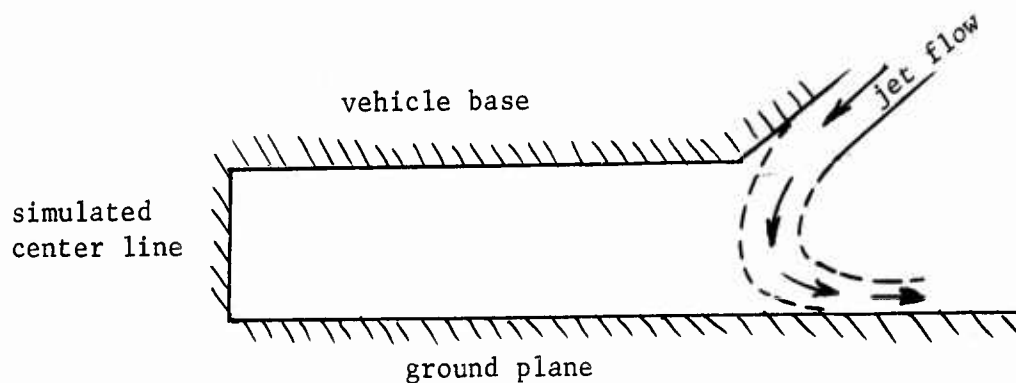
There has been considerable experimental data published regarding the annular jet since the presentation of Publication U-926. Most of the data are in the form of the basic building blocks $\frac{p_b}{p_{b_j}}$, \bar{C}_r and $\frac{t_o}{t_e}$ with modifications

found necessary in experimentation. This section will summarize the data and compare them with theoretical estimates.

2.2.1 Comparison with Strand Theory

Reference 2 describes the detailed, large scale, two-dimensional investigations by Aeronutronic directed specifically at experimentally verifying the basic annular jet performance parameters $\frac{p_b}{p_{t_j}}$, \bar{C}_r , and $\frac{t_o}{t_e}$.

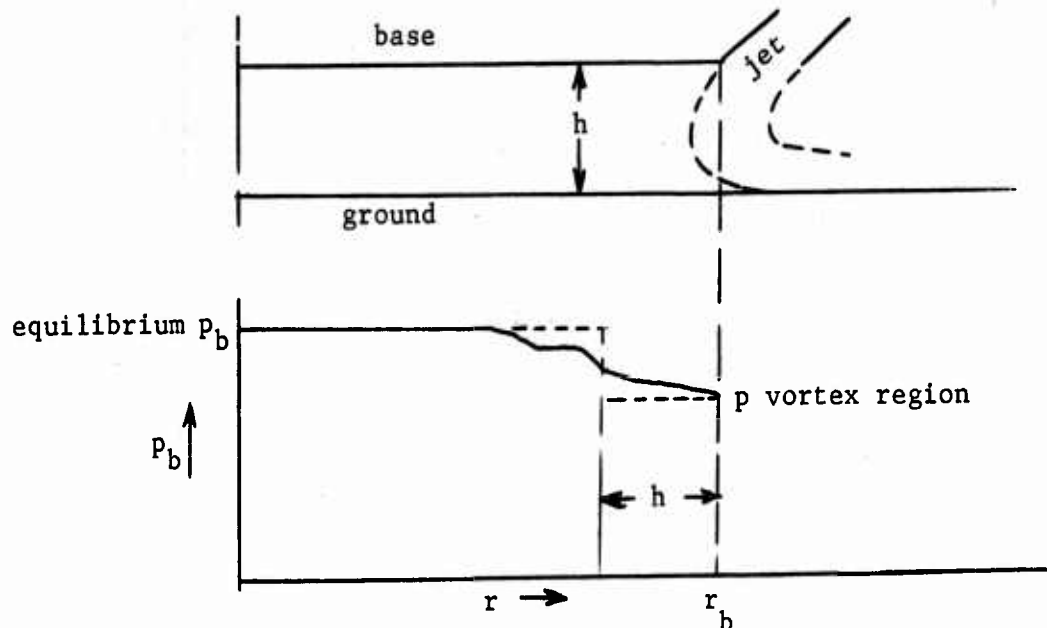
The experimental set-up is shown in the following sketch.



The experiment simulated a two-dimensional cut through a vehicle. The solid boundary for the vehicle centerline was used because of assumed symmetry with an opposite jet.

These investigations revealed shortcomings in several of the assumptions of the theory. However, sufficient data were generated to account for these assumptions.

The first of these assumptions was that constant static pressure exists all over the base area. That this is invalid (due to the action of a jet induced vortex) was quantitatively demonstrated and accounted for in Reference 2. The sketch below shows a typical variation in base pressure from the vehicle centerline to the inner edge of the jet.



The base pressure was integrated over the base area to determine the base lift. This lift was then assumed to consist of the following components:

- a. Equilibrium base pressure acting on the base out to the point h distance in from the inner edge of the jet.
- b. Some lower, but constant "vortex region" pressure acting over the base region within h of the inner edge of the jet.

The vortex region pressure (p_v) was then expressed in terms of the equilibrium base pressure as a function of $\frac{t_e}{h}$ and θ .

The equilibrium base pressure (in terms of jet total pressure) and the vortex region pressure (in terms of equilibrium base pressure) are plotted in Figures 2-2 and 2-3, respectively. The theoretical ratio of base pressure to jet total pressure is also plotted in Figure 2-2 for comparison. The experimental values of equilibrium base pressure agree quite well with theory for jet inclination angle (θ) of 30 degrees and 45 degrees but fall considerably below for $\theta = 0$ degrees. There is a moderate amount of scatter in the data for vortex region base pressure and there appears to be no consistent trend with θ .

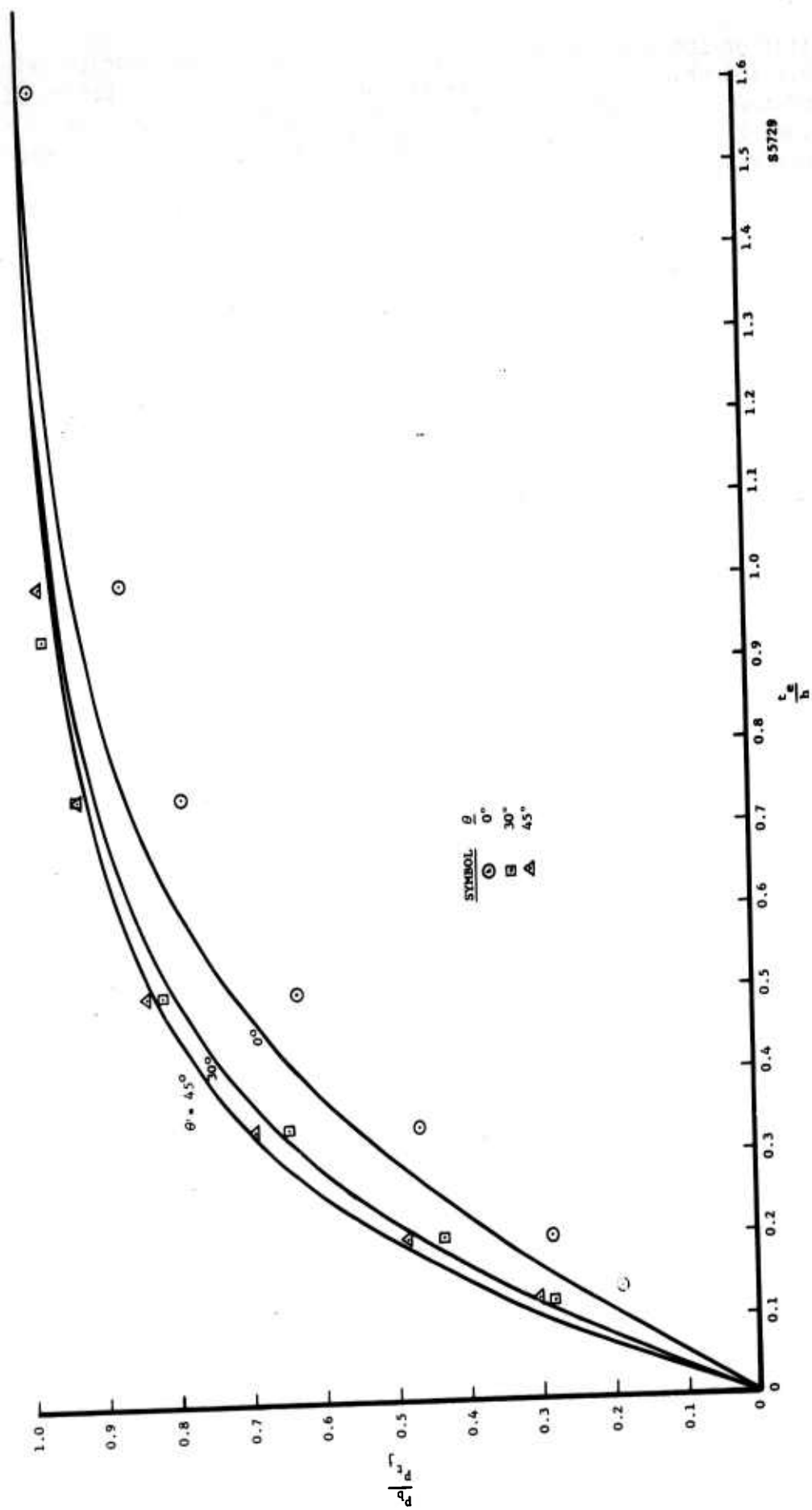
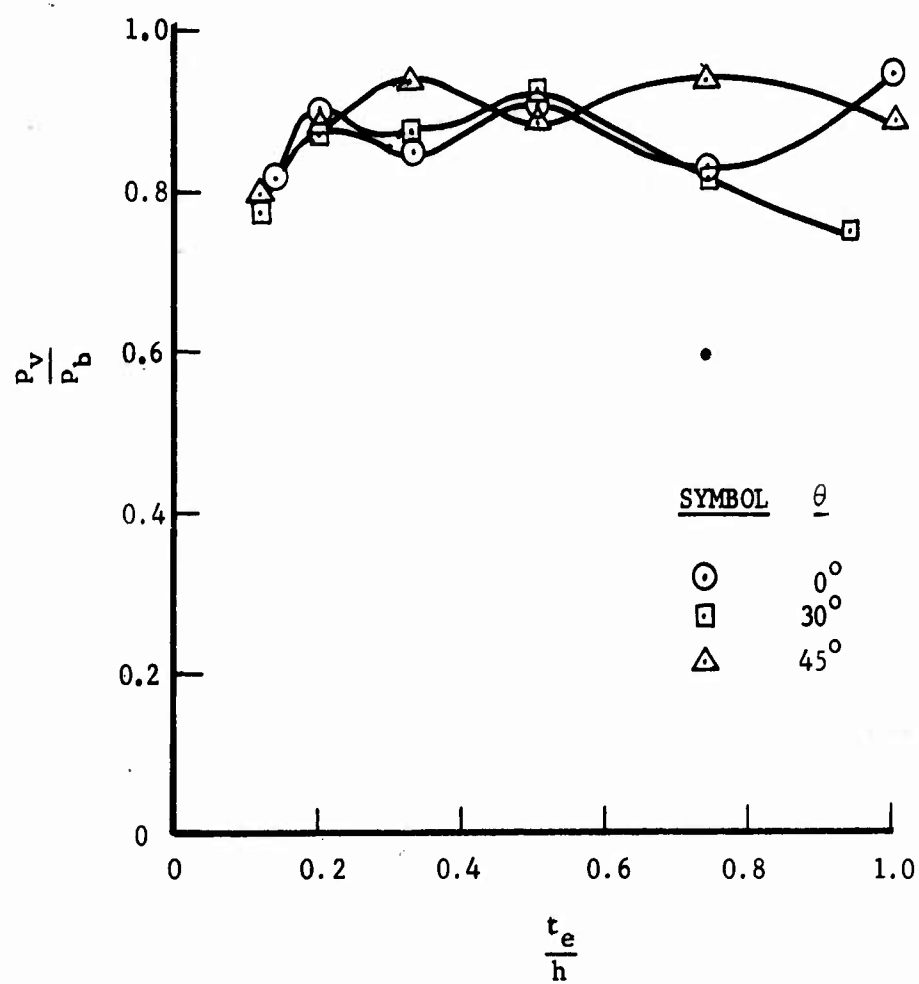


FIGURE 2-2. COMPARISON OF BASE PRESSURE THEORY (STRAND) AND DATA
- AERONAUTIC DATA (REFERENCE 2)



S5730

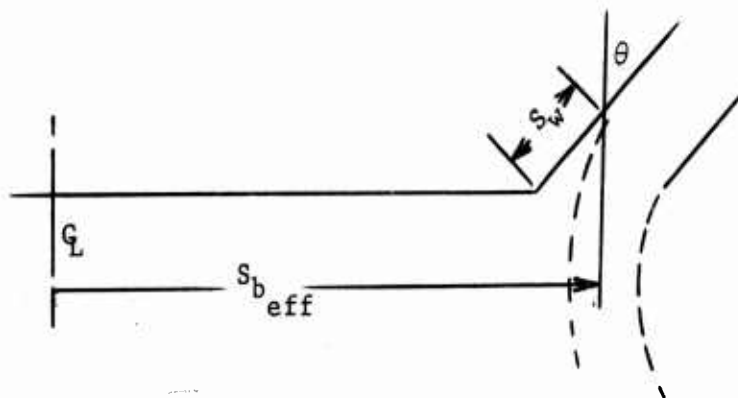
FIGURE 2-3. VORTEX REGION PRESSURE RATIO -
AERONUTRONIC DATA (REFERENCE 2)

Note that the jet total pressure term is an averaged quantity (\bar{p}_{t_j}).

Due to the viscosity of the real gas, the total pressure across the jet will not be constant, as was assumed in the inviscid theory. Therefore, an integrated average total pressure was used in the experimental work.

In addition to the above data, tests were reported in Reference 2 for $\theta = 60$ degrees. However, the data do not agree well with theory and are not included here. Reference 2 points out that the ducting necessary to assure the exit flow angle of 60 degrees came quite close to being horizontal. This geometry aided the formation of a strong vortex which reduced the static pressure at the outer edge of the jet. Thus, the pressure differential being supported by the jet is based on the reduced static pressure caused by vortex action. The flow field in the vortex was very complex and estimation of the reduction in static pressure was impossible. Since there is no clearly defined base level for the pressure differential, the utility of the base pressure data at 60 degrees is greatly reduced from that of 0, 30 and 45 degrees. For this reason these data are not presented here, although they are available in Reference 2.

The second assumption found lacking in the theory can be illustrated in the following sketch.



The jet was assumed to start turning uniformly at the point where the outer edge of the jet leaves the physical restraint of the jet wall. The base pressure was assumed to act over the "effective base area" ($S_{b \text{ eff}}$).

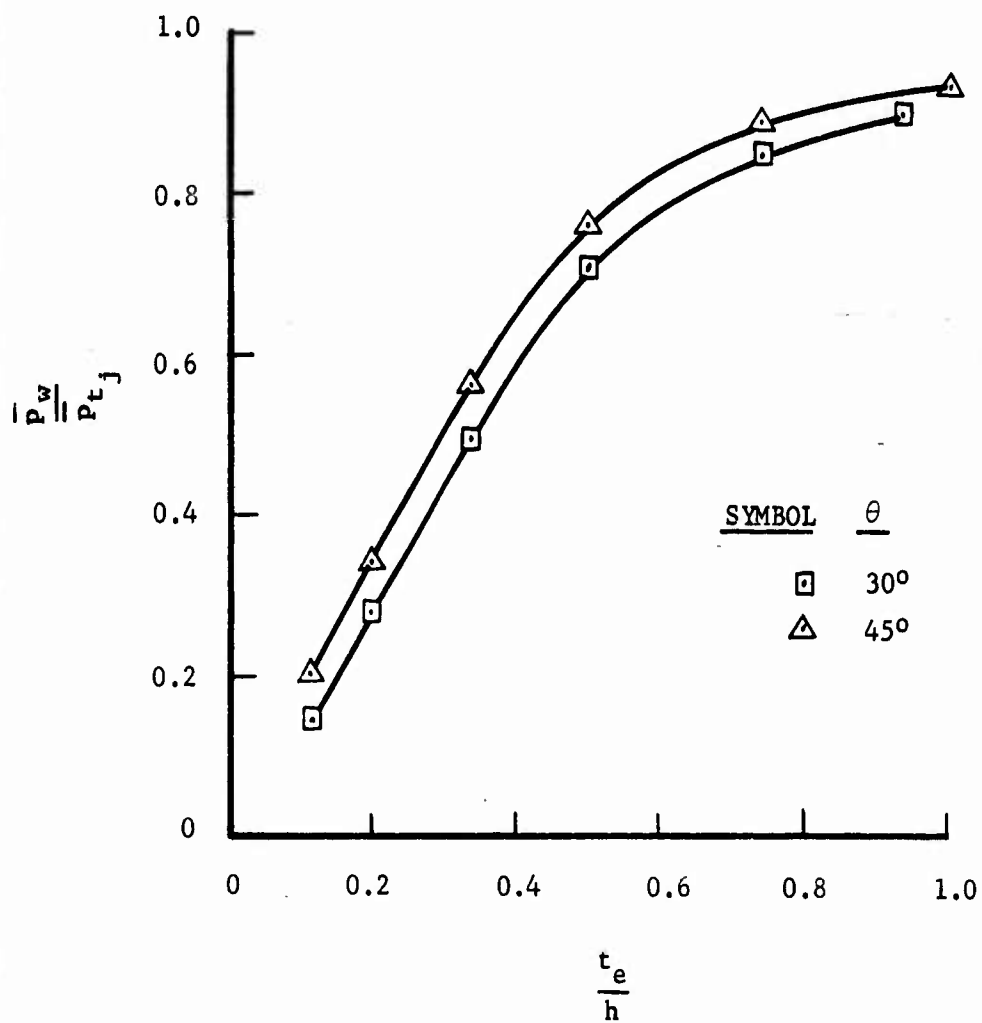
It has already been demonstrated that the vortex region has lower pressure exerted than base pressure. It is also incorrect to assume that base pressure is applied over the inner wall (S_w) of the jet up to the point where the jet was assumed to turn. Reference 2 demonstrates this, and presents pressures along S_w in terms of jet total pressure as a function of t_e/h and θ .

Figure 2-4, from Reference 2, shows this pressure variation. Stanton-Jones' theory, Reference 1, for estimating P_b/P_{t_j} is compared to the Aeronutronic experimental data in Figure 2-5. It can be seen that the data compare better with this theory at low θ than the Strand theory does. The data agree quite well with either theory at higher θ . Based on this comparison, it is advisable to further investigate Stanton-Jones' theory so that all performance parameters will be defined. These simple results might eliminate current dependence on data plots for performance estimates by providing analytical solutions.

The jet reaction coefficient (\bar{C}_r) can be shown to be a function of t_e/h and θ , as is P_b/P_{t_j} . This parameter

$$\begin{aligned}\bar{C}_r &= \frac{\text{jet lift}}{P_{t_j} t_e} \\ &= \frac{\int_{\text{jet}} (p_j + 2q_j) dt}{P_{t_j} t_e}\end{aligned}$$

The experimental determination of \bar{C}_r is compared with theory in Figures 2-6, 2-7, and 2-8. Since the theoretical and experimental values for all three angles have very much the same value, they are plotted on separate curves so that they will not be too cluttered.



S5731

FIGURE 2-4. INNER WALL PRESSURE RATIO -
AERONUTRONIC DATA (REFERENCE 2)

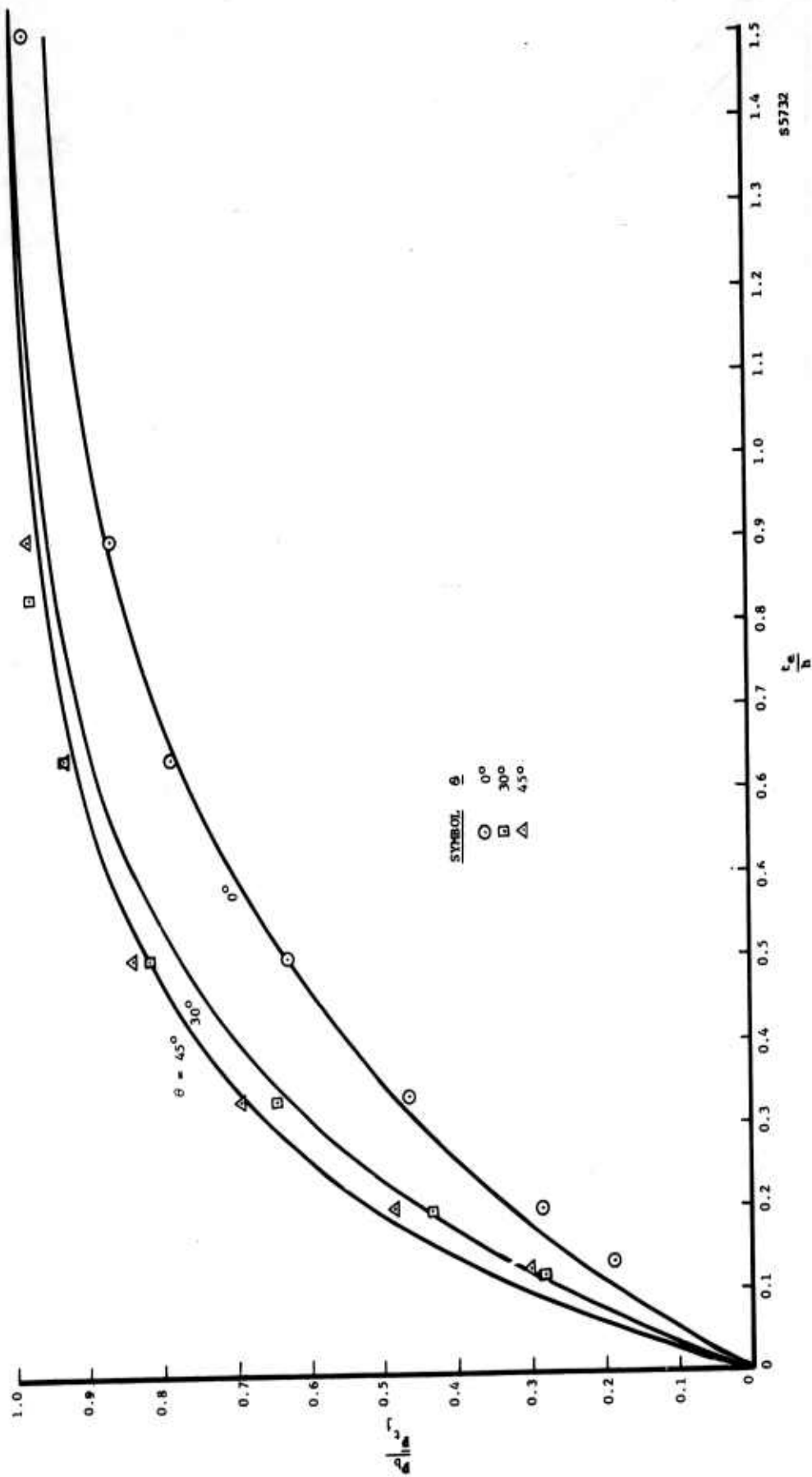
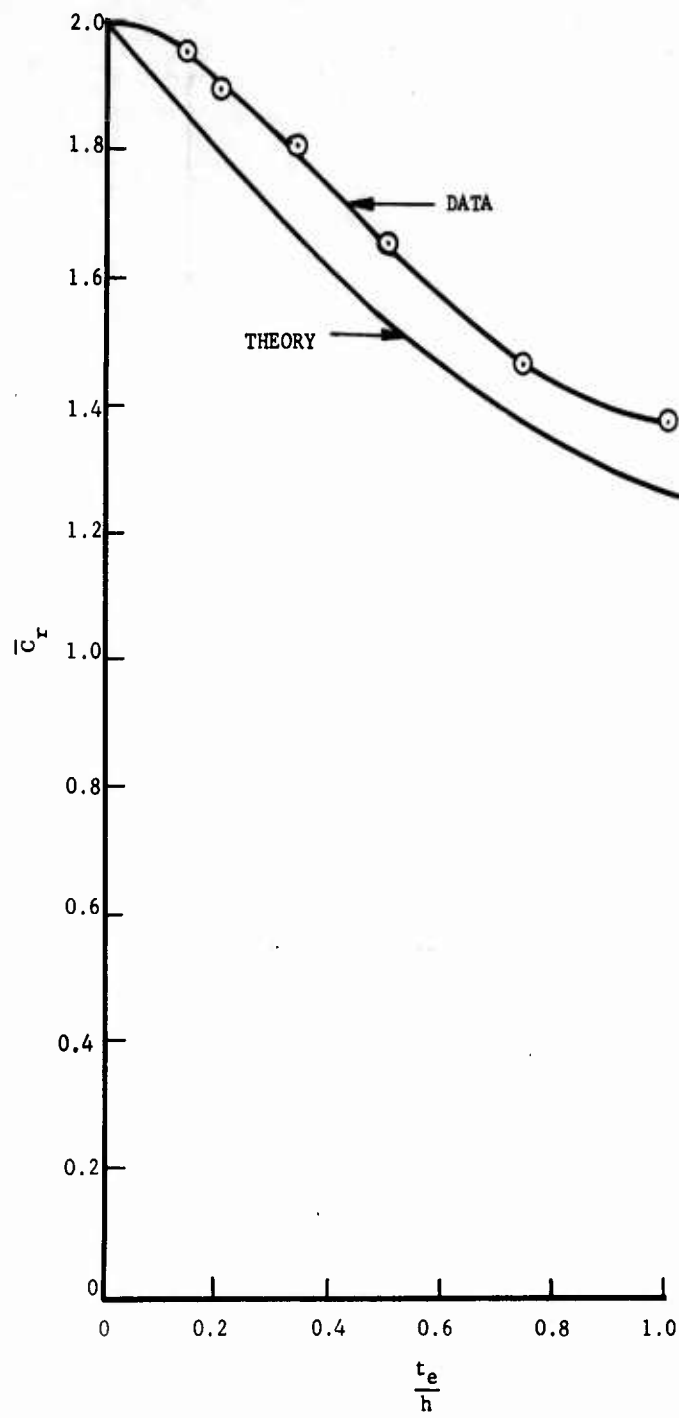


FIGURE 2-5. COMPARISON OF BASE PRESSURE THEORY (STANTON-JONES) AND DATA
- AERONAUTIC DATA (REFERENCE 2)



S5733

FIGURE 2-6. JET REACTION COEFFICIENT - STRAND THEORY COMPARED TO AERONUTRONIC DATA
(REFERENCE 2) - $\theta = 0$ DEGREES

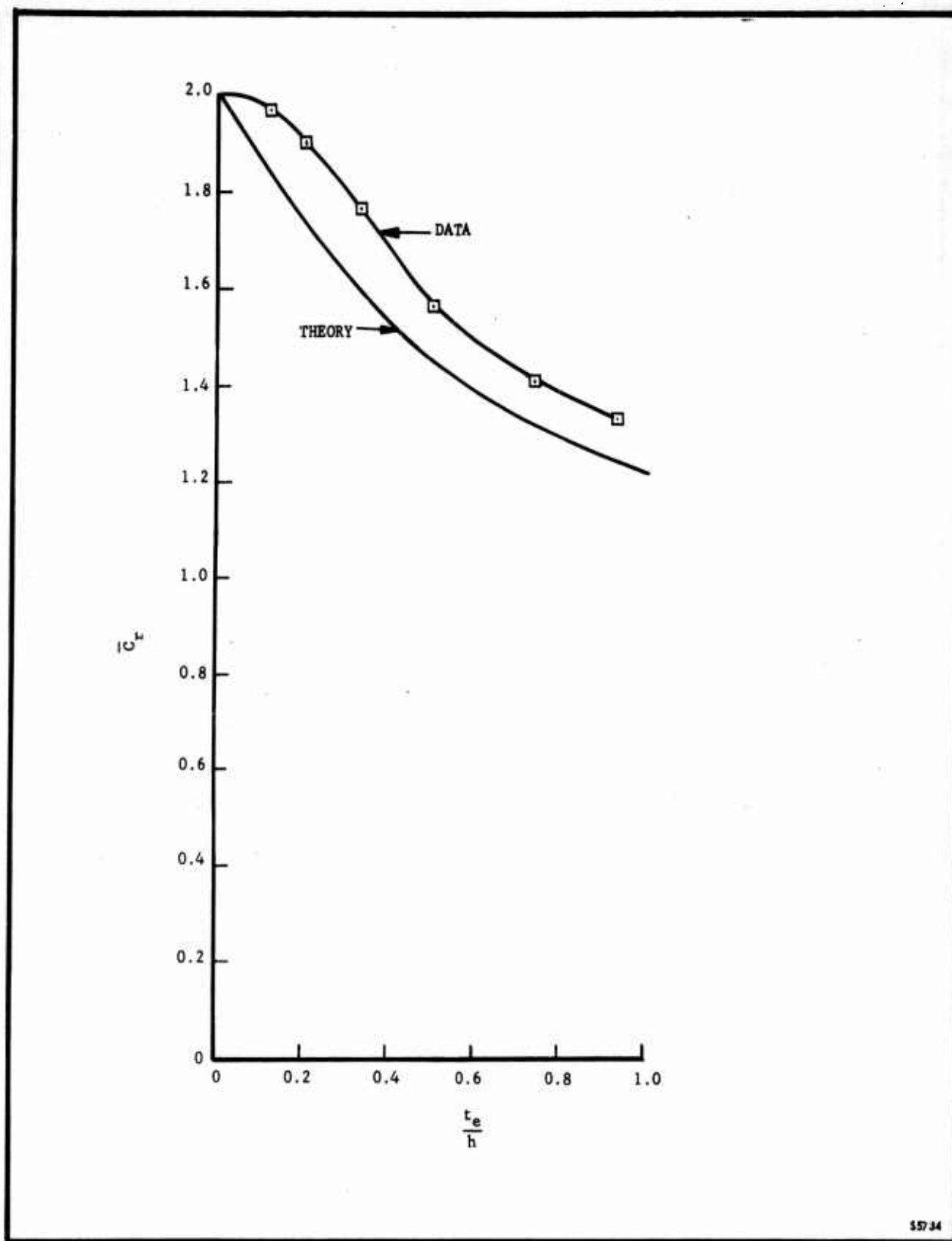
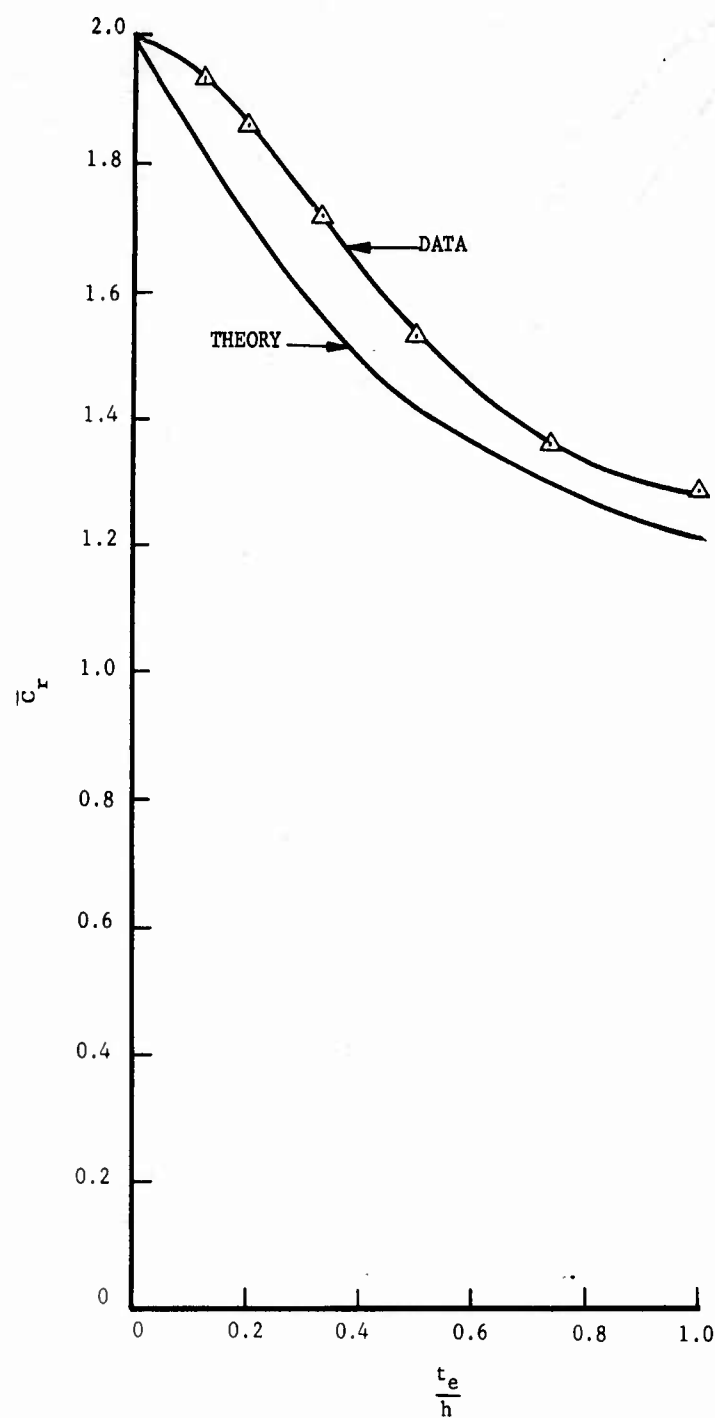


FIGURE 2-7. JET REACTION COEFFICIENT - STRAND THEORY COMPARED TO AERONUTRONIC DATA
(REFERENCE 2) - $\theta = 30$ DEGREES



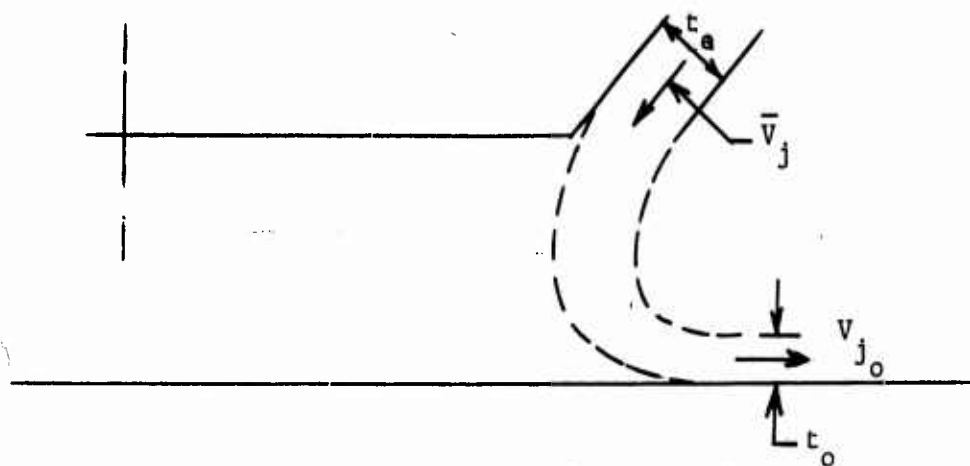
55735

FIGURE 2-8. JET REACTION COEFFICIENT - STRAND THEORY COMPARED* TO AERONUTRONIC DATA
(REFERENCE 2) - $\theta = 45$ DEGREES

The comparison shows the experimental \bar{C}_r to be higher than the theoretical. It is believed that this increase reflects the reduction in static pressure adjacent to the inner edge of the jet from that predicted in theory. Such reduction results in an increase in jet velocity which, in \bar{C}_r , overcomes the accompanying reduction in jet static pressure.

The parameter $\frac{t_o}{t_e}$ was impossible to determine experimentally. The jet flow is viscous in nature rather than inviscid as was assumed in the theory. The jet entrained considerable external flow. There was, therefore, no clearly defined jet boundary. However, from the theory, $\frac{t_o}{t_e}$ may be expressed

in terms of a jet velocity ratio, which can be determined experimentally.



$$\text{jet volume flow} = t_e \bar{V}_j = t_o V_{j_o}$$

where \bar{V}_j = average jet velocity at exit

V_{j_o} = velocity where jet total pressure has expanded to ambient pressure

$$= \sqrt{\frac{2}{\rho}} \sqrt{P_{t_j}}$$

t_o = jet thickness where V_{j_o} exists

$$\frac{t_o}{t_e} = \frac{\bar{V}_j}{V_{j_o}}$$

Since the jet was viscous, there was a boundary layer and p_{t_j} was not constant across the jet. Therefore p_{t_j} was averaged and given the symbol

\bar{p}_{t_j} . Similarly

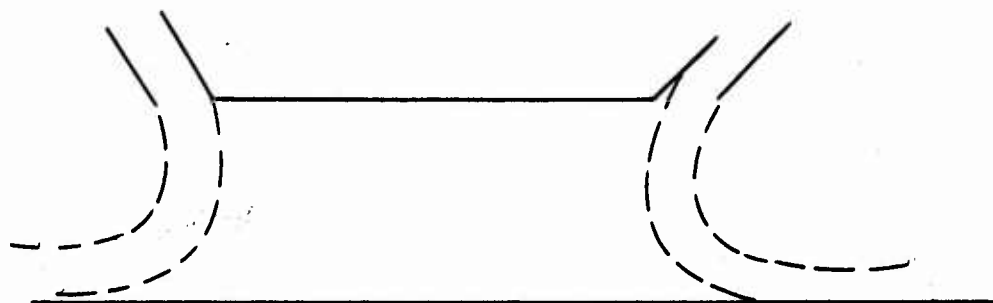
V_{j_o} becomes \bar{V}_{j_o}

$$\therefore \frac{t_o}{t_e} = \frac{\bar{V}_j}{\bar{V}_{j_o}}$$

Thus, although $\frac{t_o}{t_e}$ cannot be determined, the equivalent parameter, $\frac{\bar{V}_j}{\bar{V}_{j_o}}$,

can be used for estimating volume flow. This parameter is shown in Figures 2-9, 2-10, and 2-11, and compared to the theoretical estimates. The previously mentioned increase in jet velocity caused by reduced back pressure is demonstrated in this figure.

Recent unpublished data at Aeronutronic has shown good agreement between the preceding data, two-dimensional double opposing jet data,



and data from three-dimensional rectangular planform models. Figure 2-12, for example, compares \bar{p}_{t_j} for $\theta = 0$ degrees for the single jet configura-

tion with double jet and three-dimensional model data.

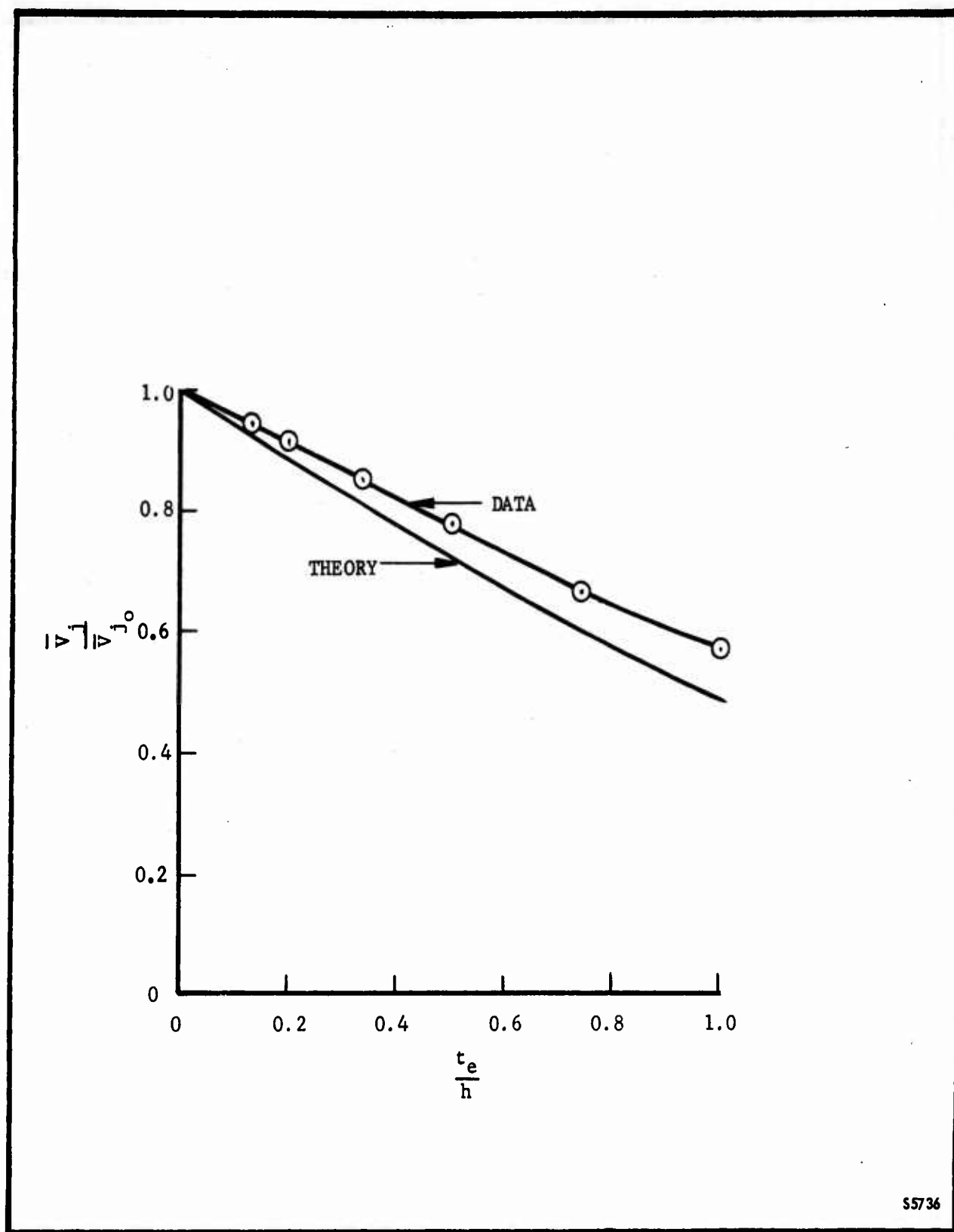
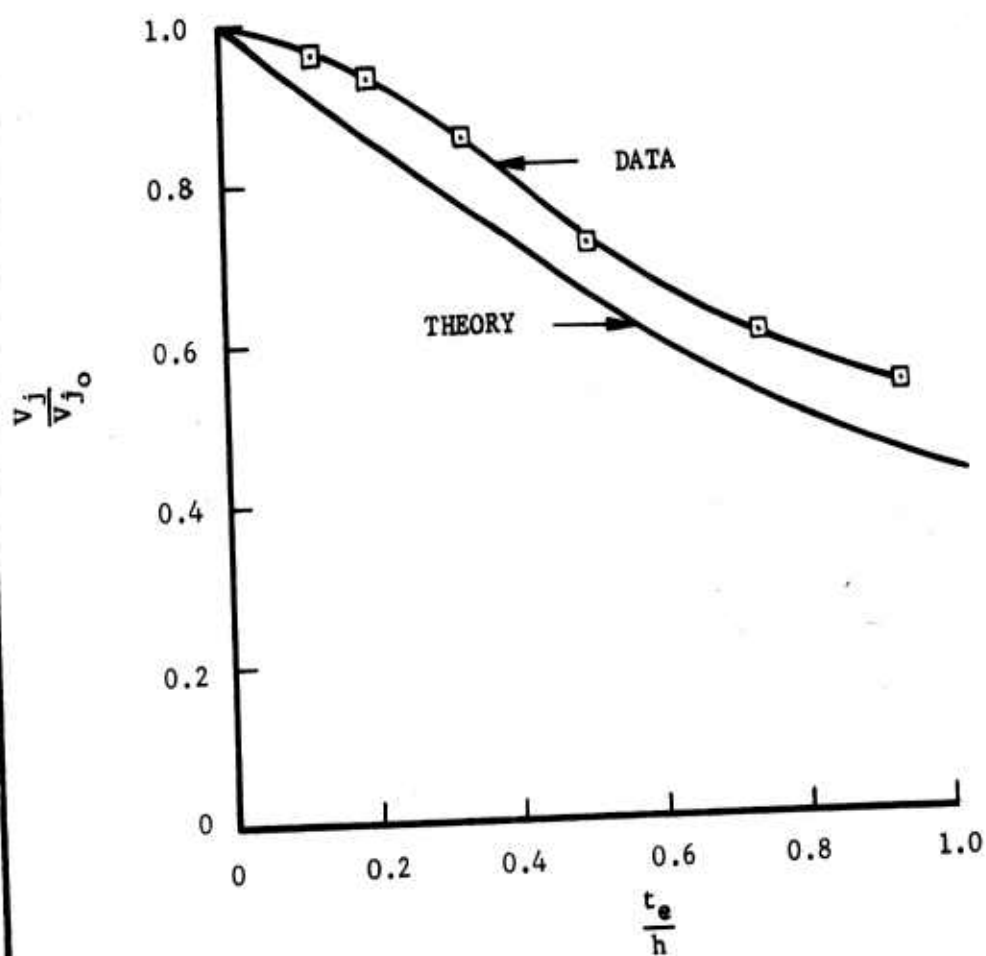


FIGURE 2-9. JET VELOCITY RATIO - STRAND THEORY COMPARED TO AERONUTRONIC DATA (REFERENCE 2) - $\theta = 0$ DEGREES



55737

FIGURE 2-10. JET VELOCITY RATIO - STRAND THEORY COMPARED TO AERONUTRONIC DATA (REFERENCE 2) - $\theta = 30$ DEGREES

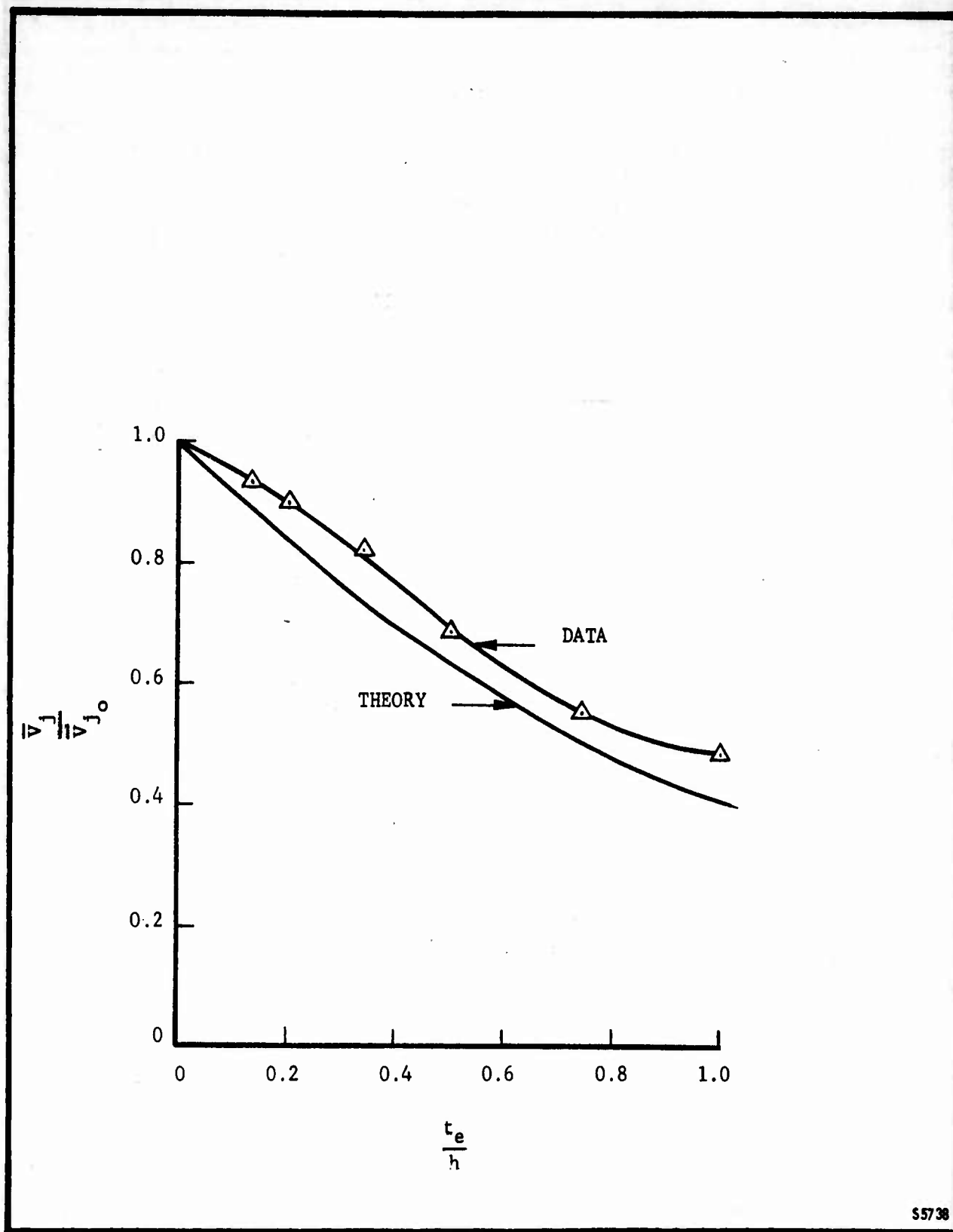
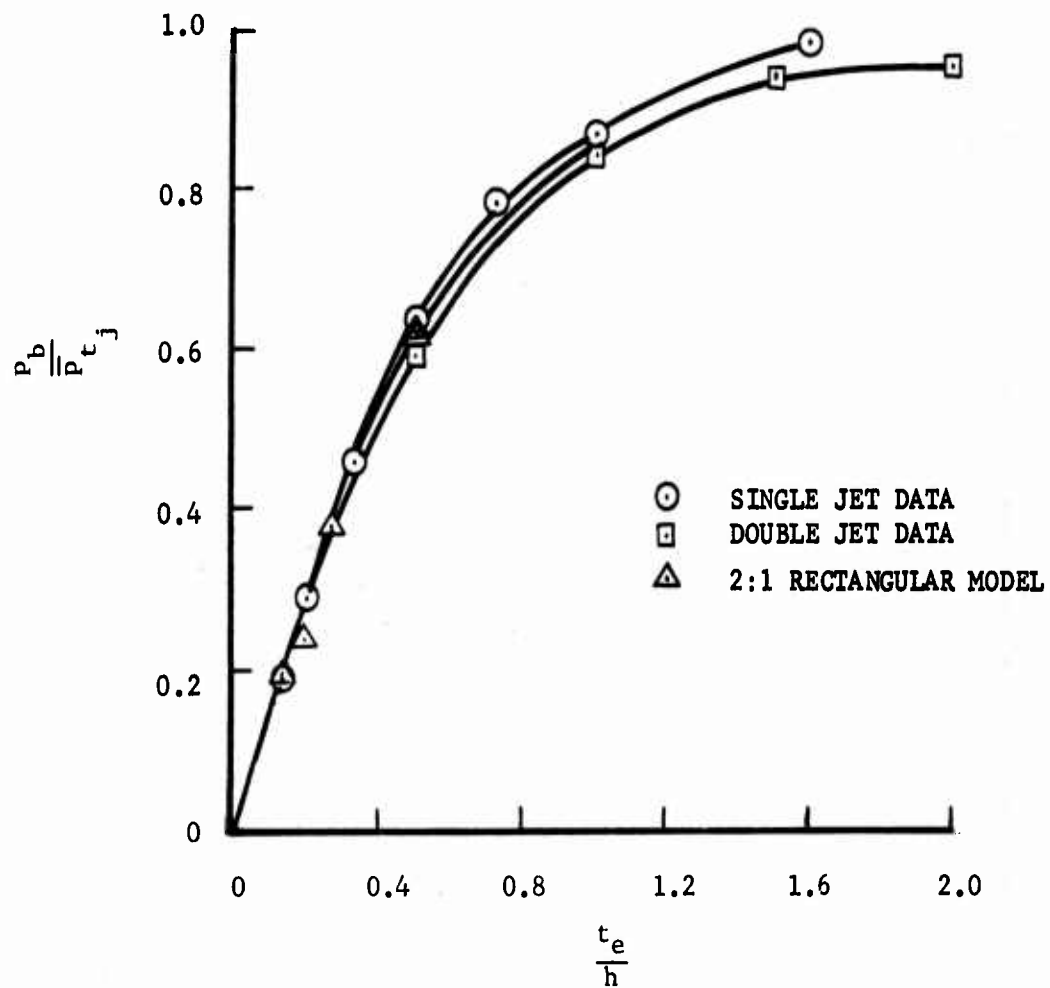


FIGURE 2-11. JET VELOCITY RATIO - STRAND THEORY COMPARED TO AERONUTRONIC DATA
(REFERENCE 2) - $\theta = 45$ DEGREES

EQUILIBRIUM BASE PRESSURE
 INTEGRATED AVERAGE JET TOTAL PRESSURE
 SINGLE-JET, DOUBLE-JET, AND THREE-DIMENSIONAL DATA



55739

FIGURE 2-12. BASE PRESSURE RATIO COMPARISON

2.2.2 Agreement of Current Data with Theory and Previous Data

The previous section described the prime reason for non-agreement of the data with theory; i.e., the jet induced vortex under the base. Another reason is that momentum is lost in the process of viscous mixing of the jet with the surrounding air. However, the Aeronutronic data agree with theory much better than previous data summarized in Publication U-926.

Figure 2-13, for example, compares the theory with faired data summarized in Publication U-926 and data included herein, for $\theta = 0$ degrees. The current data shows much better agreement with theory than does the previous data.

This is believed due primarily to the extreme care exerted in Reference 2 to insure the accuracy of the exit angle. It was not clear that the actual flow exit angle for the data reported in Publication U-926 agreed with the geometrical exit angle. Therefore, the data reported previously may be for lower angles than specified and the base pressure would not be expected to attain the level indicated by nozzle angle. The present data was taken at definitely known angles and, therefore, more closely approaches the predicted values.

2.2.3 Effect on Power Requirement and Geometry

In Publication U-926, the only experimental data available was for the ratio of $\frac{P_b}{P_{t_j}}$. A method was devised which permitted the estimation of

experimental \bar{C}_r and $\frac{t_o}{t_e}$ from the theoretical curves. This device was the

determination of an "effective" $\frac{t_e}{h}$. That this was an uncertain estimation

was noted in Publication U-926, which also noted that the best method would be to actually measure the parameters. As demonstrated in Section 2.2.1, such measurement has been accomplished. It is therefore recommended that performance estimates using the "effective" $\frac{t_e}{h}$ be discontinued and the

actual experimentally determined value be used instead.

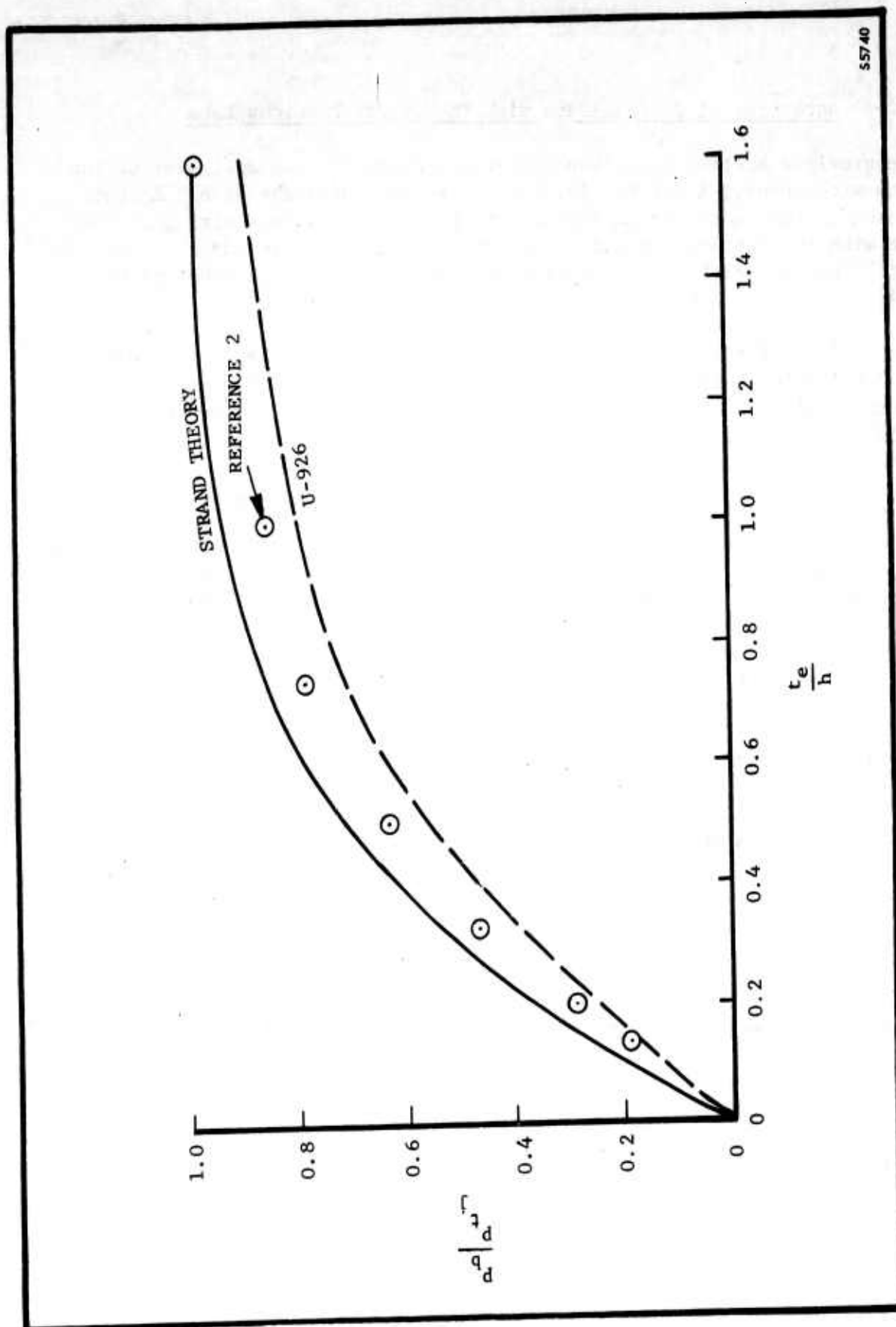
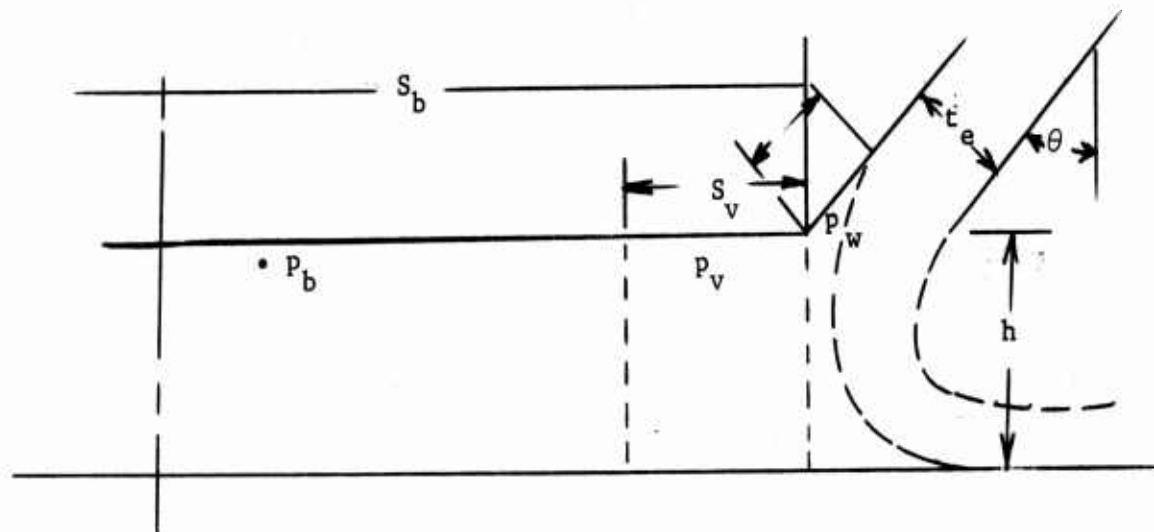


FIGURE 2-13. CURRENT AND PREVIOUS DATA COMPARISON (REFERENCE 2 DATA COMPARED WITH DATA SUMMARIZED IN PUBLICATION U-926 - $\theta = 0$ DEGREES)

In view of the previously mentioned shortcomings of the inviscid theory, and the necessity of using three separate base pressures over the region called "effective base area" in Publication U-926, a derivation of hovering ground effect power factor G will be included here using experimentally determined parameters entirely. The derivation is similar to that of Reference 2.



$$L = p_b (S_b - S_v) + p_v S_v + p_w S_w \sin \theta + R \cos \theta$$

$$= \bar{p}_{t_j} \frac{p_b}{\bar{p}_{t_j}} (S_b - S_v) + \bar{p}_{t_j} \frac{p_b}{\bar{p}_{t_j}} \frac{p_v}{p_b} S_v + \bar{p}_{t_j} \frac{p_w}{\bar{p}_{t_j}} S_w \sin \theta + \bar{p}_{t_j} \bar{C}_r S_j \cos \theta$$

$$= \bar{p}_{t_j} \left[\frac{p_b}{\bar{p}_{t_j}} S_b + \frac{p_b}{\bar{p}_{t_j}} S_v \left(\frac{p_v}{p_b} - 1 \right) + \frac{p_w}{\bar{p}_{t_j}} S_w \sin \theta + \bar{C}_r S_j \cos \theta \right]$$

$$\text{or } \bar{p}_{t_j} = \frac{L}{\frac{p_b}{\bar{p}_{t_j}} \left[S_b + S_v \left(\frac{p_v}{p_b} - 1 \right) \right] + \frac{p_w}{\bar{p}_{t_j}} S_w \sin \theta + \bar{C}_r S_j \cos \theta}$$

Jet volume flow

$$Q = s_j \bar{v}_j = s_j \frac{\bar{v}_j}{\bar{v}_{j_0}} \bar{v}_{j_0} = s_j \frac{\bar{v}_j}{\bar{v}_{j_0}} \sqrt{\frac{2}{\rho}} \sqrt{\bar{p}_{t_j}}$$

Jet power

$$P = Q \bar{p}_{t_j} = s_j \frac{\bar{v}_j}{\bar{v}_{j_0}} \sqrt{\frac{2}{\rho}} \left(\bar{p}_{t_j} \right)^{3/2}$$

$$= \frac{s_j \frac{\bar{v}_j}{\bar{v}_{j_0}} \sqrt{\frac{2}{\rho}} L^{3/2}}{\left\{ \frac{p_b}{\bar{p}_{t_j}} \left[s_b + s_v \left(\frac{p_v}{p_b} - 1 \right) \right] + \frac{p_w}{\bar{p}_{t_j}} s_w \sin \theta + \bar{c}_r s_j \cos \theta \right\}^{3/2}}$$

Multiply by $\frac{2S}{2S} \frac{1/2}{1/2}$

$$P = \frac{L}{2\sqrt{\rho}} \sqrt{\frac{L}{S}} s_j \sqrt{s} \frac{\bar{v}_j}{\bar{v}_{j_0}} 2 \sqrt{2} \cdot \left\{ \frac{p_b}{\bar{p}_{t_j}} \left[s_b + s_v \left(\frac{p_v}{p_b} - 1 \right) \right] + \frac{p_w}{\bar{p}_{t_j}} s_w \sin \theta + \bar{c}_r s_j \cos \theta \right\}^{3/2}$$

$$= p_{i_\infty} G$$

An optimization process will now be carried out for a circular planform vehicle. The area terms may be expressed in terms of $\frac{h\ell}{S}$, $\frac{t_e}{h}$ and θ .

The pressure ratios, reaction coefficient and velocity ratio were shown in Section 2.2.1 to be functions of $\frac{t_e}{h}$ and θ . Thus, G is a function of

$\frac{h\ell}{S}$, $\frac{t_e}{h}$ and θ . As demonstrated in Publication U-926, such an optimization

process will be valid to a first order approximation for vehicles with planforms other than circular, provided the actual $\frac{h\ell}{S}$ for such vehicles is used

in the resulting optimum G vs $\frac{h\ell}{S}$ Curve.

For simplicity, let

$$\frac{h\ell}{S} = N_1$$

and

$$\frac{t_e}{h} = N_2$$

$$N_1 = \frac{h(\pi\ell)}{\frac{\pi d^2}{4}} = \frac{4h}{d}$$

or $d = \frac{4h}{N_1}$

$S_j = ct_e$, where c = the circumference of the jet centerline at the plane (normal to the flow) where the jet starts to turn.

$$= \frac{t_e}{h} h \left[\pi \left(d - 2 \frac{t_e}{2} \cos \theta \right) \right] = \pi h N_2 \left(\frac{4h}{N_1} - \frac{t_e}{h} h \cos \theta \right)$$

$$= \pi h^2 N_2 \left(\frac{4}{N_1} - N_2 \cos \theta \right)$$

$$S = \frac{\pi d^2}{4} = \frac{4\pi h^2}{N_1^2}$$

$$S_b = \frac{\pi}{4} \left(d - 2 \frac{t_e}{\cos \theta} \right)^2 = \frac{\pi h^2}{4} \left(\frac{4}{N_1} - \frac{2 N_2}{\cos \theta} \right)^2$$

$$S_v = \pi \left(d - 2 \frac{t_e}{\cos \theta} - \frac{h}{2} \right) h = \pi h^2 \left(\frac{4}{N_1} - \frac{2 N_2}{\cos \theta} - \frac{1}{2} \right)$$

$$S_w = \pi \left[d \frac{2 t_e}{\cos \theta} + 2 \left(\frac{1}{2} \frac{t_e}{\cos \theta} \sin \theta \right) \sin \theta \right] \frac{t_e}{\cos \theta} \sin \theta$$

$$= \pi h^2 N_2 \tan \theta \left[\frac{4}{N_1} - \frac{2N_2}{\cos \theta} + N_2 \tan \theta \right]$$

Each of the area terms is seen to be dependent on h^2 . However, G may be rewritten so that the h^2 terms will drop out, leaving G dependent only on $\frac{hl}{S}$, $\frac{t_e}{h}$ and θ . Multiply the numerator and denominator by $\frac{1}{h^3}$

$$G = \frac{\frac{S_j}{h^2} \sqrt{\frac{S}{h^2}} \frac{\bar{V}_j}{\bar{V}_{j_0}} 2\sqrt{2}}{\left\{ \frac{p_b}{p_{t_j}} \left[\frac{S_b}{h^2} + \frac{S_v}{h^2} \left(\frac{p_v}{p_b} - 1 \right) \right] + \frac{p_w}{p_{t_j}} \frac{S_w}{h^2} \sin \theta + \bar{C}_r \frac{S_j}{h^2} \cos \theta \right\}^{3/2}}$$

G was optimized as a function of $\frac{hl}{S}$ by varying $\frac{t_e}{h}$ and θ for several values of $\frac{hl}{S}$. At each $\frac{hl}{S}$ optimum geometry was determined as the combination of $\frac{t_e}{h}$ and θ which gave the minimum G. This optimum geometry is shown in Figure 2-14, where the optimum geometry, as estimated by theory, is also plotted for comparison. Note that the optimum $\frac{t_e}{h}$ is constant and higher than the theoretical optimum.

As indicated by theory optimum θ becomes nearly vertical as $\frac{hl}{S}$ increases.

The minimum G from experiment is compared in Figure 2-15 with minimum theoretical G. The difference is roughly 10 percent.

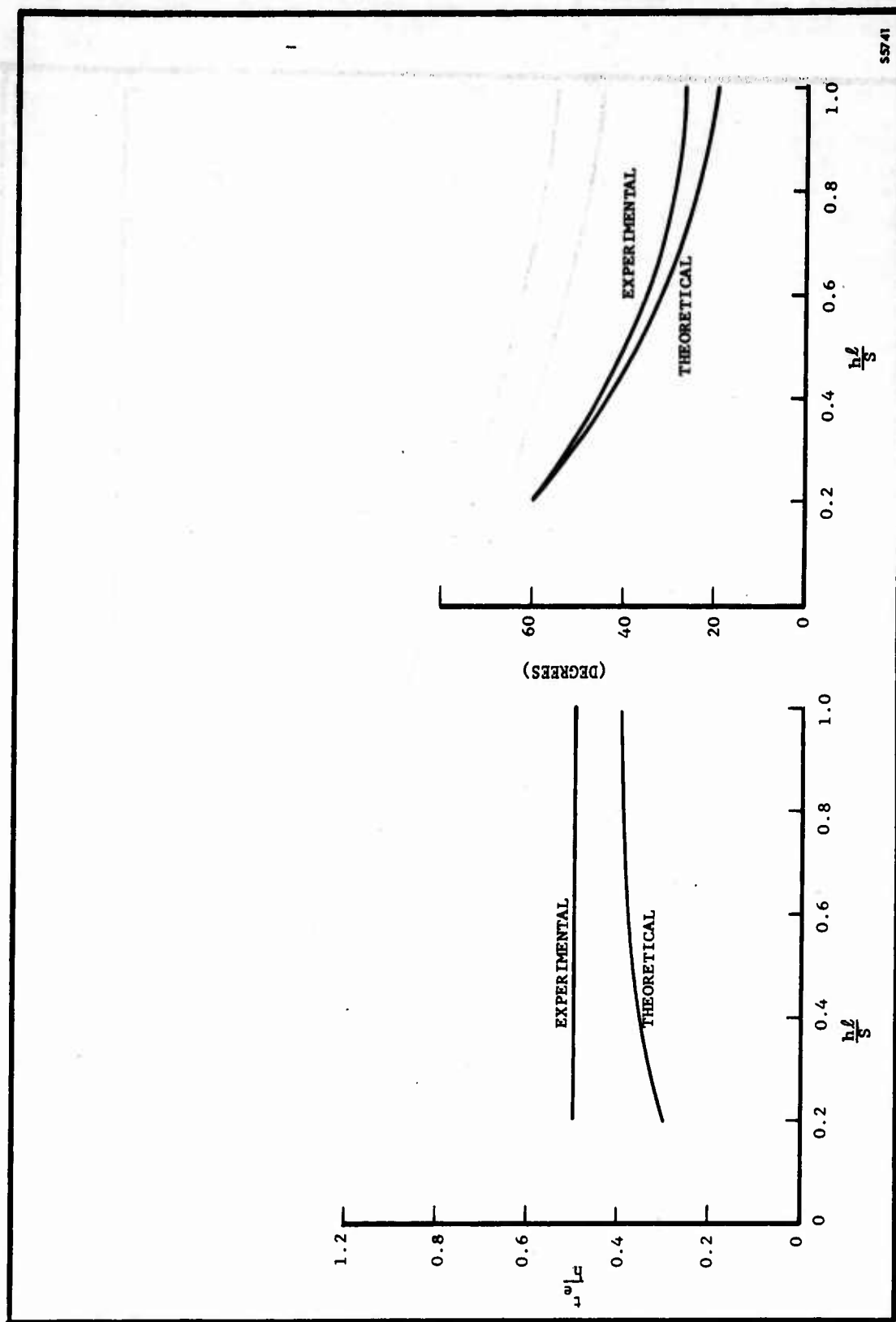


FIGURE 2-14. OPTIMUM THICKNESS TO HEIGHT RATIO AND JET INCLINATION ANGLE (EXPERIMENTAL OPTIMUM COMPARED WITH THEORETICAL OPTIMUM)

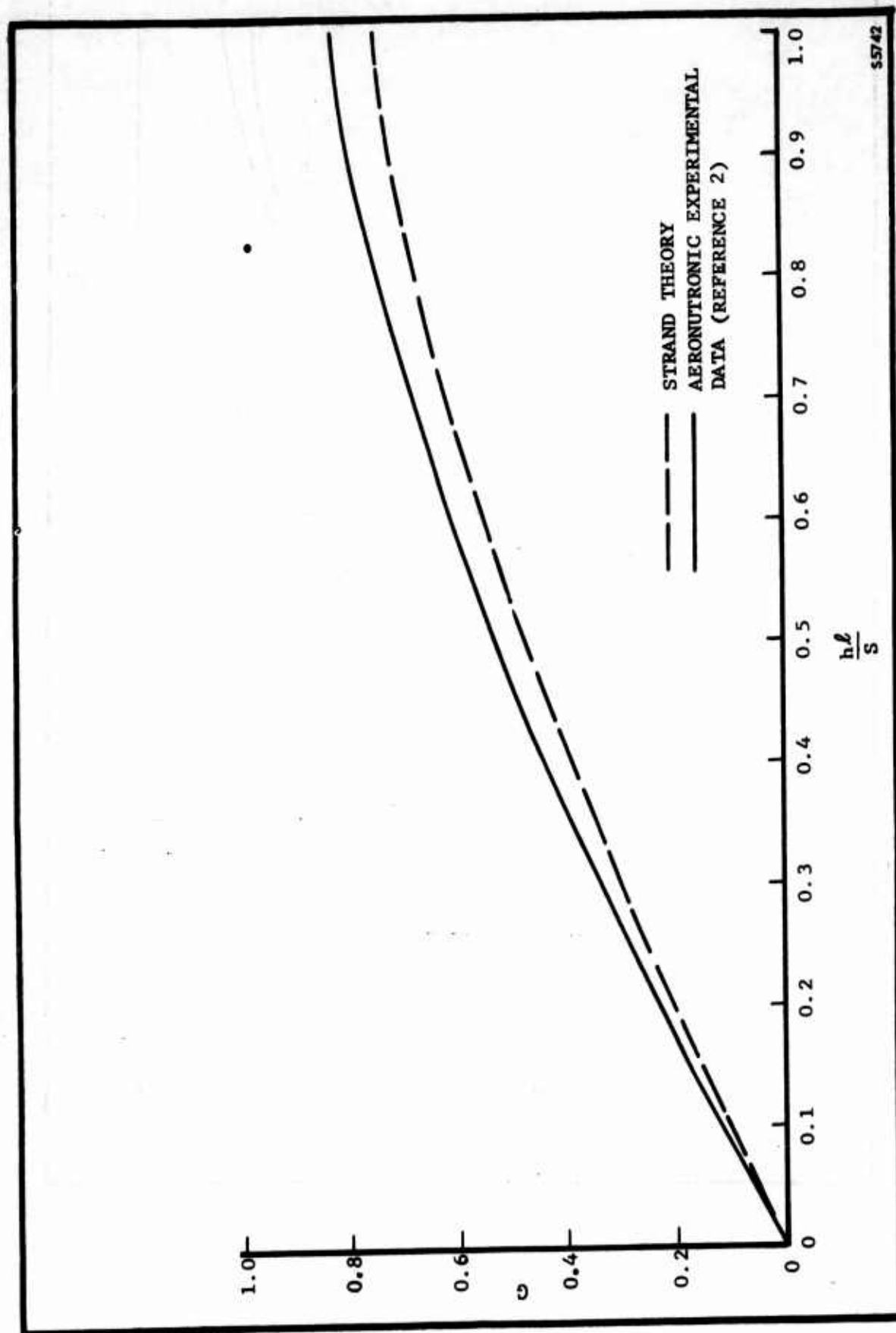


FIGURE 2-15. MINIMUM HOVERING GROUND EFFECT POWER FACTOR - G
(EXPERIMENTAL MINIMUM COMPARED WITH THEORETICAL MINIMUM)

2.3 INSTALLED POWER REQUIREMENTS - HOVERING

Several papers concerning internal flow systems for air-cushion vehicles have recently become available. Most of them discuss specific ducting geometries that are being evaluated (References 3, 4, and 5), or describe power plant-fan-duct matching problems (References 6, and 7) in much the same terms as those documented for aircraft. Reference 8 describes recent efforts by Strand towards describing in simple terms the ducting geometry required to minimize internal flow losses.

Strand pointed out that ducting loss estimation for air-cushion vehicles is more difficult than the usual ducting problems because the ducts are of such large diameter that fully developed turbulent flow (the basis of most ducting loss data) is rare. He has derived a relation expressing the minimum possible losses in terms of fan and duct geometry and air volume flow. This relation is approximate and useful for preliminary design purposes. Strand's development is outlined below.

A mean fan total pressure loss (due to blade drag) was expressed as

$$\frac{\Delta P_{tFL}}{\Delta P_{tF}} = m \frac{\epsilon}{\phi}$$

where

$$m = \frac{2}{3} \left(\frac{1-\nu^3}{1-\nu^2} \right)$$

ν is the ratio of hub radius to fan tip radius and is taken as zero in Strand's presentation.

$$\epsilon = \tan^{-1} \left(\frac{C_D}{C_L} \right) \text{ fan blade}$$
$$\phi = \frac{v_f}{u}$$

where v_f is axial velocity at the fan and u is fan tip velocity.

The ducting loss is expressed as a percentage of the duct inlet dynamic pressure.

$$\Delta P_{tDL} = \zeta q_i$$

where ζ is the duct loss coefficient which is established experimentally or estimated from empirical relations, and does not include inlet total pressure recovery η_r . It is apparent that Strand has assumed neither diffusion or effusion between the duct inlet and the fan. Written in terms of the fan total pressure rise, the ducting loss is

$$\frac{\Delta P_{tDL}}{\Delta P_{tF}} = \frac{\zeta \phi^2}{\psi}$$

where

$$\psi = \frac{\Delta P_{tF}}{\frac{\rho}{2} u^2}$$

Fan ducting losses add, to become

$$\frac{\Delta P_{tL}}{\Delta P_{tF}} = m \frac{\epsilon}{\phi} + \frac{\zeta \phi^2}{\psi}$$

based on fan total pressure rise.

Duct inlet total pressure q_∞ is known from ambient conditions. Jet exit total pressure p_{t_j} is known from performance calculations. The total pressure rise across the fan must be

$$\Delta P_{tF} = p_{t_j} - \eta_r q_\infty + \Delta P_{tL}$$

The last two equations may be combined to express the combined fan and duct total pressure losses in terms of flow parameters.

$$\begin{aligned} \frac{\Delta P_{tL}}{p_{t_j} - \eta_r q_\infty} &= \frac{m \frac{\epsilon}{\phi} + \frac{\zeta \phi^2}{\psi}}{1 - m \frac{\epsilon}{\phi} - \frac{\zeta \phi^2}{\psi}} \\ &= \frac{HP_{total}}{HP_{ideal}} \end{aligned}$$

Strand found the optimum values of the fan velocity coefficient ϕ and the fan pressure rise coefficient ψ to be

$$\phi_{\text{opt}} = \left(\frac{\epsilon'}{2\zeta} \right)^{3/7} \sigma^{-4/7}$$

$$\psi_{\text{opt}} = \left(\frac{\epsilon'}{2\zeta} \right)^{2/7} \sigma^{-12/7}$$

where σ is the fan characteristic number

$$\sigma = 2.105 Q^{1/2} \left(\frac{\Delta p_{tF}}{\rho} \right)^{-3/4} n$$

and n is the fan speed in revolutions per second. The fan total pressure rise Δp_{tF} must be known in order to evaluate σ , which is required when evaluating the optimum ϕ and ψ . Strand has written the minimum required fan pressure rise from the preceding relationships.

$$\Delta p_{tF \min} = \frac{p_{t_j} - \eta_r q_\infty}{1 - 2.4(Q \epsilon' n^2)^{2/7} \left(\zeta \frac{\rho}{\Delta p_{tF \min}} \right)^{3/7}}$$

Δp_{tF} must be found by iteration. According to Strand, three sequences are usually sufficient.

The optimum fan diameter may be determined from

$$d_{\text{opt}} = \frac{2u}{\omega}$$

$$= \frac{1}{\pi n} \left(\frac{2\Delta p_{tF}}{\rho \psi_{\text{opt}}} \right)^{1/2}$$

Estimation of the duct loss coefficient ζ is difficult because of the very low duct length to diameter ratios encountered and the complex flow paths that are often required. It is suggested in Reference 4 that the potential flow through the ducting be calculated by automatic computing machine or by electrical analogy methods. Boundary layer growth may then be computed (again with the help of automatic computers) and the losses estimated. The first technique, computing the potential flow, is almost impossible when complex three-dimensional ducting is involved.

Electrical analogy methods are practical only for two-dimensional problems. Moreover, a potential flow solution is not strictly applicable in most of the ducting because of turbulence caused by the fan. At the present time it is recommended that conventional duct loss empirical relations be used, followed by detailed component tests.

The normal procedures for estimating the minimum ducting power losses from Strand's analysis are:

- a. Determine p_{t_j} and Q from peripheral jet performance calculations.
- b. Choose values for ϵ , n and ζ based upon available fan and power plant specifications and ducting loss data.
- c. Calculate minimum Δp_{t_f} by iteration.
- d. Calculate σ , ψ_{opt} , ϕ_{opt} and d_{opt} .
- e. Calculate $\frac{\Delta p_{tL}}{\Delta p_{tF}}$ from ϕ_{opt} and ψ_{opt} .

Strand concluded that the quantities listed below should be minimized in order to minimize ducting and fan losses.

- a. Volume flow per fan (this infers that multiple fans are advantageous from an aerodynamic, if not from a mechanical viewpoint).
- b. Shaft speed.
- c. Fan blade section drag to lift ratio.
- d. Duct loss coefficient.

2.4 FORWARD MOTION

Two recent papers concerned with the effects of forward motion are reviewed herein. One analytical approach will be presented in detail.

2.4.1 Effect on Power for Lift

Unchanged

2.4.2 Momentum Drag

2.4.2.1 Definition

Unchanged

2.4.2.2 Minimum Total Power

The basic idea of this section is unchanged from that of the corresponding section of Publication U-926; i.e., momentum drag will have considerable effect on jet thickness selected as optimum. The details of the volume flow calculations are different, reflecting the experimental data contained in Section 2.2.

Since the basic intent of this section is adequately served by the corresponding section of Publication U-926, it is deemed superfluous to go through the details of the volume flow and momentum drag power calculations here.

There is however a minor computational error in the estimation of momentum drag power required on page 2-48 of Publication U-926. The relation for this quantity included a factor of $\frac{1}{.7}$ as a propulsive efficiency. This factor was not included in the actual calculation performed, and Figure 2-35 of Publication U-926 is in error. Again, since the basic intent is served, the details of this correction will not be included.

2.4.3 External Drag

Unchanged

2.4.4 Over Water Drag

Unchanged

2.4.5 Miscellaneous

In Reference 9, Stanton-Jones discussed an analysis of several geometrically similar vehicles. The analysis included typical installation losses

and was verified by 1/12 scale model tests. Some generalizations from the study are noted below.

- a. At low height to diameter ratios, the speed for maximum L/D is quite critical. As the height to diameter ratio increases (above about 0.01 to 0.03 for the configuration considered) L/D varies much more slowly with speed.
- b. Angling the side jets back more than 20 to 30 degrees increases the mass flow requirements so much that either ducting sizes or ducting losses become prohibitive.
- c. The power required to overcome profile drag is approximately equal to half the lifting power at the speed for maximum L/D.

A preliminary analysis of wind tunnel tests on one specific configuration (tests in Reference 10) is presented by Chaplin in Reference 11. The data generally correlated well with the simple theory of Reference 12 when corrections are made for aerodynamic lift. Correlation with the jets angled back 30 degrees and 45 degrees is good. When the jets are angled back 60 degrees the theory underestimates power required by as much as 20 percent.

2.4.6 Adaptation of Hovering Data for Forward Motion

The effect of forward motion on cushion power required may be estimated by adapting the data presented in Section 2.2. This method was first devised in Reference 13.

In hovering, the term p_b is the actual pressure above ambient in the base region and is supported by a jet with total pressure (p_{tj}) measured above local static pressure. If the local static pressure (p_o) is different from remote ambient pressure, for example, when the vehicle is moving, the pressure differential the jet must support (Δp_b) is $\Delta p_b = p_b - p_o$. Similarly, the p_{tj} measured with respect to local static pressure is different from the jet total pressure increment above remote ambient (p_{tj}).

Under certain conditions it may be desired to give the jet flow a component of velocity parallel to the plane of the exit (V_z). For example, this would be a way to obtain thrust and/or reduce net momentum drag. The jet total pressure must be great enough to provide this component of

velocity and still provide a velocity component normal to the plane of the exit. If the portion of p_t associated with V_z is q_z , then

$$p_{tj} = p_t - q_z - p_o$$

The pressure differential supported by a given jet is dependent on the portion of the total pressure associated with the velocity component normal to the plane of the jet exit. The ratio of $\Delta p_b/p_{tj}$ in forward motion is determined by jet geometry just as p_b/p_{tj} is in hovering. However, in motion p_{tj} is not the true indicator of jet total pressure p_t is. Jet power, for example, is the product of jet volume flow and p_t , not p_{tj} . Therefore, in forward motion, the p_t required for a given p_b is found from

$$\frac{\Delta p_b}{p_{tj}} = \frac{p_b - p_o}{p_t - q_z - p_o}$$

Similarly, \bar{V}_j/\bar{V}_{jo} and \bar{C}_r for vehicles in motion may be found from jet geometry; but for finding volume flow and jet reaction these ratios must be applied to p_{tj} , not p_t .

Each individual vehicle will have its particular variation of p_o around the perimeter. Since no generalization can be made, no discussion of p_o will be presented here.

2.5 STABILITY AND CONTROL

To date the stability and control of air-cushion vehicles have received substantially less attention than performance. Theoretical efforts in this area have produced results of only limited usefulness and which have not been correlated with experimental results. A survey of presently available theoretical analyses and test data has produced the following results:

- a. Two-dimensional experimental static stability data cannot yet be correlated with three-dimensional data.
- b. Three-dimensional experimental data are limited primarily to static test results.
- c. Data presently available from experimental vehicles has limited applicability for defining the important parameters of the dynamic characteristics of the vehicle because the data is qualitative in nature, or because the vehicles were operated relatively close to the ground.
- d. The most comprehensive dynamics analysis published is described by the authors as being primarily of qualitative usefulness.

2.5.1 Hovering Stability

2.5.1.1 Static Stability

2.5.1.1.1 Pitch and Roll

Major discrepancies have been noted between two-dimensional and three-dimensional stability data (References 9 and 14 through 19). In general, the three-dimensional models have demonstrated substantially greater static stability. A comparison of a typical configuration in both two and three dimensions is shown on Figure 2-16, from Reference 14. The stability parameter is given in center of pressure shift per degree of tilt, where the center of pressure shift is expressed in percentage of vehicle length. Thus a value of -0.2 would indicate that a 5 degree tilt would cause the vehicle center of pressure to move $(-0.2)(5) = -1.0$ percent of the vehicle length from the center line in a direction to initiate rotation back toward neutral.

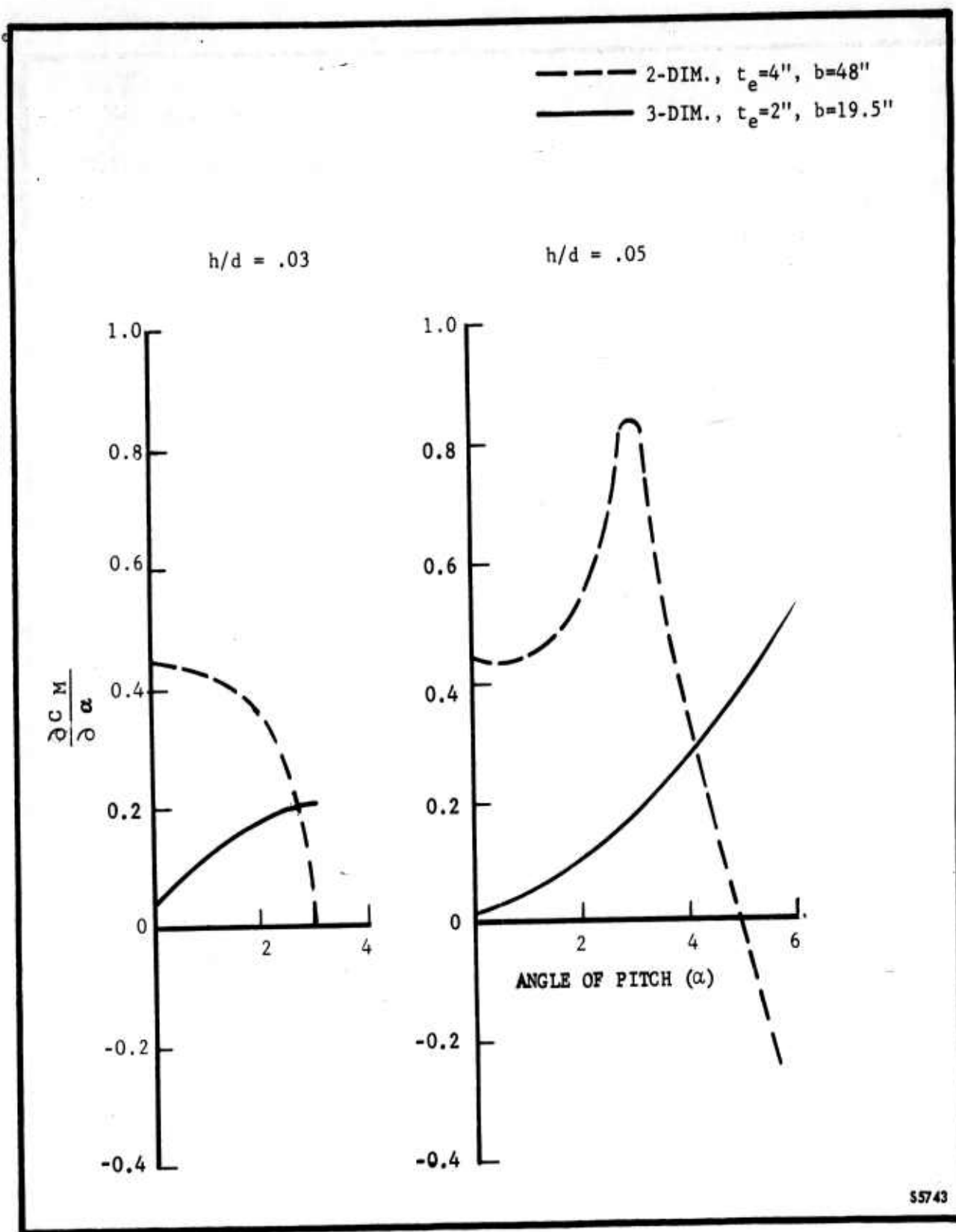


FIGURE 2-16a. COMPARISON OF TWO- AND THREE-DIMENSIONAL PITCH STABILITY
 - $\theta = 0$ DEGREES - $h/d = 0.03$ - $h/d = 0.05$

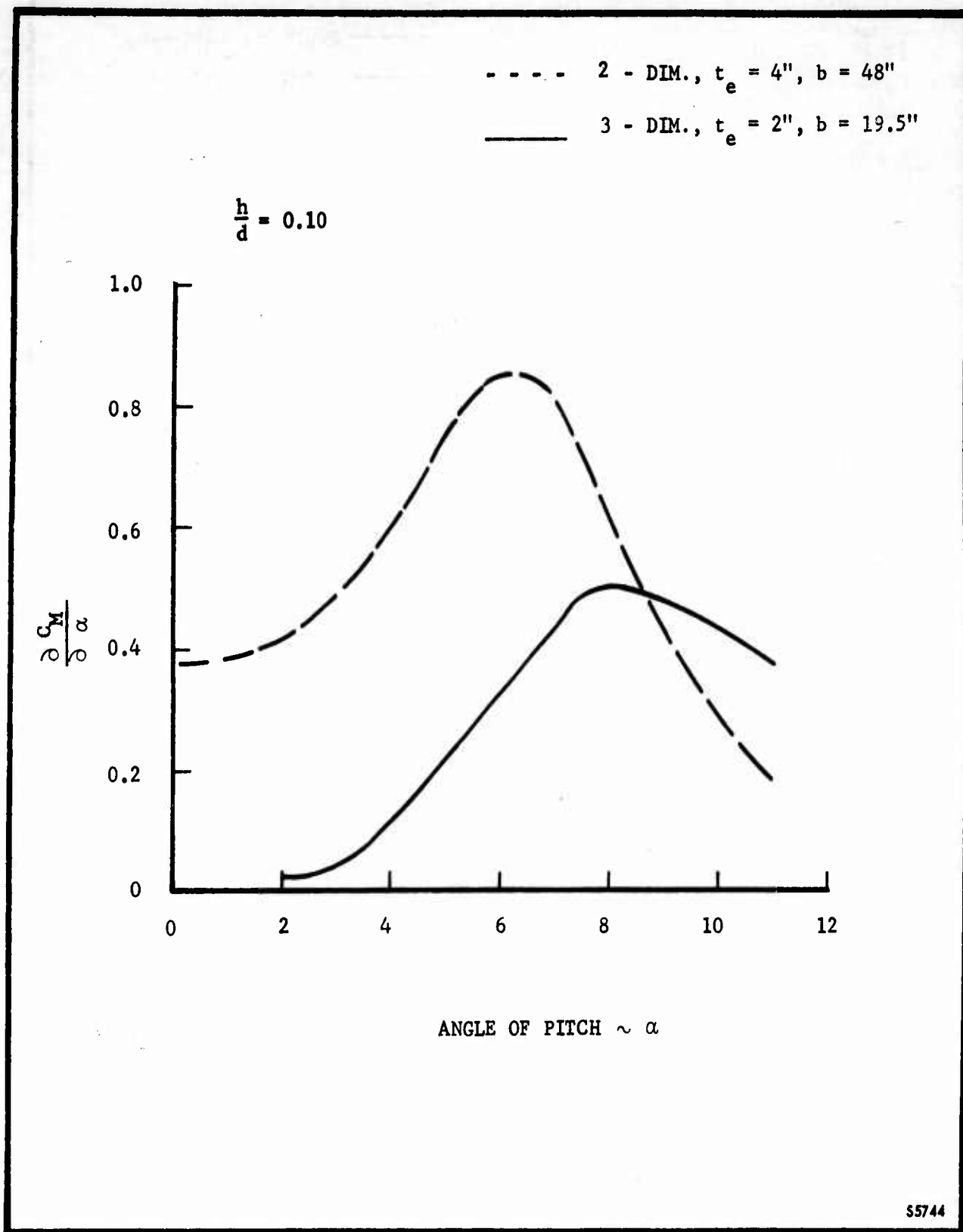


FIGURE 2-16b. COMPARISON OF TWO- AND THREE-DIMENSIONAL PITCH STABILITY
 - $\theta = 0$ DEGREES - $h/d = 0.10$

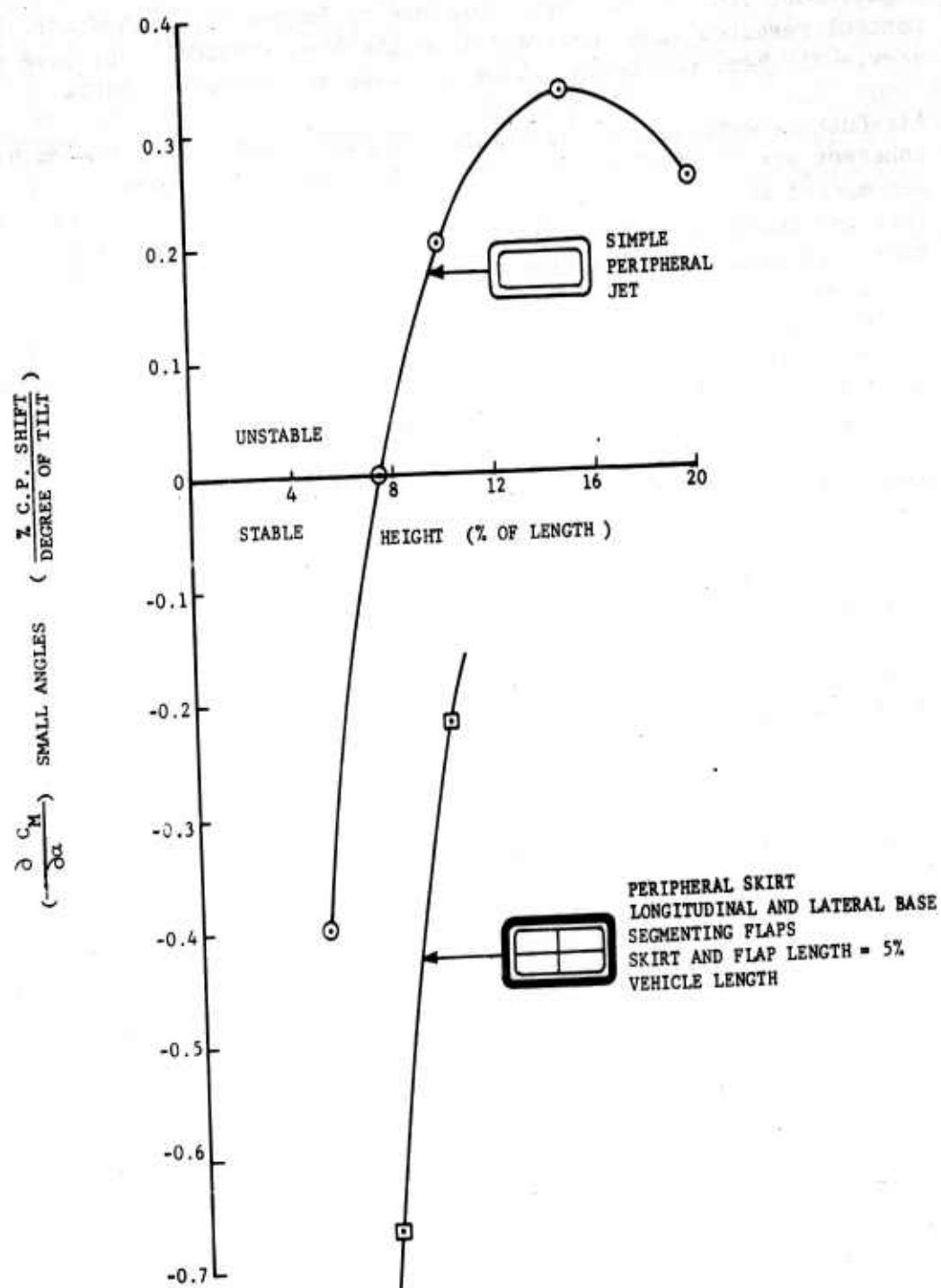
Significant results have been obtained by Aeronutronic in stability and control research under contract from the Army (TRECOM), but have not previously been published. Some of these are presented below.

Air-Cushion vehicles of the simple peripheral jet configuration have inherent static stability when hovering close to the ground (i.e., the net moment arising from vehicle tilt opposes the initial tilt). However, they are unstable in the upper height range of interest. Although the crossover point is a function of configuration, a height of 6 percent of the diameter is common to most circular model data. The effect of increasing the length relative to the width is to increase the limiting height to length ratio for static stability in pitch and to decrease the limiting height-to-width ratio in roll. In Reference 16 and in recent unpublished Aeronutronic experiments, rectangular models were found to be unstable in roll at a height-to-width ratio of 5 percent, whereas they were found to be stable in pitch at a height-to-length ratio of 5 percent; i.e., at a greater absolute height.

The upper curve of Figure 2-17 presents pitch stability data from a 2:1 rectangular Aeronutronic model employing a vertical peripheral jet with an area of 15 percent of the total area. The model was neutral at a height-to-length ratio of 7.5 percent, stable at lower, and unstable at greater heights.

The lower curve illustrates the effect on pitch stability of extending a skirt (of 5 percent of the vehicle length) beneath the vehicle around the outer periphery, and also dividing the base into four segments with 5 percent long flexible flaps on the longitudinal and lateral centerlines. This model was still stable at a height of 10 percent of the length, measuring the height from the surface to the vehicle base rather than from the surface to the skirt edge. It was found by removing the segmenting flaps that the peripheral skirt alone did not contribute much to the stability. The peripheral skirt was retained for performance reasons. The base compartmentation due to the flaps augments the stability by limiting the cross flow under the base. The base compartments now behave more like isolated air-cushion vehicles. The low areas develop a higher base pressure than the high areas and a restoring moment is obtained. It should be noted that the flaps extended two thirds of the way to the ground at the lower height tested and half-way to the ground at the higher height.

Figure 2-18 presents the effect of base segmenting jets on pitch stability. Aeronutronic models employed segmenting jets with width equal to the peripheral jet width. Both the corner lobe and longitudinal-lateral centerline jet configurations produced static longitudinal stability up to the maximum height-to-length-ratio tested



54142

FIGURE 2-17. STATIC LONGITUDINAL HOVERING STABILITY (SKIRTS)

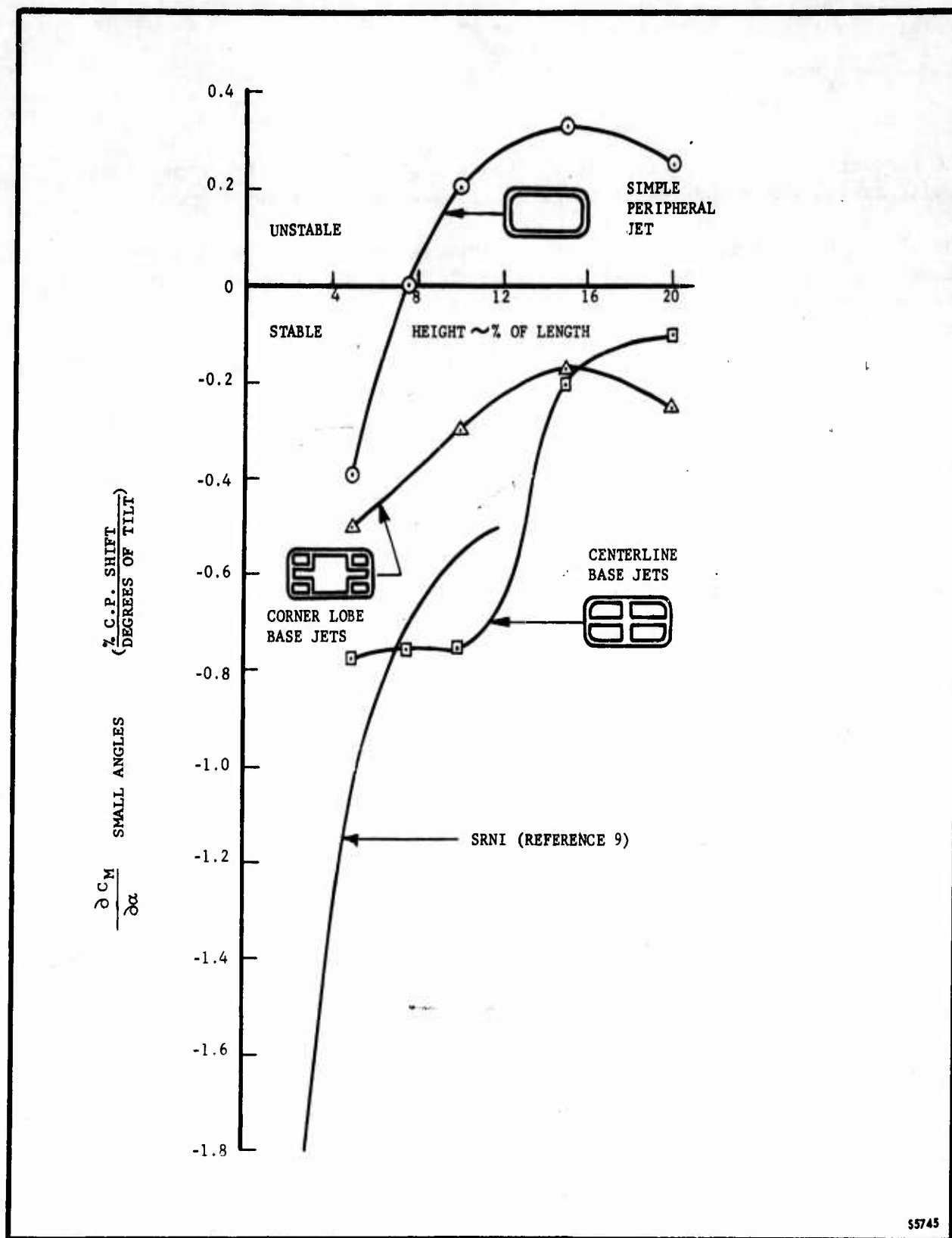


FIGURE 2-18. STATIC LONGITUDINAL HOVERING STABILITY (INTRAVENTS)

(20 percent). This is particularly notable in the case of the corner lobe configuration where the center longitudinal base strip is not segmented.

The simple peripheral jet model was unstable in roll at all heights tested (down to 5 percent of the model width) as shown by the upper curve of Figure 2-19. This is in contrast to the longitudinal case and indicates that longitudinal and lateral flow patterns with the vehicle tilted are not similar when the vehicle length is significantly greater than the width. The lower curves show the variation of static lateral stability with vehicle height-to-width ratio when a skirt and base segmenting flaps extend part way to the ground. With either two longitudinal base segmenting flaps or a single flap on the centerline, the model is seen to become stable at a height-to-width ratio of slightly less than .20, and to rapidly increase in stability as height-to-width ratio is lowered. Two longitudinal base segmenting flaps are somewhat superior to a single flap on the centerline.

The effect of the base segmenting jets on lateral stability is shown in Figure 2-20. The corner lobe configuration produces static lateral stability up to a height of 20 percent of the width. The slight instability at great heights is to be expected since there is a wide central base portion which remains unsegmented in this configuration. The center slot configuration produces static lateral stability at all heights through 40 percent of the vehicle width.

It appears that static longitudinal and lateral hovering stability can be obtained at all heights of interest through use of base segmenting jets. It should be noted that the static stability derivatives have been taken in the range of small to moderate tilt angles (up to $1/3$ the way to touchdown). In many cases where stability exists at low angles, instability occurs at large angles approaching touchdown. Two phenomena enter into this instability. As the low jet approaches the ground it splits and partially flows under the base. This results in a destabilizing base force. Concurrently, the jets tend to rotate within the nozzles in such a way that a small side force (stabilizing when the vehicle center of gravity is above the base) occurs in the direction of the low side. Little is known about the side force except that it is not sufficient to overcome the destabilizing base pressures. Several investigators are presently evaluating this force.

2.5.1.1.2 Yaw

Unchanged.

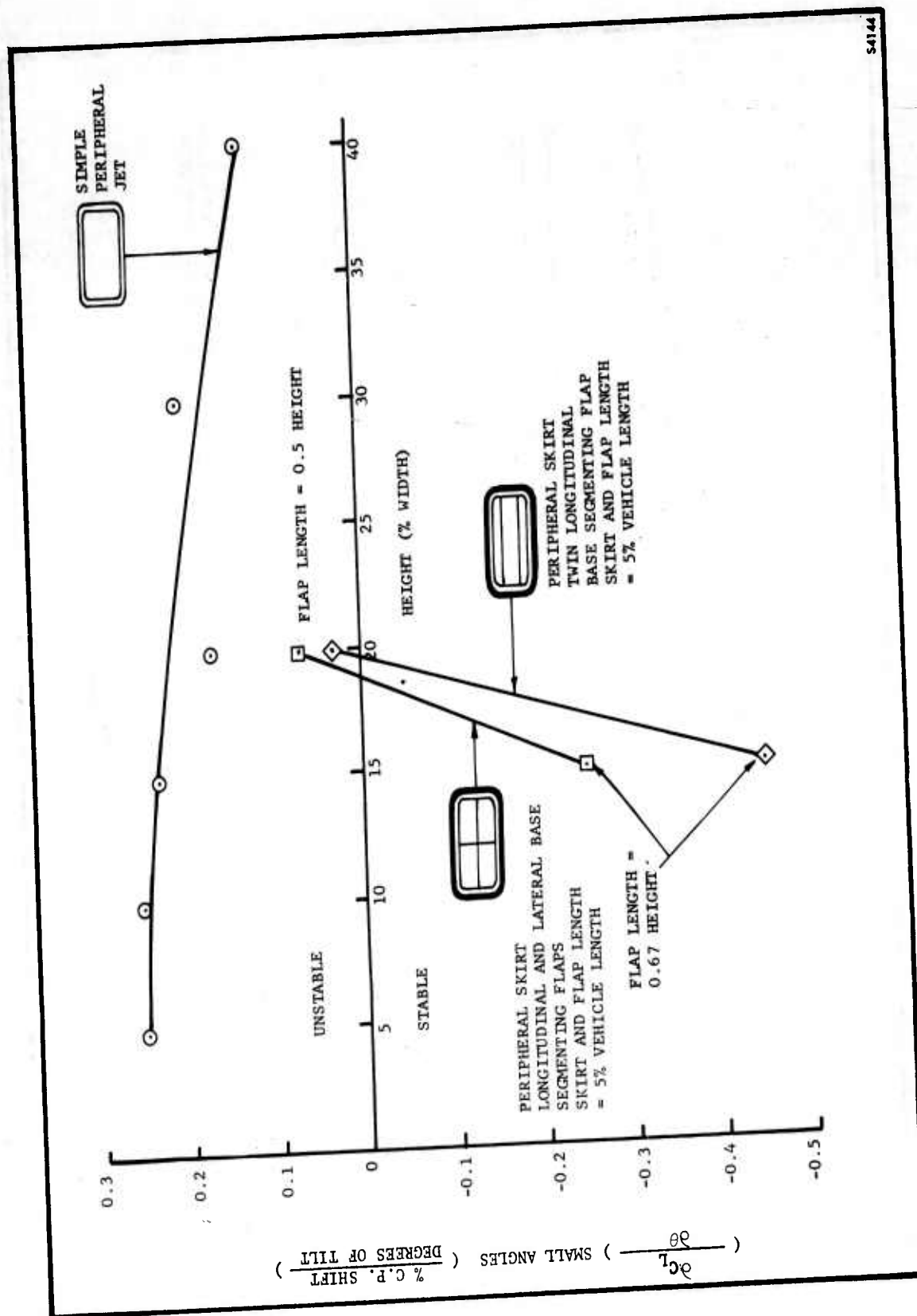


FIGURE 2-19. STATIC LATERAL HOVERING STABILITY (SKIRTS)

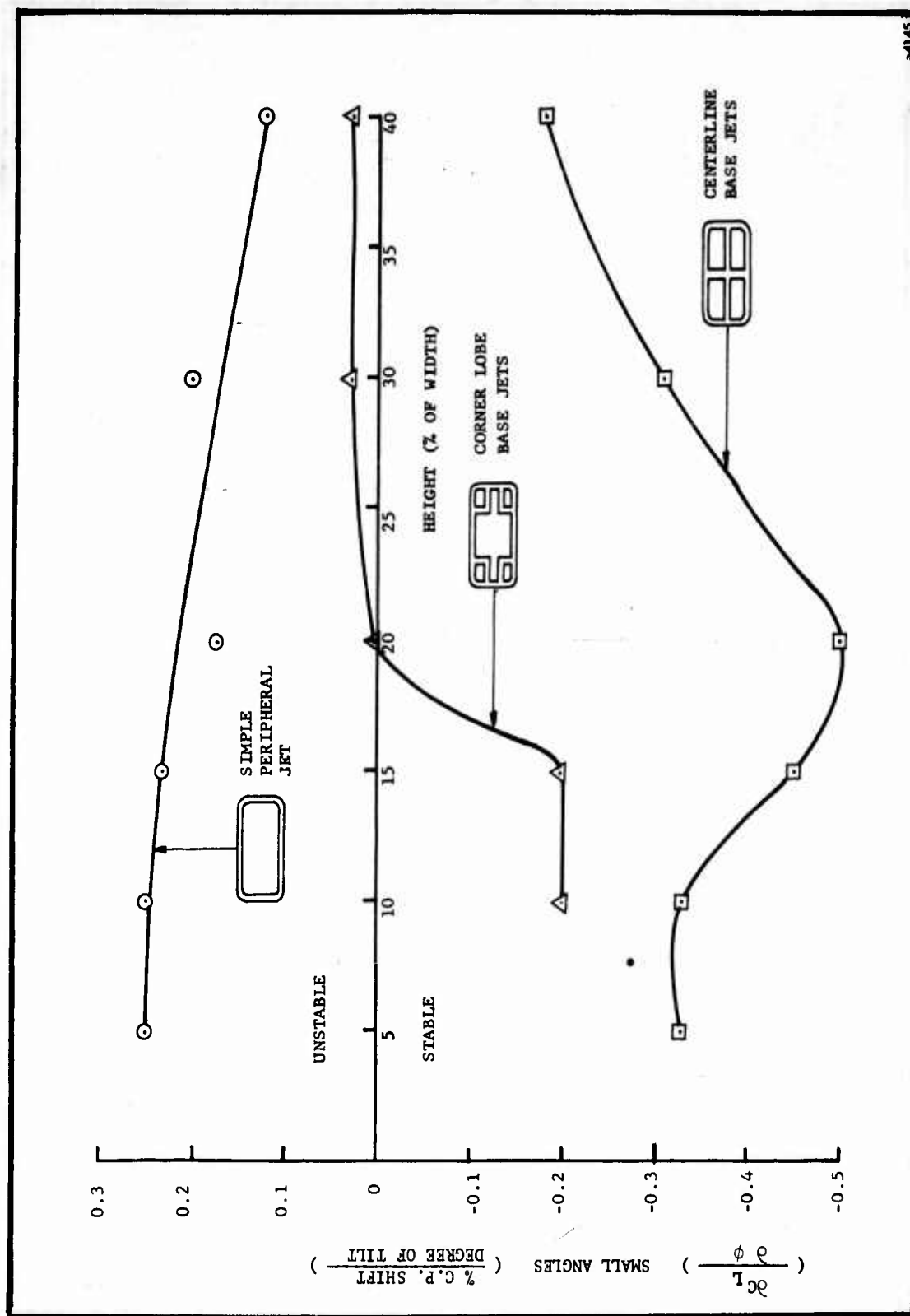


FIGURE 2-20. STATIC LATERAL HOVERING STABILITY (INTRAVENTS)

•2.5.1.1.3 Altitude

All free flight models and full-scale machines tested to date have demonstrated static heave stability at operating height-to-diameter ratios up to at least 0.15. Figure 2-21 (based on Reference 15) shows the stability of two typical circular configurations with different jet efflux angles.

•2.5.1.2 Dynamic Stability

The equations of motion for the air-cushion vehicle are complex and as yet inadequately defined. The most comprehensive dynamics analysis published, References 20 and 21, is described by the author as being primarily of a qualitative usefulness, and does not consider possible interactions between the internal flow system and the jets. Extensive systematic experimental programs are required to establish the relative importance of the various parameters in the equations of motion. AiResearch and Grumman are presently comparing dynamic model test data with the theoretical presentations of References 22 and 23, respectively.

There is at present almost no information available on damping derivatives. Figure 2-22 from Reference 15 shows that the damping in heave may decrease rapidly with increasing height. However, the model tested was very small. Stanton-Jones mentioned this general lack of information in Reference 19 and indicated that the static derivatives, together with the experimentally measured response of a dynamically similar model, were used to solve for the unknown damping. The approximations normal in aircraft stability work should not be taken for granted in air-cushion vehicle applications until data are available to verify them. More study, both theoretical and experimental is required.

2.5.2 Stability in Forward Motion

2.5.2.1 Static Stability

Forward motion alters the static stability of a vehicle in several ways. The static pressure distribution around the periphery of the vehicle affects the peripheral jet geometry and hence the base pressure distribution. Aerodynamic forces on the vehicle upper surfaces will probably cause significant shifts in the vehicle center of pressure. Large forces may be encountered in the fan inlet ducting because of the large quantities of air required.

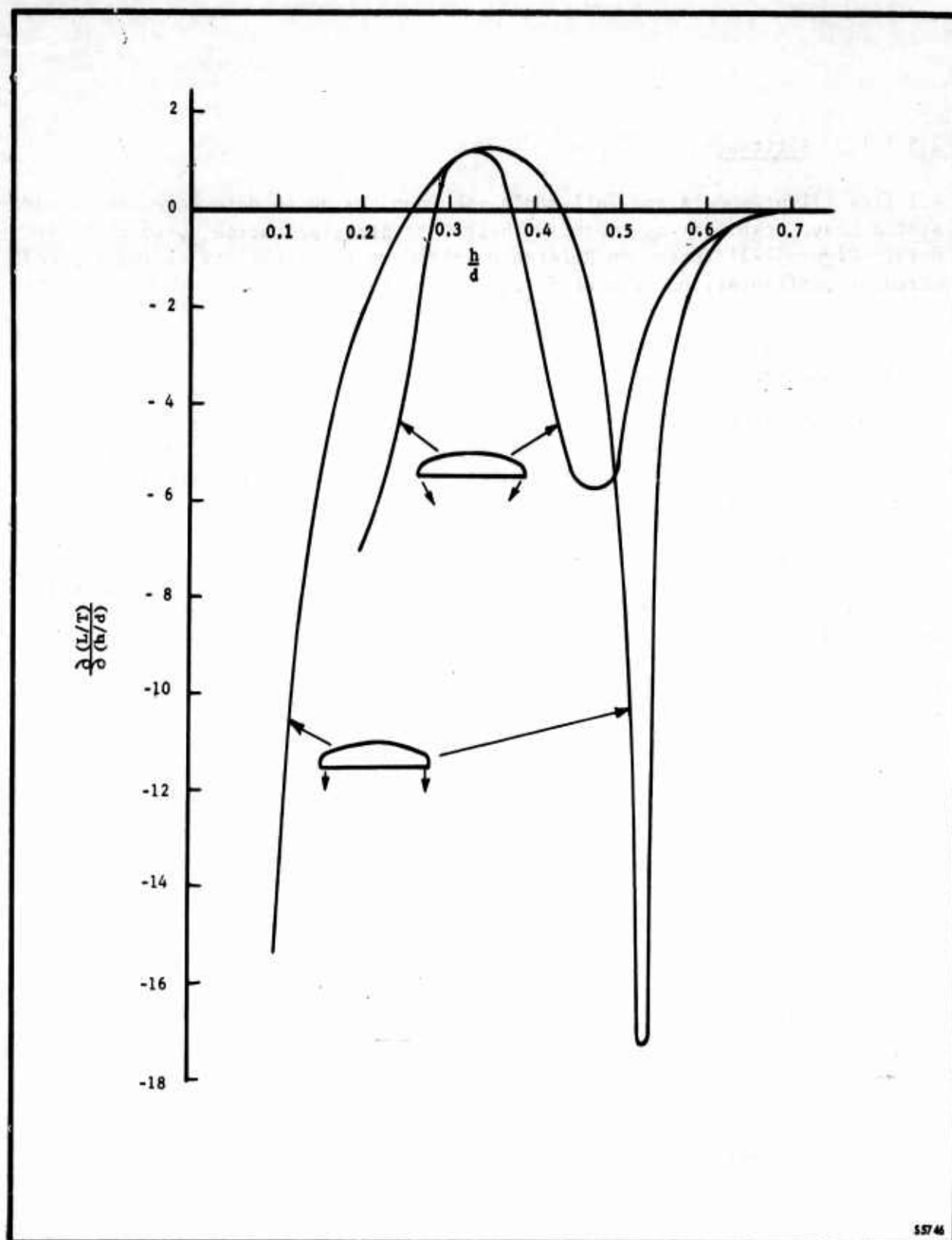
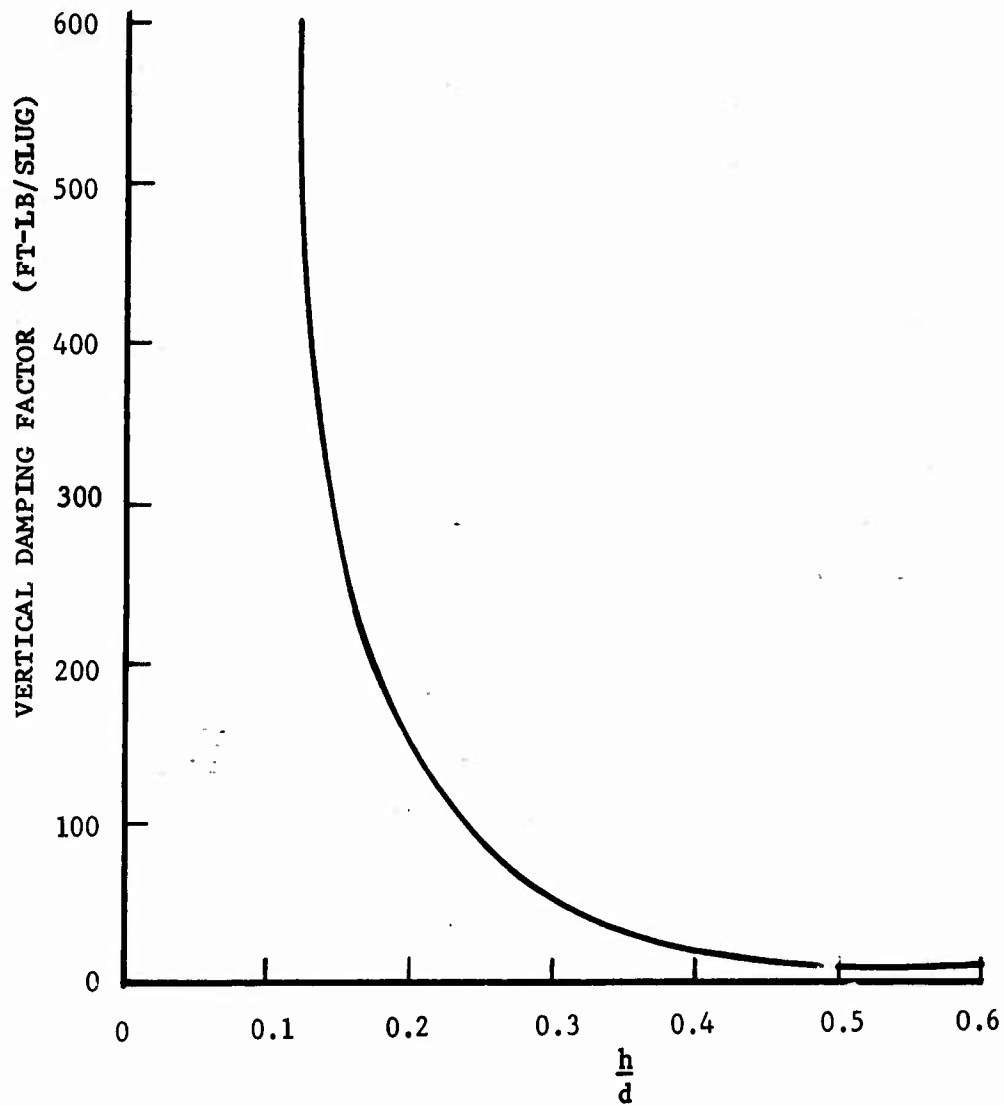


FIGURE 2-21. STATIC HEAVE STABILITY - SIMPLE PERIPHERAL JET (BASED ON REFERENCE 15)

NOTE: PERIPHERAL JET WITH
CIRCULAR BASE

FROM SMALL SCALE MODEL
TEST (MODEL SIZE NOT
SPECIFIED)



S5747

FIGURE 2-22. DAMPING IN HEAVE (REFERENCE 15)

2.5.2.1.1 Pitch and Roll

Air-cushion models tested to date (References 15, 16, 17, and 24) have demonstrated a decrease in static longitudinal stability and a change in trim with increase in forward speed caused by external aerodynamics and a shift in cushion center of pressure. Figure 2-23, taken from Reference 17, is typical. It is unlikely that the center-of-gravity location can be designed far enough forward to help, since there is insufficient longitudinal trim to permit level hovering. A large amount of intraventing may alleviate this situation. It may be necessary to employ an aerodynamic tail surface to counteract the forward movement of the center of pressure with increasing airspeed. The tail surface design may require development, since it must operate in a flow field somewhat different from aircraft practice. Another possible solution is described in Section 6.1.

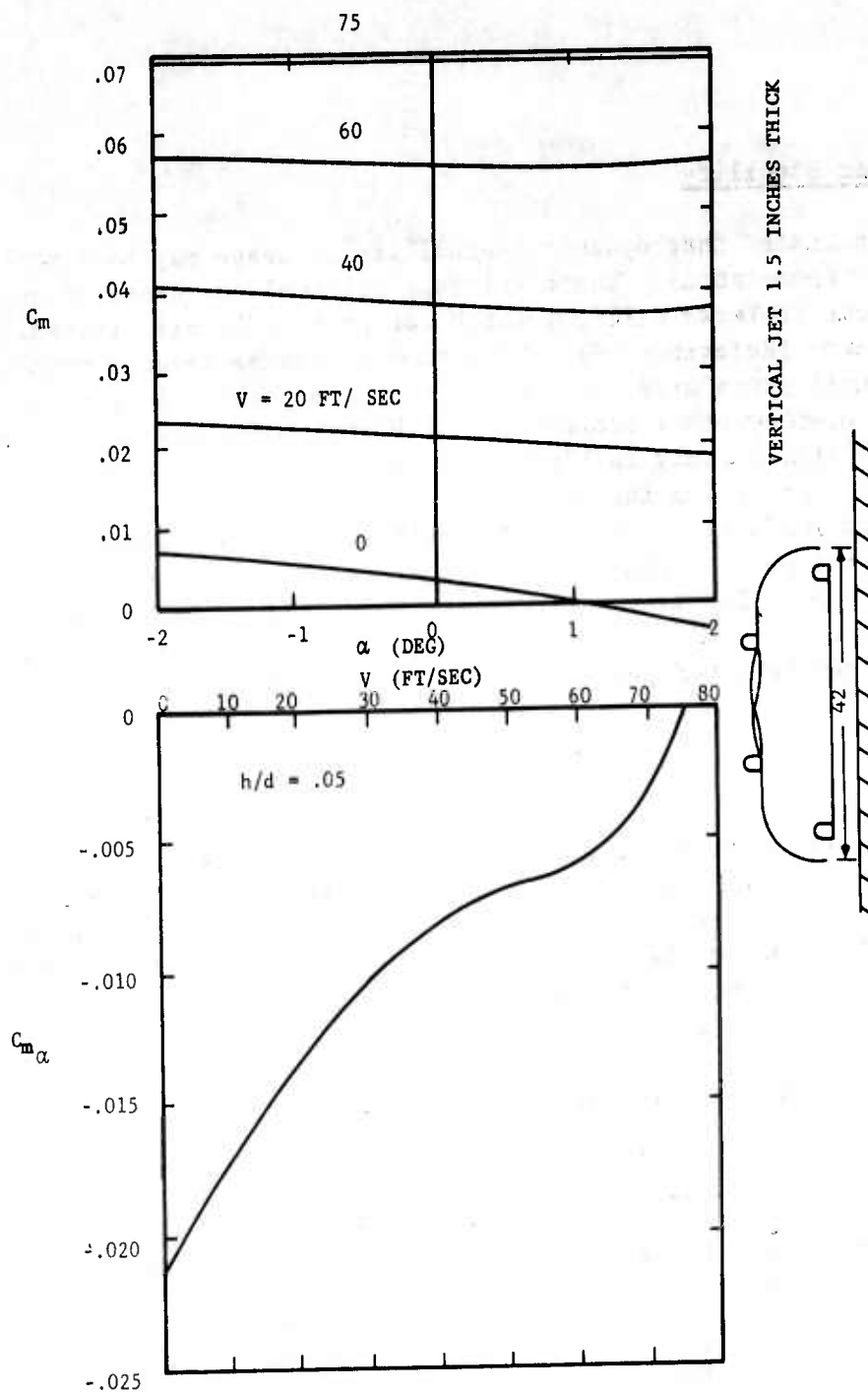
The flow patterns which affect lateral stability are transverse to the flight direction and nominally symmetrical about the longitudinal center-line. Therefore, speed-induced changes in lateral stability would not be expected to be as large as in pitch, where fore and aft symmetry of flow is modified by speed. Also, the external airload should be relatively insensitive to roll angle. Work presently under way at David Taylor Model Basin indicates that static lateral stability is insensitive to air speed at a height equal to 5 percent of the vehicle width.

2.5.2.1.2 Yaw

The directional stability problem of the air-cushion vehicle requires serious study. Vehicle shapes with low fineness ratio are inherently unstable in yaw under forward flight conditions. In addition, the practical demands of vehicle design often dictate placing the centroid of the air intakes forward of the vehicle center of gravity. Air inlets ahead of the center of gravity can produce an additional large destabilizing moment, and the size of vertical tail required to neutralize these effects may become impractical. Air inlets or propellers aft of the center of gravity are stabilizing; the magnitude of the effect depends on their size. A typical complete air-cushion model had an apparent center of pressure in yaw which was 17 percent of the vehicle length ahead of the nose of the model (Reference 24).

2.5.2.1.3 Altitude

Present information shows little effect of forward motion on static heave stability.



S4147

FIGURE 2-23. EFFECT OF FORWARD SPEED ON PITCHING MOMENT AND STABILITY
(REFERENCE 17)

2.5.2.2 Dynamic Stability

Present data indicate that dynamic instability in heave may be a problem under special circumstances. There exists a critical frequency of encounter with wave systems in forward flight which can produce dynamic instability in pitch and heave (Reference 19). This problem can be reduced through proper operational procedures. At the present time, there is perhaps some question as to whether other troublesome stability modes may also be encountered. Analytical study is hindered by the effects of the ground and forward speed in increasing the number of important derivatives; the effect of the ground in producing non-linearity (including slope reversal) in these derivatives; and the general absence of reliable values for the important derivatives. The flow patterns are sufficiently complex so that analytical prediction of derivatives is also unreliable. General stability prediction is therefore not possible at the present time.

2.5.3 Control

Tentative stability, control, and handling criteria for air-cushion vehicles have been proposed in Reference 25. These criteria appear, in general, to be realistic and are based on aircraft and helicopter concepts (but not standards). Since control data for peripheral jet vehicles are virtually non-existent, Aeronutronic instituted a hovering control program. The following methods were individually investigated:

- a. Differential jet throttling
- b. Differential jet width
- c. Differential jet angle
- d. Differential jet angle combined with differential jet width

Experiments were carried out at two heights (approximately 10 and 15 percent of the vehicle length). The model had a peripheral jet only, and was rectangular with a length-to-width ratio of 2. The results presented in Figure 2-24 reveal:

- a. Jet width control is superior to the other schemes. Thinning the jet width on one end of the vehicle to 30 percent of the value at the other end shifts the center of pressure 4 percent of the vehicle length.

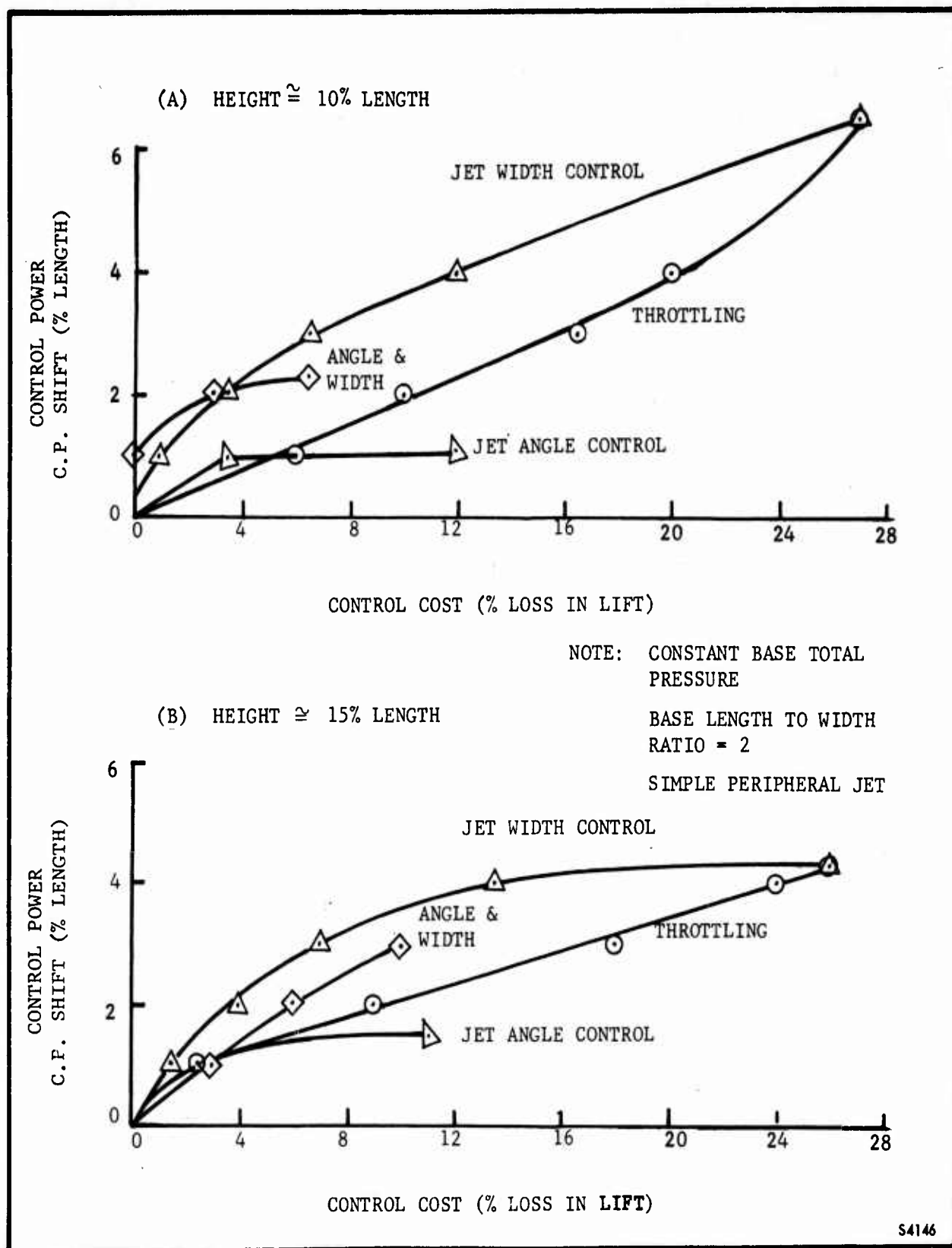


FIGURE 2-24 COMPARISON OF POWER AND COST OF FOUR LONGITUDINAL CONTROL SCHEMES

- b. If jet throttling is used the losses in lift are 6 to 8 percent higher than with the jet width control for the same center of pressure shift.
- c. Jet angle control was the poorest method investigated. For a practical range of control deflections the center of pressure shift was limited to 1 percent of the length.
- d. Combining jet angle control with jet width control leads to disappointing results. The same center of pressure shift was obtained with only slightly less jet width differential than for the case where the jet angle was fixed. The shift was obtained at a slightly higher loss in lift than for the case where jet angle was fixed.
- e. Jet width control not only produced the strongest control action at the lowest cost in lift loss, but was also most nearly linear in action and most nearly independent of angle of pitch.

The above model was neutrally stable at the lower height and unstable at the higher height. A base segmenting jet was then added at the transverse centerline of the model. The model was then stable at both heights, but the control effectiveness was improved only slightly. (The center of pressure shift was increased by less than 1 percent of the vehicle length.)

At a very minimum, an air-cushion vehicle must be able to trim itself to a horizontal attitude. The degree of control power will dictate the maximum permissible deviation of the center of gravity from the design location. From the foregoing it would appear that deviations of up to ± 4 percent of the length can be trimmed. This would amount to a total travel of 4 feet on a 50-foot vehicle and would leave little margin for control or emergency trim. It appears that differential control of the peripheral jet might be adequate for trim purposes.

Another possible use of the peripheral jet control would be as a stabilizer for a vehicle which has a slight inherent instability. The variable jet width tests were conducted first at a height of approximately 10 percent of the vehicle length, where the vehicle was neutrally stable and the control was adequate for stabilization purposes. A second series of tests was

conducted at a height of approximately 15 percent of the vehicle length, where a strong degree of inherent static instability existed. When the tilt angle exceeded 60 percent of the touchdown angle, the control was not strong enough to overcome the divergent moment. For this height, the variable jet should probably be augmented by intraventing.

2.6 OPERATIONAL PROBLEMS

Most of the problems associated with jet impingement on the ground are not much closer to solution now than when Publication U-926 was released. A substantial effort is required towards better defining the jet impingement - induced problems of air-cushion vehicles before any concerted effort may be put forth towards solving the problems. VTOL downwash research will yield part of the answers required in air-cushion technology, but because of some fundamental differences in operating environment additional work will be required. Some basic differences between air-cushion vehicles and VTOL aircraft are:

- a. Ground pressures are substantially higher for an air-cushion vehicle.
- b. Jet velocities are much higher for an air-cushion vehicle.
- c. The air-cushion vehicle must continuously operate in an environment that is transient for a VTOL aircraft.
- d. Deflectors, of demonstrable effectiveness on air-cushion vehicles, are probably not practical for VTOL aircraft.

VTOL research, then, is of distinct usefulness in the air-cushion field, but leaves many important questions unanswered.

Considerable work is being done in the VTOL field regarding erosion from downwash impingement (Reference 26), but as yet no experimentally verified conclusions have been reached. The most promise for air-cushion vehicle operation lies in the field of deflectors rather than soil stabilizing devices. Deflection appears especially promising in overwater applications.

The problem of propeller - blade damage caused by foreign-object ingestion was discussed in Publication U-926. Reference 27 describes some of the work done to alleviate propeller damage by using nickel plating. Two aluminum propellers, one nickel-plated and the other unplated, were subjected to identical water-spray conditions. The unplated blade was severely eroded, while the plated blade showed very little damage. This demonstrates that even if ingestion remains a problem for air-cushion vehicles, there are proven means for alleviating the damage.

2.7 OTHER CONSIDERATIONS

2.7.1 Structural

A large-scale study of structures for air-cushion vehicles has recently been completed (Reference 28). Preliminary designs were completed for several vehicles, each intended to fulfill a different operational requirement. Conclusions reached were:

- a. Steel structures weigh less than aluminum (at least for an amphibious assault vehicle), and both weigh less than wood. For any specific mission, vehicle cost varies inversely with structural weight.
- b. The ratio of structural-to-gross weight will be near the range 0.11 to 0.18 for the following vehicle types: amphibious assault, anti-submarine warfare and cargo lighter. (All vehicles considered had payloads of 10,000 to 40,000 pounds.)
- c. The ratio of structural weight to planform area for an amphibious assault vehicle will be about 3 to 5 pounds per square foot, depending upon the structural material. This ratio will increase to about 6 for an aluminum cargo lighter.

Although the results of the studies discussed in Reference 27 are valuable, a more generalized study is needed to relate the ratio of structure-to-gross weight to mission-defined parameters, such as payload, range, planform, cargo floor loadings, and external loadings.

2.7.2 Power Supply System

Unchanged.

2.8 CONCLUSIONS

2.8.1 Five Components of Power Requirements

Unchanged.

2.8.2 Relative Importance of Components

Unchanged.

2.8.3 Component Importance for Army Missions

Unchanged.

2.8.4 Stability and Control Power Requirements

Recent work has indicated that annular jet vehicles can be made stable throughout most of the range of heights of interest for Army utilization. The power cost for such stability fixes has not yet been estimated. However, work currently in progress should soon make it possible to estimate power cost.

Control of annular jet pitch and roll only by means of differential jet control appears adequate for cg position variations of ± 4 percent of vehicle length or width. Power cost of such control will vary between 10 and 30 percent of total vehicle lift power.

2.8.5 Structural and Power Plant Weight

Unchanged.

2.8.6 Mission Capabilities

Unchanged.

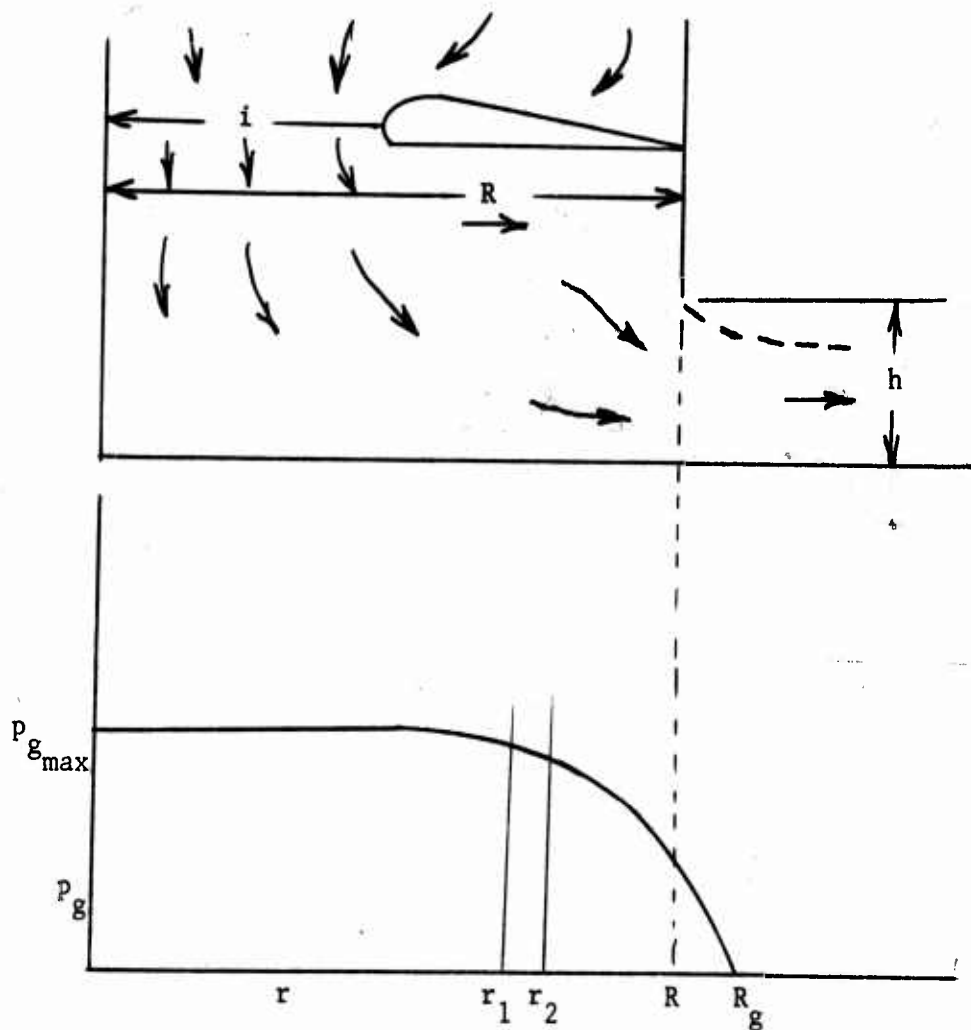
3.0 PLENUM CHAMBER

3.1 THEORIES FOR POWER REQUIRED - HOVERING

Unchanged.

3.2 TEST DATA

There are still no experimental data available for the evaluation of η_p (base pressure to base total pressure ratio) or K (total pressure loss from diffuser to plenum chamber). However, Reference 29 contains information which permits an experimental evaluation of G versus $h \ell / S$ in spite of the lack of η_p and K . The sketch below shows the test setup, and a typical variation in pressure measured along the ground plane.



The value of $p_{g_{\max}}$ is actually air flow total pressure, since the air stagnates against the ground board near the simulated centerline. The integration of ground plane pressure yields vehicle lift.

$$L = \int_0^R p_g \pi r dr \quad \text{assuming a circular vehicle.}$$

Since there is no analytical equation for the variation of p_g with r , it is necessary to evaluate the integral graphically.

$$L = \sum_g p_g \pi (r_2^2 - r_1^2)$$

This relation may be expressed in terms of $p_{g_{\max}}$, R , and pressure and area ratios.

$$\begin{aligned} L &= \sum_g \left(\frac{p_g}{p_{g_{\max}}} \right) p_{g_{\max}} \pi R^2 \left(\frac{r_2^2 - r_1^2}{R^2} \right) \\ &= p_{g_{\max}} \sum_g \frac{p_g}{p_{g_{\max}}} \left(\frac{r_2^2 - r_1^2}{R^2} \right) \end{aligned}$$

The lift is seen to be equal to the total pressure applied over the planform area corrected by the sum of the product of the two dimensionless ratios.

The power required

$$\begin{aligned} P &= p_{g_{\max}} Q = p_{g_{\max}} S_x V_{j_0} \\ &= p_{g_{\max}} h \ell \bar{C} \sqrt{\frac{2}{\rho}} \sqrt{p_{g_{\max}}} \\ &= h \ell \bar{C} \sqrt{\frac{2}{\rho}} (p_{g_{\max}})^{3/2} \\ &= h \ell \bar{C} \sqrt{\frac{2}{\rho}} \left(\frac{L}{S} \right)^{3/2} \\ &= \left[\sum_g \frac{p_g}{p_{g_{\max}}} \left(\frac{r_2^2 - r_1^2}{R^2} \right) \right]^{3/2} \end{aligned}$$

By simple manipulation this may be written as

$$P = \frac{L}{2\sqrt{p}} \sqrt{\frac{L}{S}} \left[\frac{2\sqrt{2} C \frac{h\ell}{S}}{\left[\sum_{S_g} \frac{p_g}{p_{g_{\max}}} \left(\frac{r_2^2 - r_1^2}{R^2} \right) \right]} \right]^{3/2}$$

$$= P_{1\infty} G$$

Thus, we have a relation for G based on an integration of ground pressure. Sufficient data were presented in Reference 29 to evaluate G for two values of the ratio $\frac{1}{K}$ or $\frac{S_d}{S}$. They are $\frac{S_d}{S} = 0.25$ and 1.0 rather than 0.25 and 0.5 as in Publication U-926. G versus $\frac{h\ell}{S}$ is plotted in Figure 3-1 as heavy lines. Also plotted is G as evaluated by the two theories described in Publication U-926 for the same values of $\frac{S_d}{S}$. The theories are presented here for convenience, without derivation.

Hiller theory

$$G = \frac{2\sqrt{2} C \frac{h\ell}{S} \left[1 + \frac{K C^2 \left(\frac{h\ell}{S} \right)^2}{\left(\frac{S_d}{S} \right)^2} \right]}{\left[1 + C^2 \left(\frac{h\ell}{S} \right)^2 \right]^{3/2}}$$

Aeronutronic theory

$$G = \frac{2\sqrt{2} C \frac{h\ell}{S} \left[1 + \frac{K C^2 \left(\frac{h\ell}{S} \right)^2}{\left(\frac{S_d}{S} \right)^2} \right]}{\left[\eta_p + \frac{S_d}{S} (1 - \eta_p) + \frac{C^2 (K + 1) \left(\frac{h\ell}{S} \right)^2}{S_d/S} \right]^{3/2}}$$

In both relations

C = discharge coefficient ≈ 0.6

$$K = \left(1 - \frac{S_d}{S} \right)^2$$

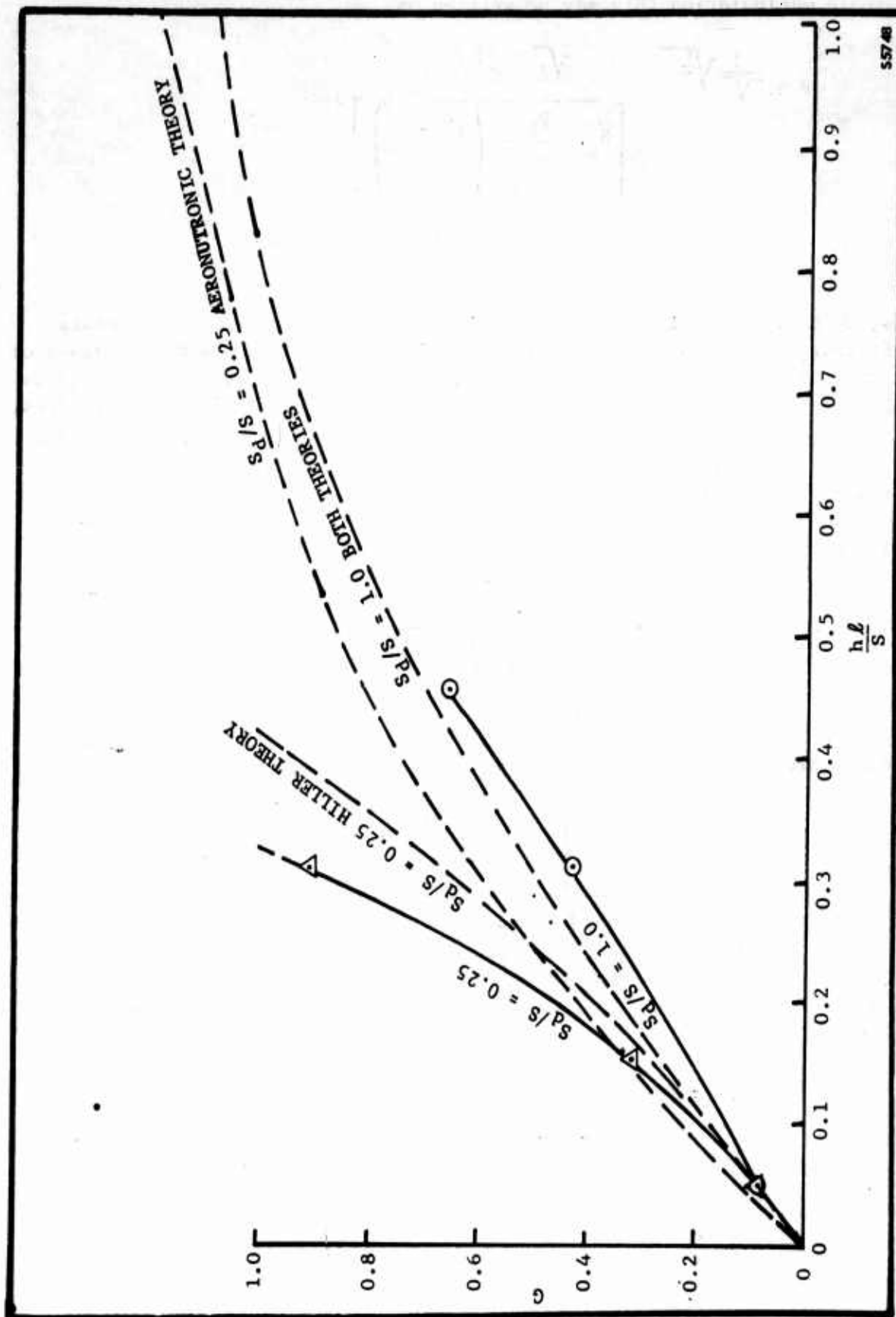


FIGURE 3-1. PLENUM CHAMBER HOVERING GROUND EFFECT POWER FACTOR
- EXPERIMENT COMPARED TO THEORY

In the Aeronutronic relation

$$\eta_p = 0.8$$

The two theories differ only in the denominator. At $\frac{S_d}{S} = 1.0$ the two relations become identical. As $\frac{S_d}{S}$ decreases, the curve for G for both theories moves up. From the Aeronutronic theory, G increases faster at low $\frac{h\ell}{S}$ than from the Hiller theory, and vice versa at high $\frac{h\ell}{S}$.

For $\frac{S_d}{S} = 0.25$ the Aeronutronic theory predicts G fairly well at $\frac{\eta_1}{S} \leq 0.15$, but is very optimistic as $\frac{h\ell}{S}$ increases. The Hiller theory estimates G about 20 to 30 percent low over the range of $\frac{h\ell}{S}$ covered by the data. It should be remembered that K is not accurately known in either theory.

For $\frac{S_d}{S} = 1.0$, either theory is adequate over the range of $\frac{h\ell}{S}$ covered by data. Both theories estimate G high by about 20 percent.

From the meager data presented here, it appears that the Hiller theory more accurately depicts the general trend of G at $\frac{S_d}{S} < 1.0$. However, it should be remembered that the factor η_p in the Aeronutronic theory is an unknown quantity. In the curves shown, η_p was assumed constant, where it may actually be varying. Such variations may alter the shape of the Aeronutronic theory curve considerably.

Figure 3-2 compares plenum chamber experimental G for $\frac{S_d}{S} = 1.0$ with annular jet experimental G . The two concepts have competitive power requirements only at low $\frac{h\ell}{S}$.

3.3 INSTALLED POWER REQUIRED - HOVERING

Unchanged.

3.4 FORWARD MOTION

Unchanged.

3.5 STABILITY AND CONTROL

Unchanged

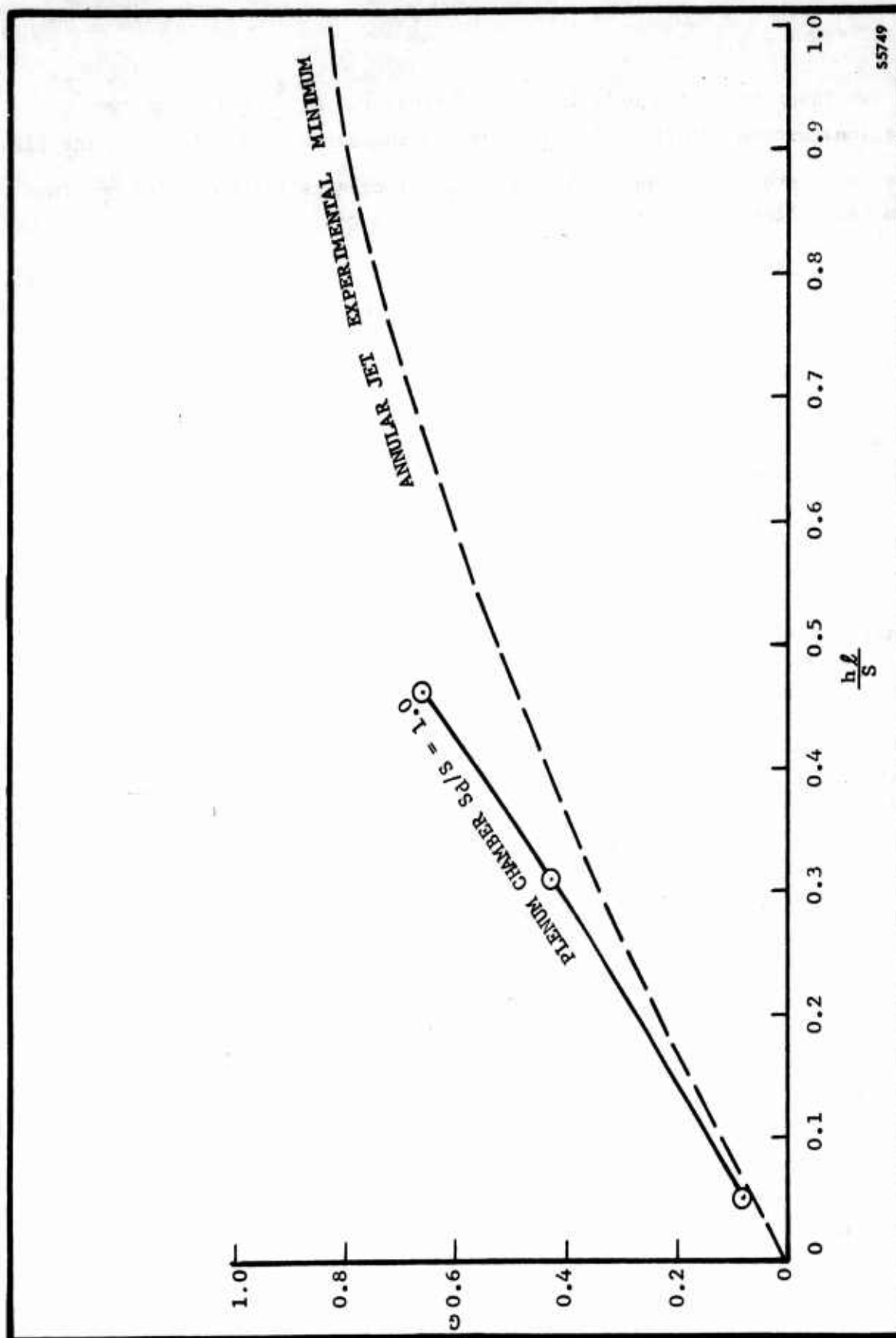


FIGURE 3-2. PLENUM CHAMBER G COMPARED TO ANNULAR JET MINIMUM G

S5749

3.6 OPERATIONAL PROBLEMS

Unchanged.

3.7 OTHER CONSIDERATIONS

Unchanged.

3.8 CONCLUSION

3.8.1 Power Required

The flow field within a plenum chamber is still very vague. None of the parameters of the two theories have been determined experimentally. The Hiller theory, at $\frac{S_d}{S} < 1.0$, appears to predict general trends of G fairly well, but the accuracy is rather poor, based on the assumption regarding loss factor made herein. It may be that when the K term is adequately defined, the theory will serve well. The same may be said of the factor η_p and the Aeronutronic theory.

3.8.2 Stability and Control

Unchanged.

3.8.3 Operational Problems

Unchanged.

4.0 HILLER DIFFUSER

4.1 POWER REQUIRED

4.1.1 Diffuser-Recirculation Concept

The paragraph beginning at the bottom of page 4-4 of Publication U-926 contains some inappropriate assumptions. The paragraph will be repeated here for convenient reference and then corrected later.

"At this point it is advisable to point out the inherent restriction in the original assumptions of the theory. The prime intent of the theory was to develop a concept which used over and over again the same air; i. e., no air escapes from the vehicle. Continuity considerations, therefore, restrict

$$S_j \equiv S_1 \text{ since } p_j = p_1 (\Rightarrow V_j = V_1)$$

This means that for a given vehicle (fixed S_j) there is only one height at which the vehicle may operate at equilibrium. Therefore, in order to operate at different heights a vehicle must be provided with the capability of varying S_j . Since S_j is varying then the areas of the rest of the duct system must also vary. Inherent in this requirement is the necessity for the capability to vary the quantity of air that is being circulated. It is possible that this requirement will cause such complexity as to preclude the use of such vehicles."

The paragraph should read as follows:

At this point it is advisable to point out an inherent requirement in the original assumptions of the theory. The prime intent of the theory was to develop a concept which used the same air over and over again; i. e., no air escapes from the vehicle. Continuity considerations, therefore, restrict

$$S_j \equiv S_1 \text{ since } p_j = p_1 (\Rightarrow V_j = V_1)$$

This means that for a given duct geometry (S_j) there is only one height at which the vehicle may operate at equilibrium. Therefore in order to operate at varying heights (S_1) a vehicle must be provided with the capability of varying S_j . This might be accomplished by hinging the outer wall of the duct so that the duct may vary from its design geometry to either a converging nozzle (for lower heights than design) or a diverging nozzle (for higher heights). The volume flow will vary approximately in response to height. This means that there is an attendant change in power required and that fan efficiency will decrease because of the departure from design operating total pressure rise and volume flow. The variable geometry of the lower portion of

the outer wall should be no more complex than the variable jet geometries proposed for annular jet type air-cushion vehicles.

The rest of this section is unchanged from that of Publication U-926.

4.1.2 Diffuser-Plenum Concept

Section 4.1.2 of Publication U-926 derived an expression for G_{fan} for the diffuser plenum concept. From page 4-8 the relation is:

$$G_{fan} = \frac{C \left(\frac{hl}{S} - \frac{S_j}{S} \right) \left(1 - K_{j-2} \right)^{1/2} 2\sqrt{2}}{\left[1 - \left(\frac{S_j}{S_d} \right)^2 - K_{j-2} \right]^{3/2}}$$

Publication U-926 then went on to make an arbitrary assumption as to S_j (jet area) in terms of hl (height times perimeter). This assumption was superfluous, since S_j may be expressed analytically in terms of hl . The inflow of air through station j is exhausted out the periphery of the vehicle, less, of course, the inlet area S_j .

$$S_j V_j = V_{j_o} (hl - S_j) C$$

where V_{j_o} is the velocity attained by expanding base total pressure (from the plenum) to ambient pressure.

$$= \sqrt{\frac{2}{\rho}} \sqrt{P_{t_b}}$$

C = discharge coefficient

$$S_j (V_j + V_{j_o} C) = V_{j_o} Chl$$

$$S_j = \frac{V_{j_o} Chl}{V_j + V_{j_o} C} = \frac{Chl}{\frac{V_j}{V_{j_o}} + C}$$

$$v_j = \sqrt{\frac{2}{\rho}} \sqrt{q_j}$$

$$v_{j_0} = \sqrt{\frac{2}{\rho}} \sqrt{p_{t_b}} = \sqrt{\frac{2}{\rho}} \sqrt{p_{t_f} - (K_s + K_g + K_d) q_j}$$

$$= \sqrt{\frac{2}{\rho}} \sqrt{q_j - q_j K_{j-2}}$$

$$= \sqrt{\frac{2}{\rho}} \sqrt{q_j} \sqrt{1 - K_{j-2}}$$

$$\therefore \frac{v_j}{v_{j_0}} = \sqrt{\frac{1}{1 - K_{j-2}}}$$

$$\therefore S_j = \frac{Ch\ell}{\left(\frac{1}{\sqrt{1 - K_{j-2}}} + C \right)}$$

Substitute for S_j in G_{fan}

$$G_{fan} = \frac{\frac{Ch\ell}{S} \left[1 - \frac{C (1 - K_{j-2})^{1/2}}{1 + C (1 - K_{j-2})^{1/2}} \right] (1 - K_{j-2})^{1/2} 2\sqrt{2}}{\left[1 - \left(\frac{S_j}{S_d} \right)^2 - K_{j-2} \right]^{3/2}}$$

The same values of K_{j-2} , C and $\frac{S_j}{S_d}$ will be used here as in Publication U-926 for estimating G_{fan} as a function of $\frac{h\ell}{S}$.

$$K_{j-2} = .285$$

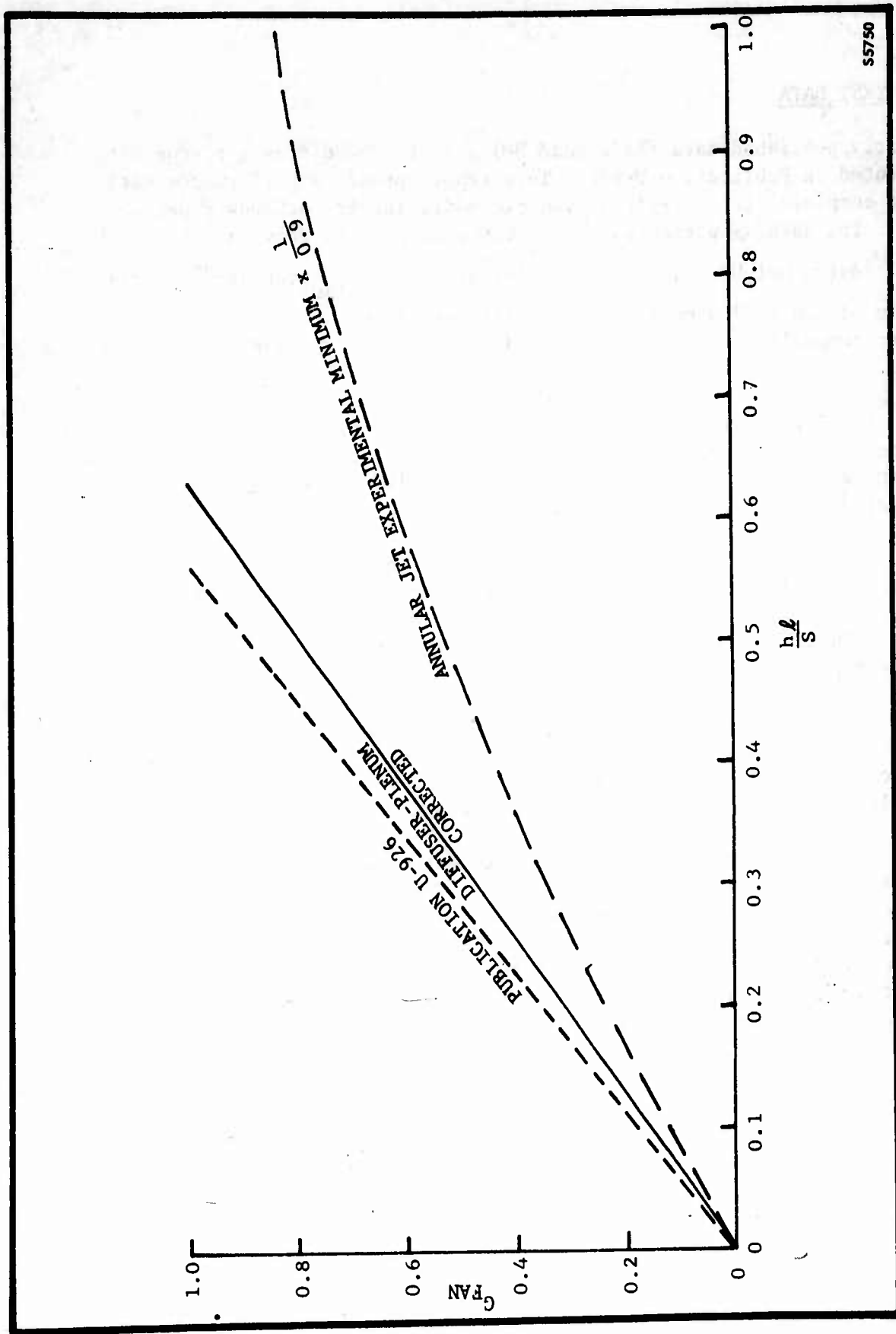
$$\frac{S_j}{S_d} = 0$$

$$C = 0.6$$

If these values are substituted into G_{fan} ,

$$G_{fan} = 1.58 \frac{h\ell}{S}$$

Figure 4-1 shows this curve as the solid line. The light broken line is the G_{fan} taken from Publication U-926 for comparison. The heavy broken line is the curve for annular jet G from Figure 2-1 of this report multiplied by 1/.9. Although the G_{fan} for the diffuser plenum has been reduced by the correction made here, the annular jet curve has been moved down even more by the use of the recently acquired data of Reference 2. As before, the diffuser plenum is competitive with the annular jet at low $\frac{h\ell}{S}$ but is inferior at higher $\frac{h\ell}{S}$.



S5750

FIGURE 4-1. DIFFUSER-PLENUM FAN GROUND EFFECT HOVERING POWER FACTOR

4.2 TEST DATA

Recently published data (Reference 30) adds to the diffuser plenum data presented in Publication U-926. This report presents performance data for a complete diffuser-plenum vehicle model in air horsepower per unit lift. The data is presented over a range of heights above and below the model design height. Since Figure 4-1 presents G_{fan} versus $\frac{h}{S}$ for a family of "rubber" annular jet and diffuser-plenum vehicles the only proper comparison to be made from model data is at the design $\frac{h}{S}$ of the model.

Figure 4-2 repeats the annular jet and diffuser-plenum curves of Figure 4-1 and shows one data point for the diffuser-plenum model at its design $\frac{h}{S}$ (0.08). The model data shows over 100 percent greater G than estimated from theory and loss factor data.

There are several reasons for this as indicated by personal correspondence with the author of Reference 30. The model trimmed out to a positive angle attack rather than zero angle on which the theory is based. In addition there were two stability fixes made to the model which affected performance. The outlet geometry was varied and the diffuser inlet was vented to atmospheric pressure. There is no accounting for these fixes in the theory. It should be remembered that the annular jet curve of Figure 4-2 includes no power requirements for stability fixes. It seems probable that the annular jet will incur power penalties for stability fixes, thus causing the annular jet G_{fan} curve to rise.

The theory makes no attempt to estimate the effect of the three dimensional radial flow in the diffuser. The air is flowing two-dimensionally through the throat of the diffuser, but further down stream, the air must begin turning to flow out beneath the sides of the model. Similarly the flow in the plenum is turning in its outflow path. One effect of such action is to increase the effective diffusion angle. This may be great enough to cause separation and its attendant losses.

In addition, Gates believes scale effects are playing an appreciable part in the losses.

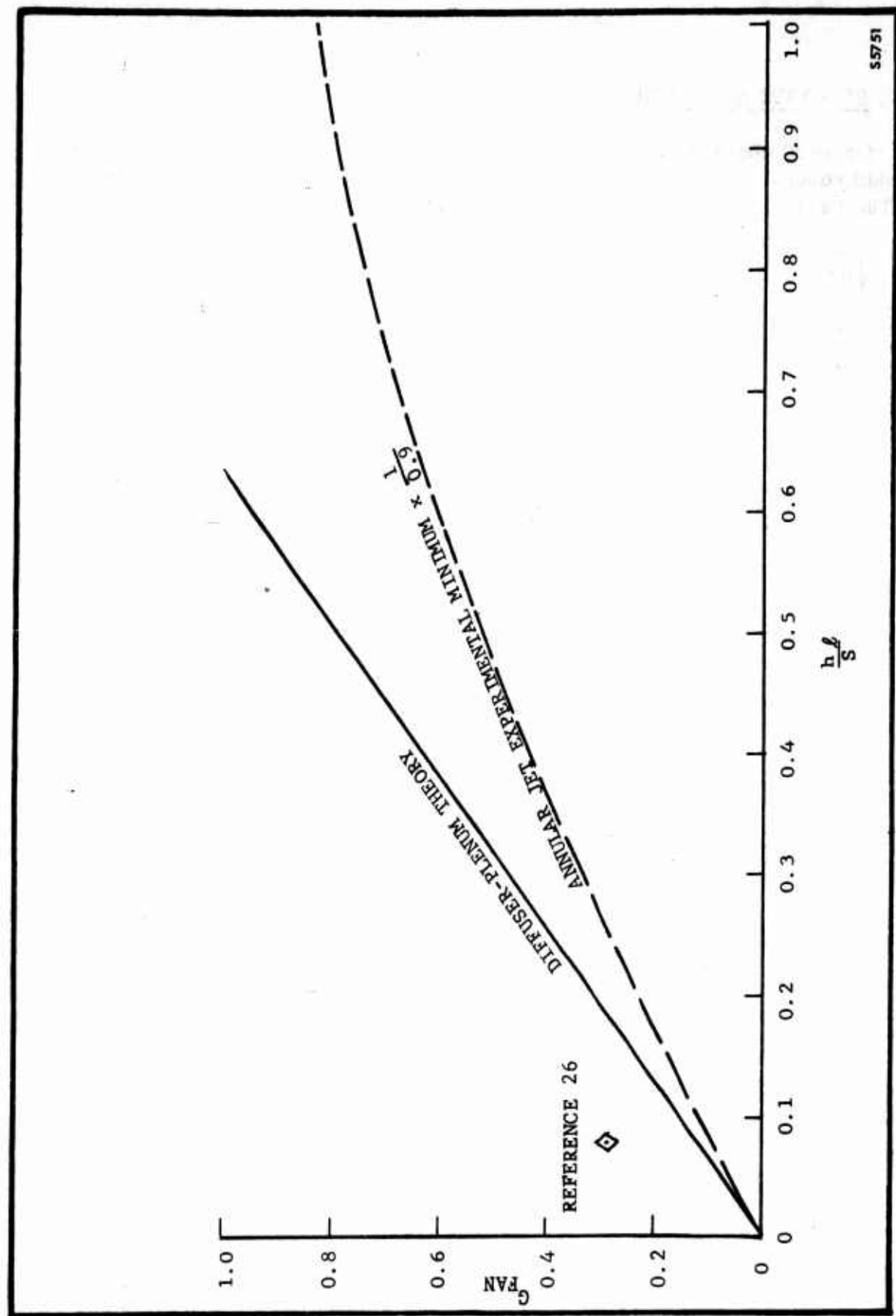


FIGURE 4-2. DIFFUSER-PLENUM DATA POINT COMPARED WITH THEORY AND ANNULAR JET

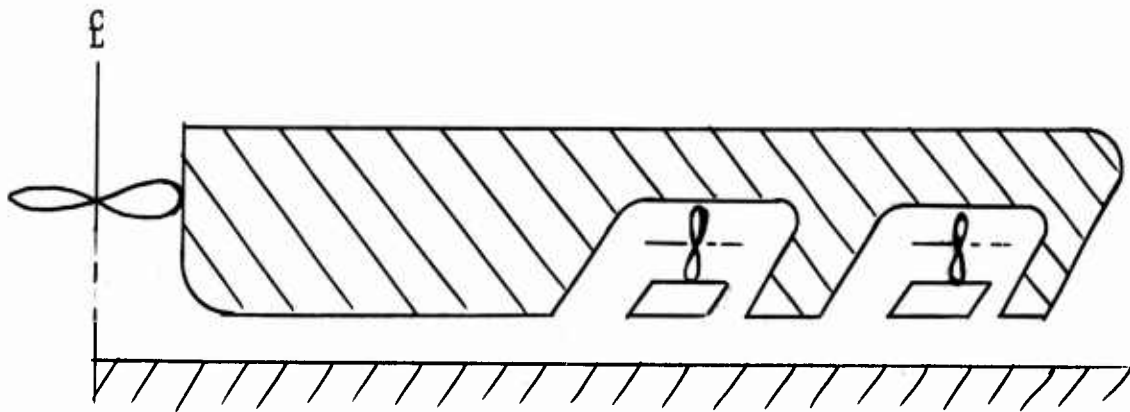
55751

4.5 STABILITY AND CONTROL

Reference 30 contains a small amount of stability data for the diffuser-plenum concept. As stated in Reference 30, there is no definable trend in the variation of $C_{m\dot{\alpha}}$ with model clearance height. Qualitatively, the model is stable in pitch throughout the range of α ($-1^\circ < \alpha < 4^\circ$) and $\frac{h\dot{\ell}}{S}$ ($\frac{h\dot{\ell}}{S} < 0.1$) covered in the tests. The model was also stable in the heave mode.

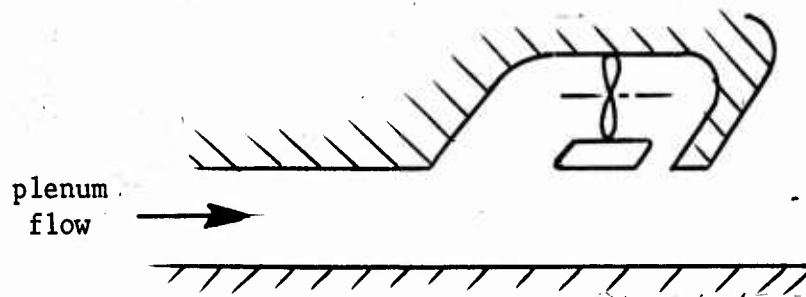
5.0 LABYRINTH SEAL

The labyrinth seal type air-cushion vehicle, as proposed by Weiland in Reference 31, is basically a plenum chamber with a peripheral air "seal". Air is compressed and supplied to the underside of the vehicle. Rather than allow the plenum air to immediately escape through a peripheral gap as from a plenum chamber, a series of "labyrinth seals" retards the plenum air as it flows outward. Each labyrinth seal is generally equipped with an auxiliary fan.

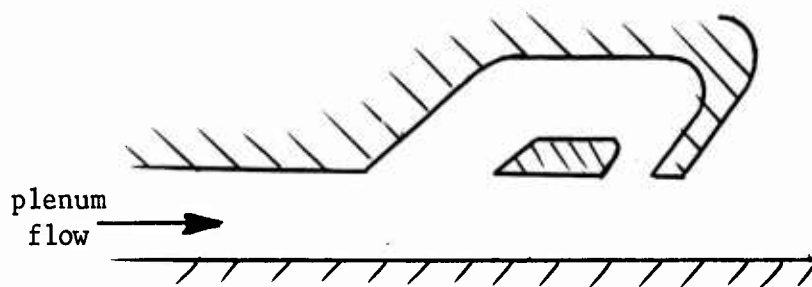


Weiland explains the labyrinth seal in general terms as a device for sealing by turbulent mixing. His description infers that the seal is effected either by a vortex which extends from the labyrinth passage into the plenum air flow path, or by an internal friction process somewhat analogous to the friction encountered by air flowing through a rough-walled duct.

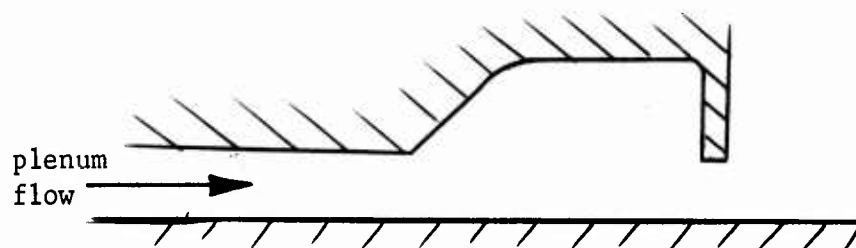
Three labyrinth configurations are described by Weiland. These are sketched below.



LABYRINTH CONFIGURATION A



LABYRINTH CONFIGURATION B



LABYRINTH CONFIGURATION C

In configuration A, the fan circulates plenum air through the labyrinth cavity. Weiland indicates that plenum air should be pumped in a clockwise direction in configuration A. Configuration B and C develop turbulence solely through natural mixing in and beneath the labyrinth cavity.

Qualitative experiments reported in Reference 32 compare several variations of configuration A with the labyrinth fan blowing in each direction and with the labyrinth fan off. The same test model was evaluated qualitatively as a recirculation type air-cushion vehicle by blocking off the plenum inlet. These experiments are discussed in Section 5.2.

5.1 POWER REQUIRED

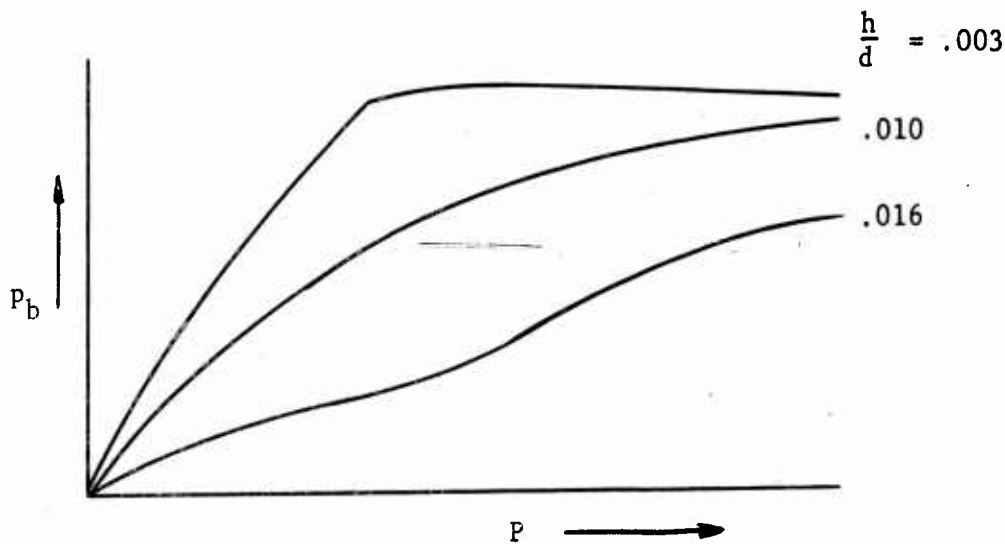
Unchanged.

5.2 TEST DATA

As stated in Publication U-926, data curves of Reference 31 are insufficiently detailed to offer a realistic comparison between the labyrinth seal and annular jet configurations.

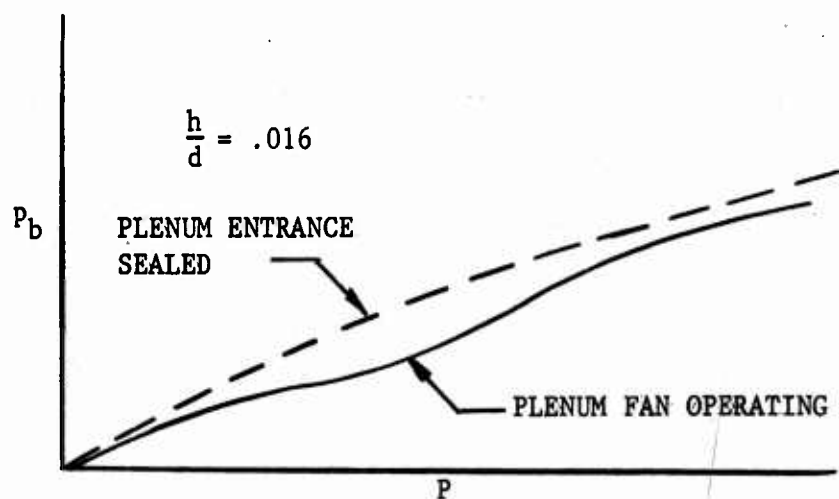
Unfortunately, according to Reference 32, recent experiments at Grumman were not sufficiently instrumented to produce reliable performance data. Moreover, the height-to-diameter ratios investigated were very low (maximum $h/d = 0.016$). The Grumman work does shed some light on labyrinth seal operation, and, as an extra benefit, shows that a recirculating jet type vehicle is probably more efficient.

Reference 32 describes tests of a two-dimensional labyrinth seal model. Several labyrinth configurations, including the reversing of the labyrinth fan direction, were investigated. Because of the instrumentation employed, only relative base pressure and fan power measurements could be made. The sketch below shows the effect of varying shaft power on base lift for a typical configuration. All configurations tend towards this pattern. To the left of the break, all power is input to the plenum fan. From the break towards the right, plenum power is held constant and labyrinth power is increased. It is apparent that the vehicle must reach a certain "critical" height before the labyrinth seals become effective.

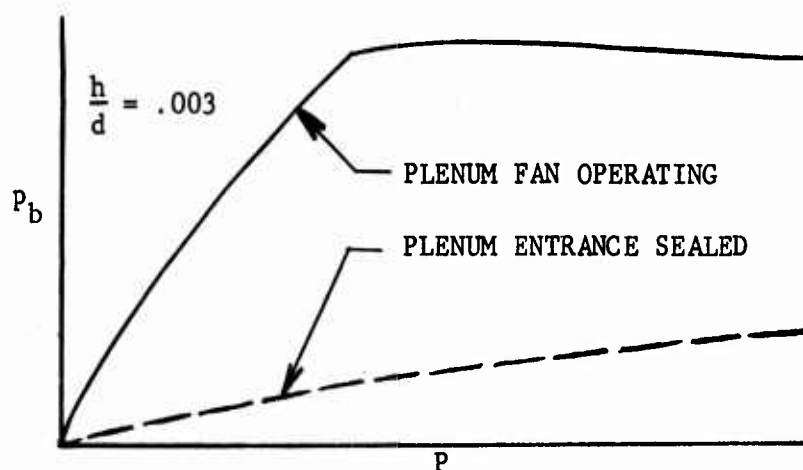


EFFECT OF SHAFT POWER ON BASE LIFT

The plenum inlet was blocked during several runs and the model was operated as a recirculation vehicle. The sketches below show the effect of sealing the plenum inlet at two base heights. It is interesting to note that at the greater height (which is really quite low), where the labyrinth concept appears most effective, the recirculation vehicle is superior in lifting capability.



COMPARISON OF
LABYRINTH SEAL AND
RECIRCULATION MODELS



It was concluded in Reference 32 that several labyrinth seal configurations show potential power savings over a plenum air-cushion vehicle. This conclusion was based on the assumption that when the labyrinth fans were unpowered, the models tested were at least as good as a plenum air-cushion model. It should be noted that tests were conducted at height-to-base-length ratios substantially under those required of a practical vehicle.



5.3 INSTALLED POWER REQUIREMENTS

Unchanged.

5.4 FORWARD MOTION

Unchanged.

5.5 STABILITY AND CONTROL

The tests of Reference 32 indicate that the labyrinth seal vehicle will be stable in heave up to the maximum height-to-diameter ratio tested, 0.016.

Some heave instability was exhibited by the recirculation configuration, but at such low height-to-diameter ratios that it is of little practical importance (h/d less than about 0.005 to 0.010, depending on labyrinth configuration, or t_e/h less than 0.5).

5.6 OPERATIONAL CONSIDERATIONS

Unchanged.

5.7 OTHER CONSIDERATIONS

Unchanged.

5.8 CONCLUSIONS

5.8.1 Power Required

Recent model tests (Reference 32) indicate that a recirculation vehicle would be more efficient than the labyrinth seal configuration, but that the labyrinth configuration is probably more efficient than the plenum air-cushion configuration. The highest height-to-base length ratio investigated was 0.016. No quantitative comparisons of either the labyrinth seal or recirculation configurations could be made with other air-cushion concepts because of insufficient test instrumentation.

5.8.2 Stability and Control

Heave stability appears satisfactory, but has not been investigated at height-to-base length ratios greater than 0.016.

5.8.3 Operational Problems

Unchanged.

6.0 RAM WING

Two recent papers, one theoretical and the other experimental, extend the state-of-the-art of the ram wing concept, and hence the high speed capabilities of other air-cushion vehicle concepts. These papers are discussed in Sections 6.1 and 6.2, and again in Section 6.5.

6.1 POWER REQUIRED

T. Strand has presented, in Reference 33, two lifting theories for a two-dimensional wing in ground effect. In Reference 34, Royce and Rethorst have extended Strand's second theory to describe a three-dimensional vehicle with side jets.

Strand's first theory is concerned with the lift and moment coefficients of a flat plate; hence, it is of somewhat limited interest.

Strand's second theory estimates lift and pitching moment coefficients for a two-dimensional "thick" airfoil with an arbitrary pressure distribution. This theory is based upon the distributed vortex and source concept, wherein the airfoil is replaced with a series of vortices (representing circulation, hence lift), and a series of sources and sinks (representing thickness). A second airfoil is located in such a manner that it is a mirror image, about the ground plane, of the first airfoil. The mathematical development has not been included in this report because of time and space limitations.

Assume that side jets or walls are put between a wing and the ground. Flow under the wing will become two-dimensional, while the flow over the wing remains three-dimensional in nature. As a result, induced drag is developed on the upper surface only. The theory of Reference 33 will facilitate lowering vehicle induced drag through the careful distribution of lift between the upper and lower vehicle surfaces. Moreover, profile drag may be reduced through the choice of pressure distributions that delay separation.

Royce and Rethorst have presented, in Reference 34, the fundamentals of a theory which describes the flow about a wing of finite span and with side jets, but with infinitesimal thickness. The theory has the same basis as the two-dimensional airfoil theory of Strand. As is usually the case with a mathematical treatment of three-dimensional flow problems, the equations which result must be solved by digital computers.

The distributed vortex and source theory for airfoils away from the ground has been well documented; when the new theories are correlated with test data from airfoils in ground effect, they too will be useful tools.

Two recent papers, one theoretical and the other experimental, extend the state of the art of the ram wing concept, and hence the high speed capabilities of other air-cushion vehicle concepts. These papers are discussed in Sections 6.1 and 6.2, and again in Section 6.5.

6.2 TEST DATA

Some NASA tests of three-dimensional rectangular wings near the ground are summarized in Reference 35. Airfoil profiles tested are not specified. The appropriate curves from Reference 35 are presented on Figures 6-1 through 6-4. Figure 6-1 compares the drag polars and lift curve slopes of a wing of aspect ratio one when very close to the ground and when completely out of ground effect. A substantial increase in lift curve slope will be noted in ground effect. Note that height-to-span ratio h/b_w is used rather than $h/l/S$. Also, the height h of the wing above the ground is defined in two ways. The curves of Reference 35 are based on the height of the airfoil lower surface at the quarter chord point. This means that vehicle clearance height varies with angle of attack. It is felt that trailing edge height is a better parameter because it will nearly always be the lowest point on the airfoil. The two curves for $h/b_w = 0.090$ on Figure 6-2b show the difference between measuring h/b_w at the two locations noted above. The curves of Figure 6-2a were prepared from unpublished NASA data taken from a different model than the curves of Reference 35. The fact that L/D reaches a maximum in Figure 6-2b (when h/b_w is measured to the trailing edge) appears to refute one of the hypotheses put forth in Reference 33: that L/D will increase continuously with C_L when h/b of trailing edge is held constant. Strand in Reference 33 was discussing the airfoil lower surface only. He tacitly assumed an "ideal air-cushion airfoil" that generates neither lift nor drag from the upper surface. A "real air-cushion airfoil" will have an upper surface that produces a small amount of lift and profile drag. When a low-lift upper surface and viscosity are added to the airfoil of Strand's discussion, it takes on more conventional characteristics. Then L/D will reach a maximum at some C_L less than maximum C_L , albeit higher than the C_L for maximum L/D with a conventional airfoil. The point of Strand's comments is that L/D will maximize at a higher C_L if the upper surface lift is kept to as small a percentage of total lift as possible.

Maximum L/D is shown for several aspect ratios in Figure 6-3. It is evident that high aspect ratios are helpful even in ground effect, but the side gaps of the airfoils are not sealed. Figure 6-4 shows the effect of sealing the side gaps and also the effect of thickening the airfoil.

Maximum L/D values of 10 to 25 appear attainable for thin wings of conventional profile and low aspect ratio. Higher L/D 's may be attainable with airfoils optimized for air-cushion vehicle use or with higher aspect ratio planforms. On a practical configuration, L/D may be substantially reduced because of the protrusion of crew compartments and air inlets, thickened trailing edge, etc.

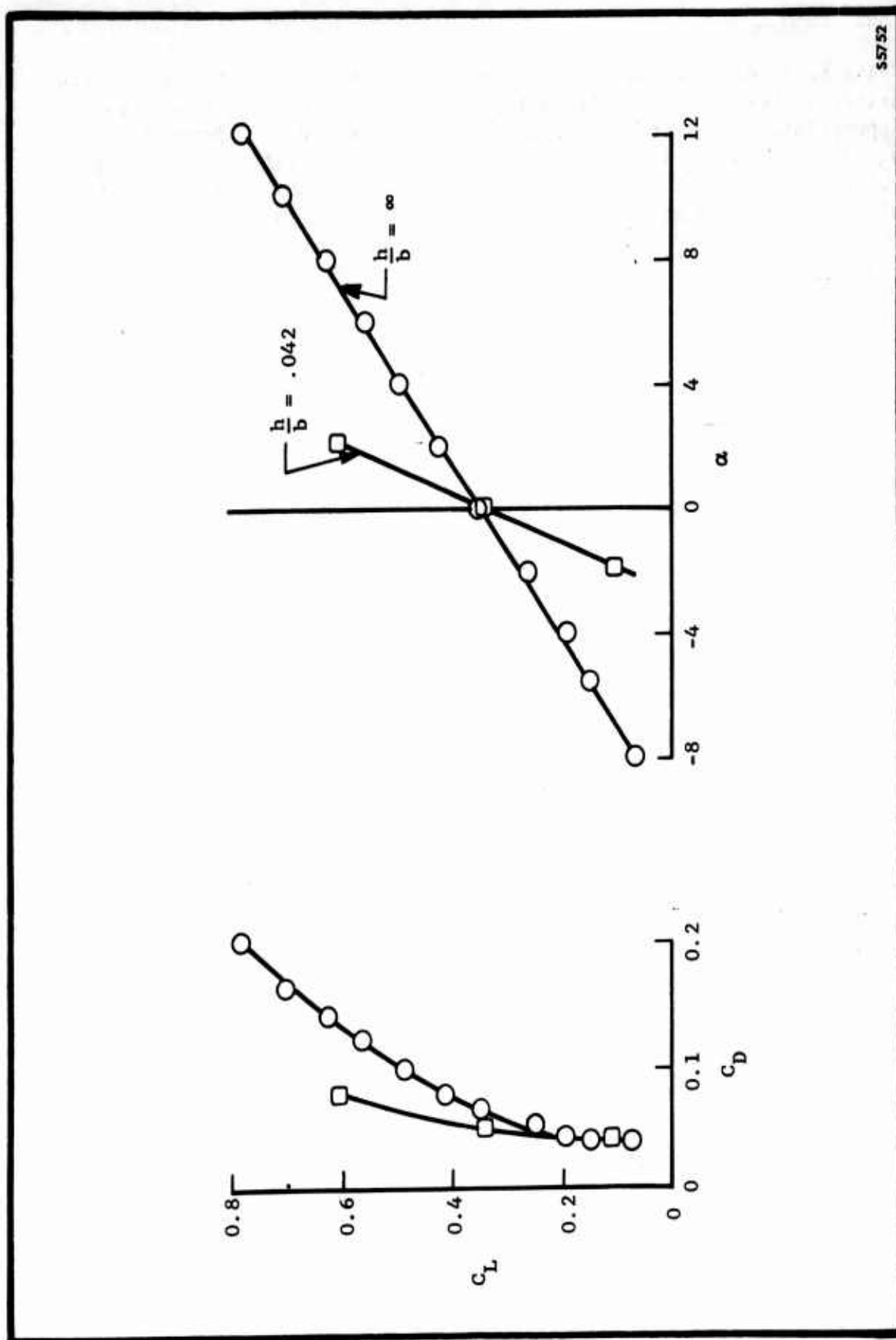
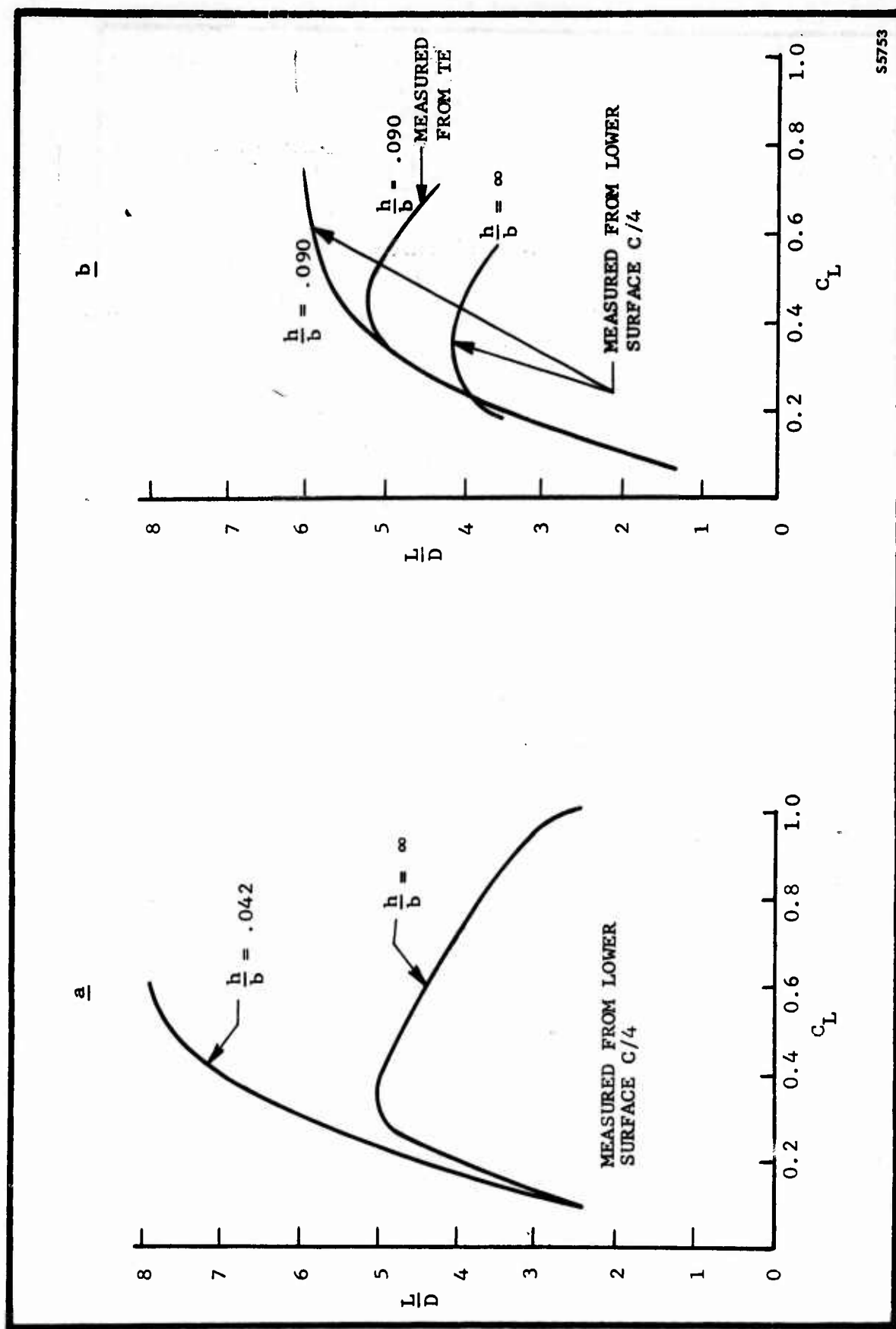


FIGURE 6-1. EFFECT OF THE GROUND ON LIFT AND DRAG

$AR = 1$; $t/c = 0.22$



S5753

FIGURE 6-2. EFFECT OF GROUND ON L/D

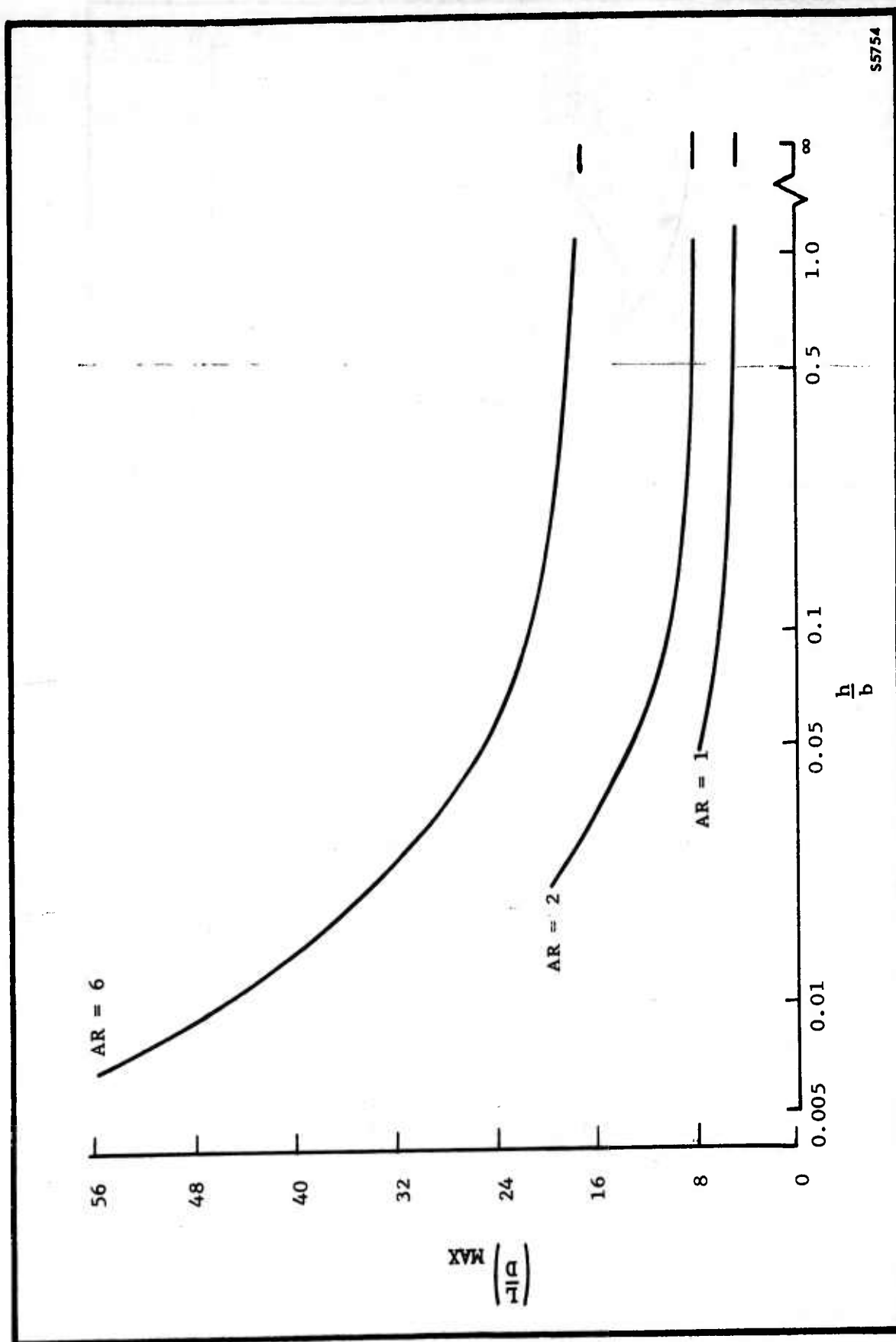
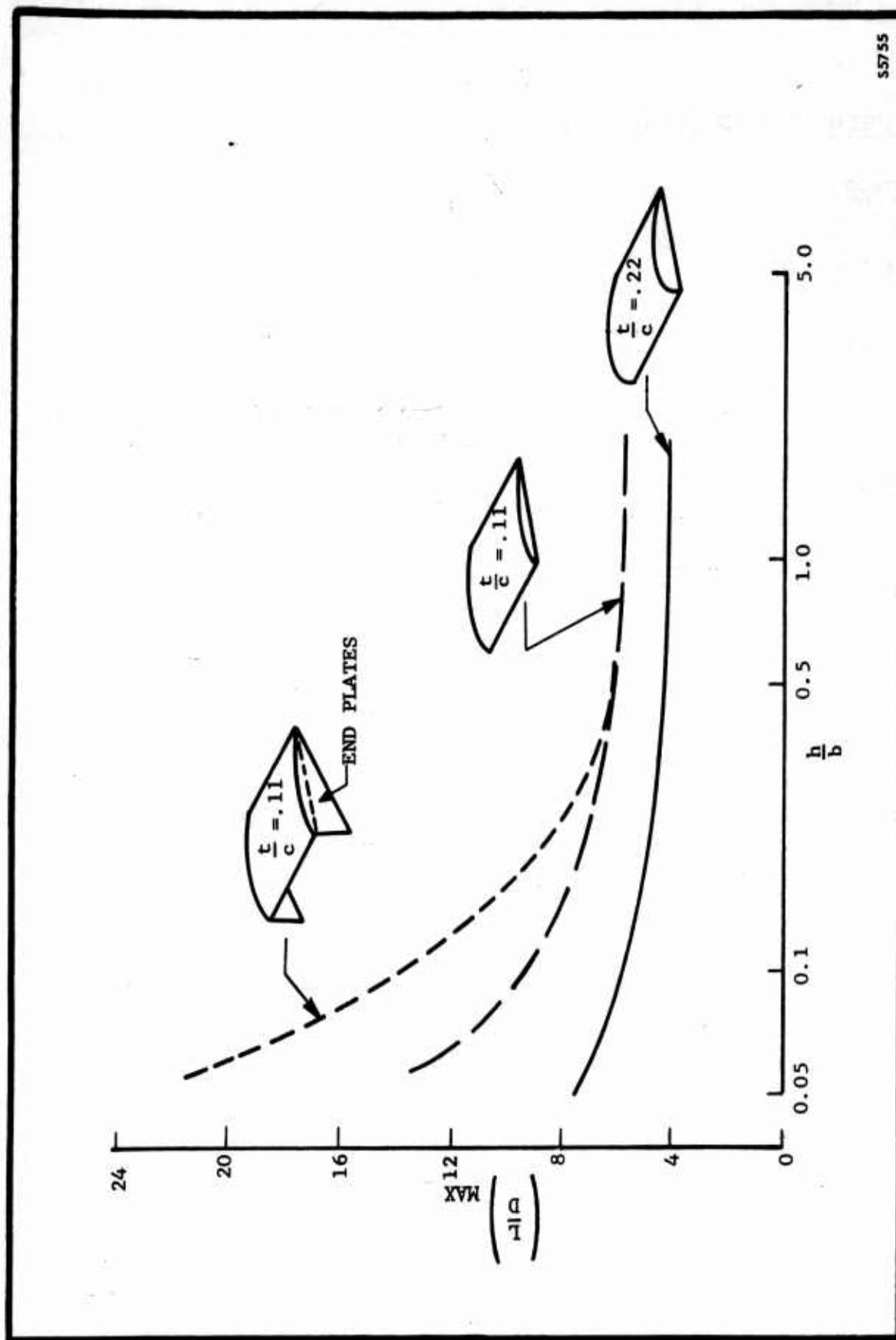


FIGURE 6-3. EFFECT OF ASPECT RATIO ON $\left(\frac{L}{D}\right)_{MAX}$
 $\frac{t}{c} = 0.22$



55755

FIGURE 6-4. EFFECT OF THICKNESS AND ENDPLATES ON $\left(\frac{L}{D}\right)_{MAX}$
AR = 1

6.3 INSTALLED POWER REQUIREMENTS

Unchanged.

6.4 FORWARD MOTION

Unchanged.

6.5 STABILITY AND CONTROL

The discussion below is based on the premise that a practical vehicle must be of finite thickness and will be well streamlined, with only small protuberances.

At low forward speeds, essentially all of the lift is due to base pressure. The center of pressure will therefore be very near the base centroid. As forward speed increases, aerodynamic lift becomes a major factor. Since the center of pressure of an airfoil is normally at the quarter chord point, the vehicle center of pressure will gradually move from the base centroid forward towards the quarter chord point as speed increases. For a rectangular planform with a conventional airfoil, this means a center of pressure shift of about 25 percent of the vehicle length. Since the center of gravity location of an airplane is usually limited to a total travel of about 20 percent of the wing chord, it may be deduced that the ram wing vehicle described above will require a stabilizing device at least as powerful as the horizontal tail of an airplane.

A possible solution, discussed in Reference 33, is the use of an airfoil with the center of pressure at mid-chord. A sample calculation is included in the reference to show the procedures involved in designing this type airfoil and the shape that results.

Airfoils can be designed to be stable in pitch. Whether a practical airfoil can be designed with pitch stability and a center of pressure at the mid-chord is not known.

6.6 OPERATIONAL PROBLEMS

Unchanged.

6.7 OTHER CONSIDERATIONS

Unchanged.

6.8 CONCLUSIONS

6.8.1 Power Required

Two theoretical methods have been developed for designing airfoils in ground effect. When these theories are correlated with experiment, they will provide a method for reducing both profile and induced drag.

NASA tests of low aspect ratio wings in ground effect indicate that the maximum L/D values of 10 to 25 are attainable with thin wings of conventional profile and low aspect ratio. Higher L/D's may be reached with airfoils optimized for an air-cushion vehicle, or with high aspect ratio planforms.

6.8.2 Stability and Control

Extremely powerful stabilizing devices will be required to overcome the center of pressure shift with speed if appreciable upper surface lift is generated by a conventional airfoil profile.

The theory of Reference 33 provides a method for designing airfoils with little or no center of pressure shift as speed increases. The theory has not been correlated by experiment.

6.8.3 Operational Consideration

Unchanged

7.0 GETOL

In Publication U-926 the air-cushion phase of operation of the GETOL concept is adequately discussed in the section dealing with the annular jet concept. Operation free of the ground effect is covered in the existing aviation technology. The prime area of concern, then, is that during transition from air-cushion operation to airplane operation. There is a current study program which will specifically investigate such transition, but results are not yet available.

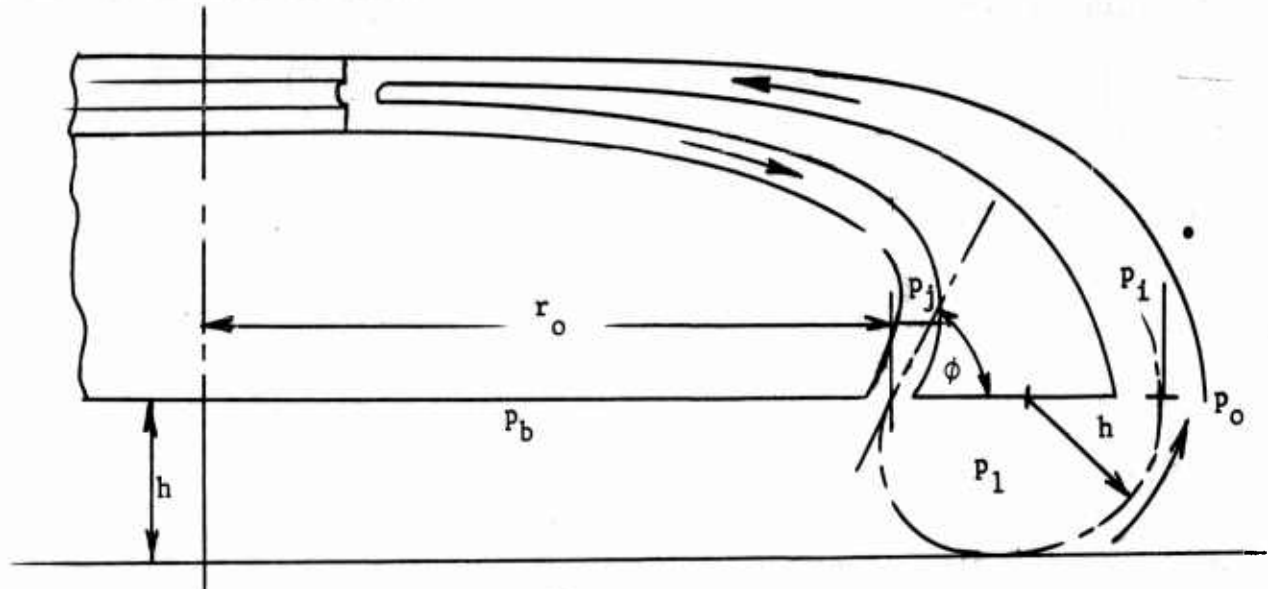
A summary report will be published by Vertol in December 1961, and will include results from wind tunnel, tow track, and dynamic flight model tests. In addition this program will investigate flow distribution problems peculiar to wing-thickness airfoils.

8.0 LEVAPAD

Unchanged.

9.0 RECIRCULATING ANNULAR JET

The recirculating annular jet sketched below has been described by Bowden in Reference 36. An air jet is exhausted through an annular nozzle in the same manner as in the peripheral jet vehicle of Section 2. The nozzle is located somewhat inboard from the periphery of the vehicle and an inlet surrounds the vehicle base.



9.1 POWER REQUIRED

Bowden developed a semi-"zero loss" expression relating the lift of a circular vehicle to the momentum loss between the jet exit and the jet inlet. No internal ducting losses or fan losses were included. He used the same reasoning and made the same type of assumptions as Chaplin in his thin jet theory. The resulting lift equation was:

$$L = J_j \left[\frac{r_o \cos \Gamma}{2h} - 2 + \cos \Gamma \tan \frac{\Gamma}{2} + \left(1 - \frac{J_i}{J_j}\right) \left(\frac{r_o}{2h} + 2 + \tan \frac{\Gamma}{2} \right) \right]$$

where

$$\Gamma = 90^\circ - \theta$$

and J_j and J_i are the jet momenta at the nozzle exit and inlet face, respectively.

Power required relationships were not derived in Reference 36. They have not been developed herein because of time restrictions.

Bowden optimized the jet efflux angle for the maximum lift to momentum addition ratio $\frac{L}{J_j - J_i}$ and compared this to similarly optimized annular jet and plenum chamber vehicles. The optimization procedure followed was not always clear, but indicated that the recirculating jet vehicle would be more efficient than the conventional annular jet vehicle when h/d is less than 0.125. This includes a large portion of the operating height range of air-cushion vehicles. It should be noted that many simplifying assumptions have been made by Bowden, including the following:

- a. No losses in the fan or ducting system. (Ducting requirements are roughly twice as great as for a non-circulating annular jet vehicle.)
- b. The problem of air loss during forward flight is dismissed by assuming that the lift induced by forward velocity will be sufficient to balance the increase in lifting power as the recirculation air is blown away. This could be an extremely optimistic assumption.

Before definite conclusions can be drawn concerning the practicality of the recirculating annular jet concept, the effects of internal ducting losses and forward motion must be more carefully investigated.

10.0 ANNULAR WATER CURTAIN VEHICLE

Reference 37 describes an overwater vehicle that is under full-scale testing at Hughes Tool Company - Aircraft Division. A peripheral water jet is used to seal in air that is pumped into a central plenum by a fan. In essence this is a plenum chamber vehicle with a very low discharge coefficient corresponding to the leakage area in the water curtain.

According to Hughes, the primary advantage of a water curtain over an air curtain is that due to the high density of water, a given momentum flux ($\dot{m}V$) may be obtained with a lower jet velocity, hence with a smaller power expenditure ($\dot{m}V^2$). In addition, a given water mass flow rate requires much smaller ducting than air because of the high density of water.

Using water as the jet medium presents several disadvantages. Separate ducting and pumping systems for cushion air and curtain water increase the mechanical complexity of the vehicle. The weight of the water in the curtain ducting system may be considerable. The vehicle is limited to overwater operation with the capability of overland operation as a plenum vehicle at greatly reduced operating height.

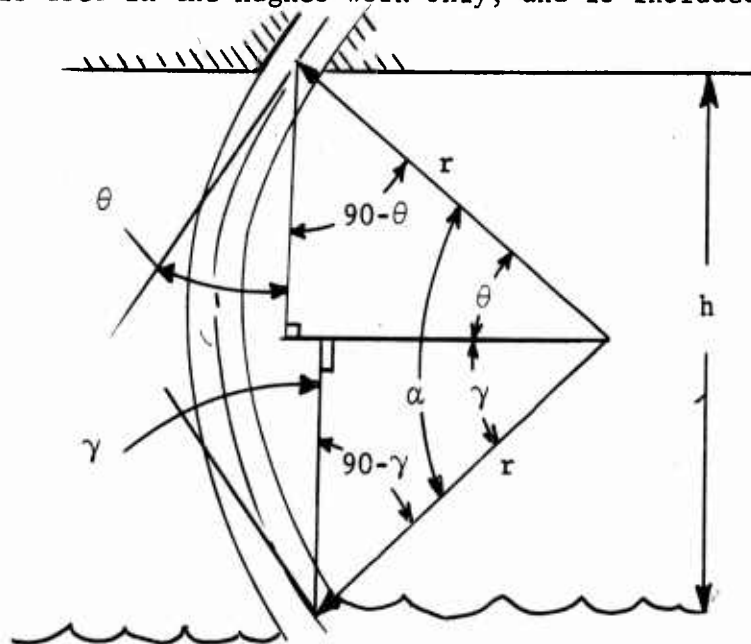
10.1 HOVERING THEORY

The power requirements at the plenum inlet (for the air) and at the jet exit (for the water) will be derived below in a manner consistent with the plenum and annular air jet derivations in Publication U-926. This will present vehicle performance differently than in Reference 37 but in a form consistent with other work in this report and in U-926.

As with other air-cushion concepts, the power required is a function only of vehicle and jet geometry ; but the jet geometry is significantly different. When an air curtain operates at equilibrium the air jet is always tangent to the ground at the jet-ground plane intersection. The water curtain, however, meets the ground plane at an angle which may be established more or less at will. As a result, it is apparent that air curtain "jet geometry" consists only of the vehicle jet efflux angle, jet thickness, and vehicle height. "Jet geometry" for the water jet must also include the jet-ground plane intersection angle which Hughes has accounted for with the jet shape parameter δ .

Water jet geometry will be defined and the parameters needed in the power required equation will be developed. Then the power required equation will be written in a form so that separate installation losses may be conveniently included for both the water and air systems. The power equation will be derived in two forms; the first will be based on Aeronutronic plenum theory, and the second will be based on a much simpler plenum theory.

Jet geometry is sketched below. The jet efflux angle used in this section is consistent with other vehicles described in this report and in Publication U-926. Note that this is not the same as the definition used in Reference 36. The angle α is used in the Hughes work only, and is included here for reference.



JET GEOMETRY

$$\frac{h}{r} = \sin \theta + \sin \gamma$$

Discharge coefficient test data for the air escaping through the water curtain has been correlated in Reference 36 with a jet turning parameter, δ .

$$\delta = 2 \frac{\text{containing force on air cushion}}{\text{momentum flux in water curtain}}$$

$$= 2 \frac{p_b h \ell}{\rho_w t_e \ell V_j^2}, \quad V_j^2 = \frac{2}{\rho_w} q_j$$

Some assumptions from the Hughes work are now required. The water jet is assumed to be so thin that velocity is constant across the jet width. The jet is of constant thickness and jet static pressure is equal to ambient pressure. The Hughes experimental work tends to justify these assumptions. Now, jet total pressure equals jet dynamic pressure and the jet turning parameter becomes

$$\delta = \frac{p_b}{p_{t_j}} \frac{h}{t}$$

The water jet nozzle width t_e has been replaced with the constant jet thickness t . This notation will apply for the remainder of the water jet vehicle analysis. From Chaplin's two-dimensional thin jet theory,

$$\begin{aligned} p_b &= \frac{j}{r} \\ &= \frac{\rho_w t V_j^2}{r} \\ &= 2 p_{t_j} \frac{t}{r} \\ t &= \frac{p_b}{p_{t_j}} \frac{r}{2} \end{aligned}$$

Substitute this t into the jet turning parameter equation

$$\delta = \frac{h}{r} = 2 \frac{h}{r}$$

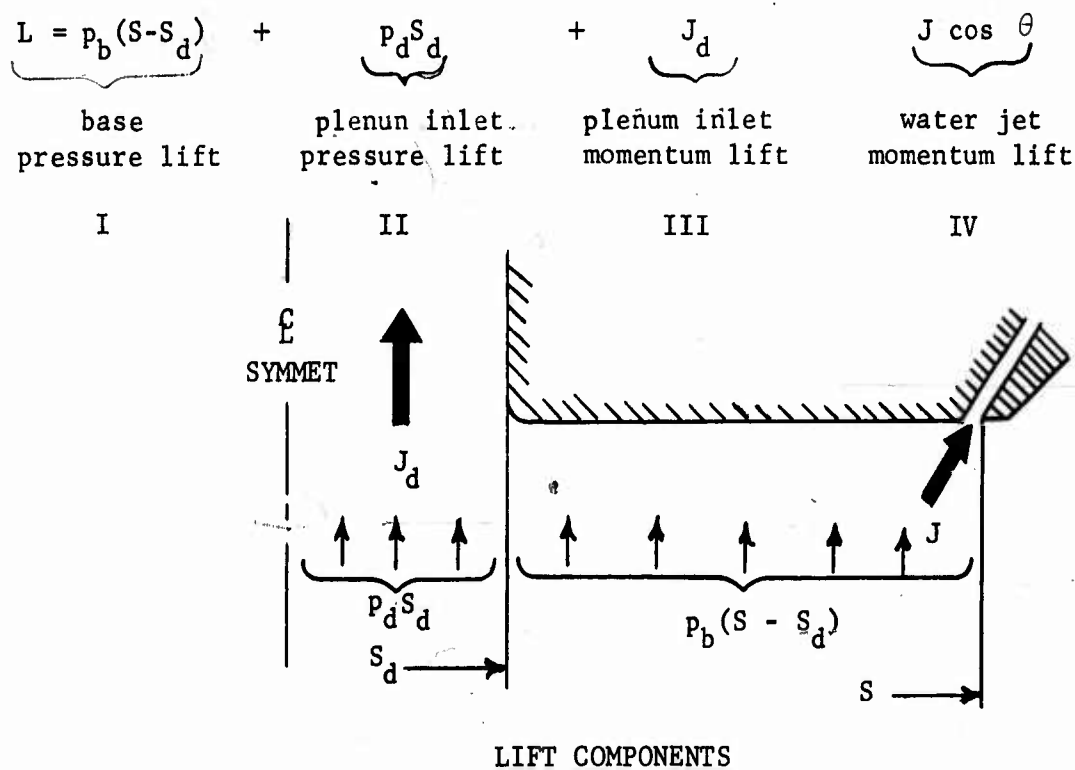
But h/r was related earlier to the jet angular geometry. The following equalities may be established between the jet turning parameter δ and the jet geometry:

$$\delta = \frac{p_b}{p_{t_j}} \frac{h}{t} = 2 \frac{h}{r} = 2(\sin \theta + \sin \gamma)$$

One of the parameters that occurs in the power equations is base pressure. This may be written directly from the jet turning relationships.

$$p_b = p_{t_j} \delta \frac{t}{h}$$

Jet total pressure will now be derived. To accomplish this, the vehicle lift equation is written assuming ambient pressure on the upper surface of the vehicle. Base lift will be presented to a manner similar to the Aeronutronic plenum chamber theory in Publication U-926.



The lift components will be expanded individually, then combined.

Component I:

$$p_b (S - S_d) = p_{t_j} \delta \frac{t}{h} (S - S_d)$$

Component II:

For evaluation of Component II, the factors K and η_p , as defined in Section 3 of Publication U-926, are required. For convenience, they are redefined here.

$$\eta_p = \frac{p_b}{p_{t_b}}$$

$$K = \frac{p_{t_d} - p_{t_b}}{q_d}$$

q_d is evaluated below from continuity.

$$Q_d = Q_a$$

where Q_a is the outflow through the water curtain. Hughes has defined a discharge coefficient C which is a function of base static pressure. This assumes negligible velocities under the base, an assumption not made in the Aeronutronic plenum chamber theory. The Hughes definition will be followed herein because all of the Hughes experimental discharge coefficient data are presented as a function of base static pressure.

$$Q_a = S_x C \sqrt{\frac{2p_b}{\rho_a}}$$

The discharge coefficient has been evaluated experimentally by Hughes in terms of δ . A fairing, by Aeronutronic, through the available data is shown in Figure 10-1 and has been used in the calculations that follow.

$$\rho_a S_d V_d = \rho_a S_x C \sqrt{\frac{2p_b}{\rho_a}}$$

$$S_d \sqrt{\frac{2}{\rho_a}} q_d = S_x C \sqrt{\frac{2}{\rho_a} p_b}$$

$$q_d = p_b \frac{S_x}{S_d} C$$

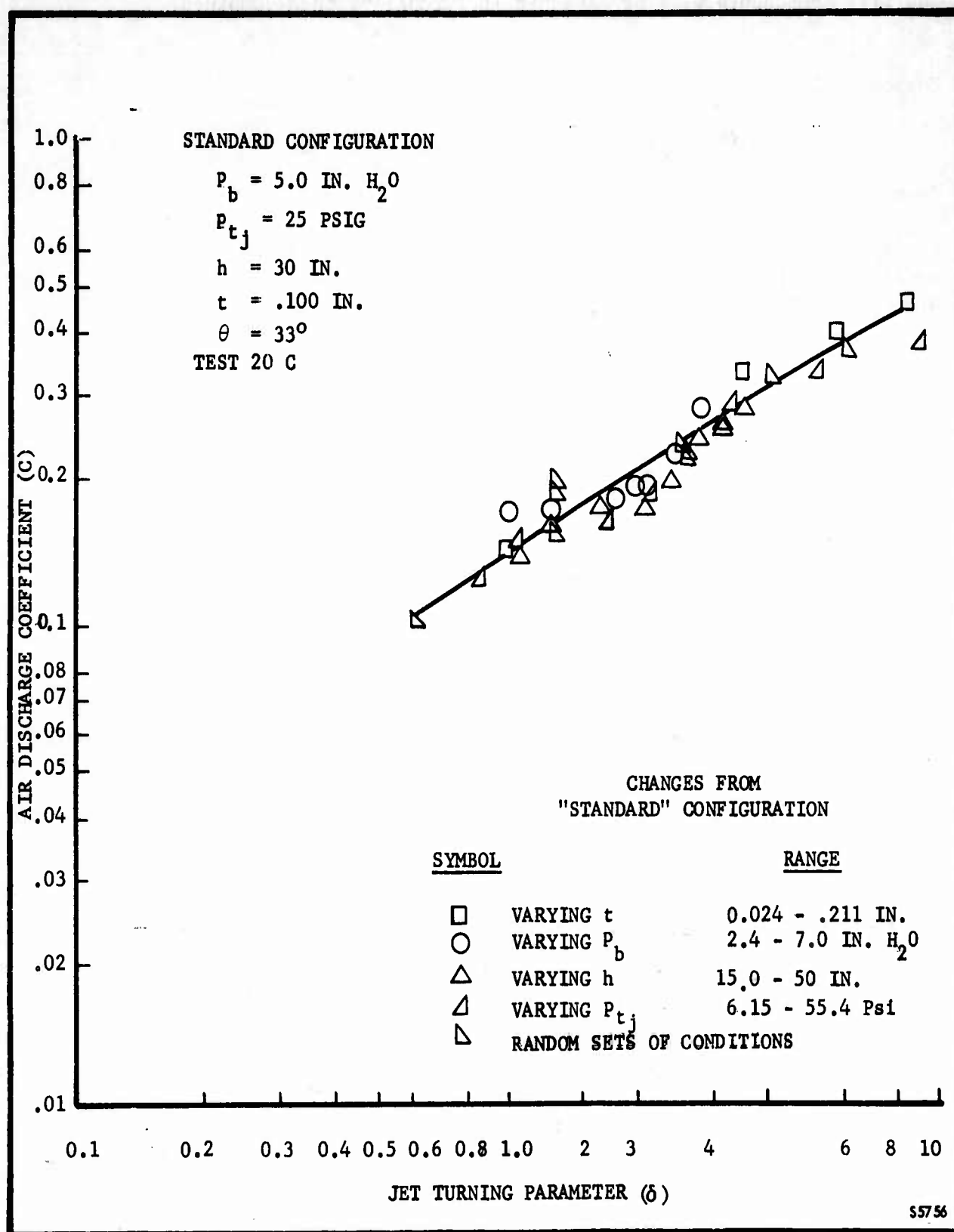


FIGURE 10-1a. EFFECT OF OPERATIONAL AND DESIGN VARIABLES ON AIR LEAKAGE
 - (REFERENCE 37) AERONUTRONIC FAIRING - C VERSUS δ

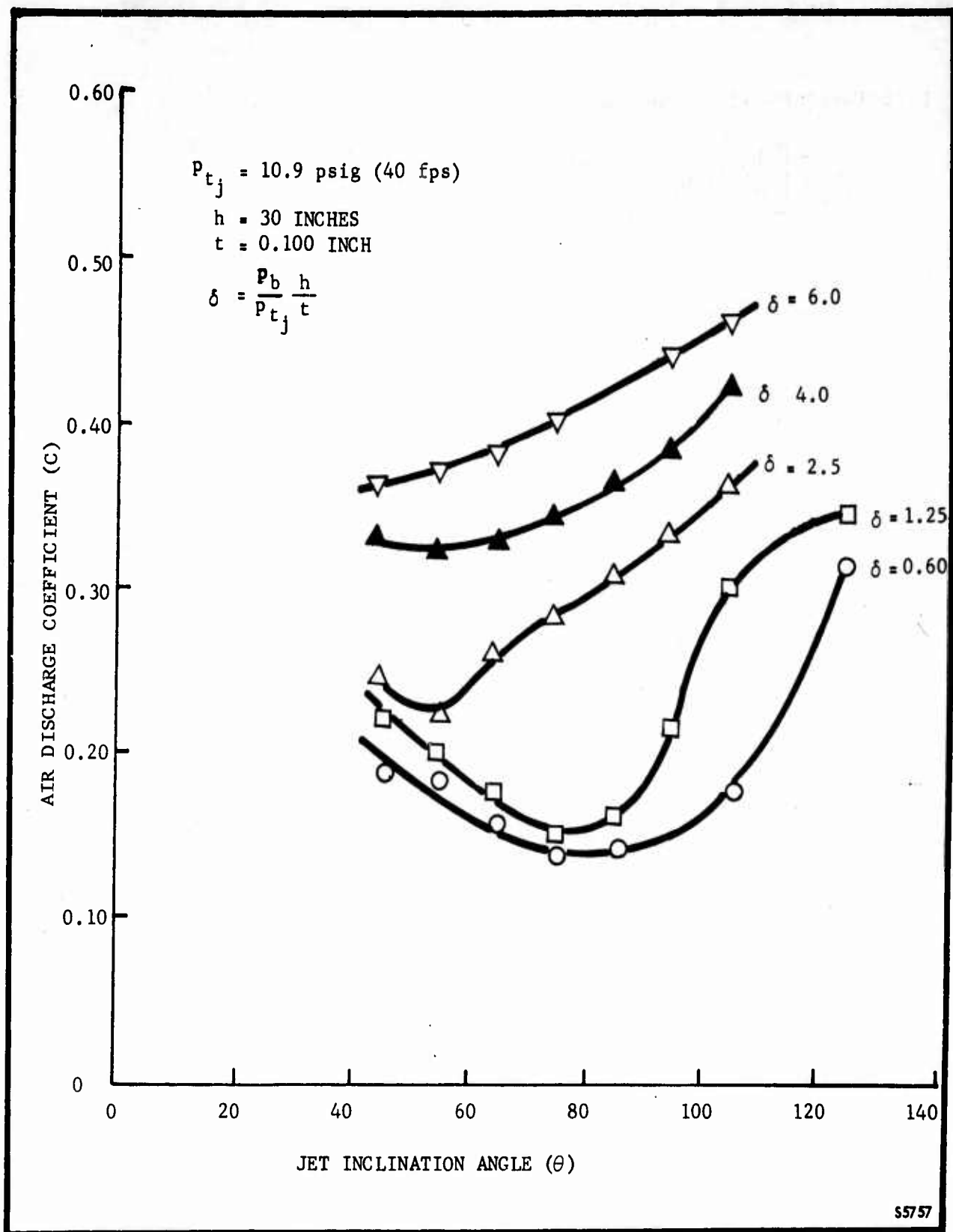


FIGURE 10-1b. EFFECT OF OPERATIONAL AND DESIGN VARIABLES ON AIR LEAKAGE
- (REFERENCE 37) C VERSUS θ

Lift Component II now becomes

$$\begin{aligned}
 p_d S_d &= \left[\frac{p_b}{\eta_p} + p_b \left(\frac{S_x}{S_d} c \right)^2 (K-1) \right] S_d \\
 &= p_{t_j} \delta \frac{t}{h} S_d \left[\frac{1}{\eta_p} + \left(\frac{S_x}{S_d} c \right)^2 (K-1) \right]
 \end{aligned}$$

Component III:

$$\begin{aligned}
 J_d &= \rho_a S_d V_d^2 \\
 &= 2 S_d q_d \\
 &= 2 S_d p_b \left(\frac{S_x}{S_d} c \right)^2 \\
 &= 2 p_{t_j} \delta \frac{t}{h} S_d \left(\frac{S_x}{S_d} c \right)^2
 \end{aligned}$$

Component IV:

$$\begin{aligned}
 J \cos \theta &= \rho_w S_j V_j^2 \cos \theta \\
 &= 2 p_{t_j} S_j \cos \theta
 \end{aligned}$$

The complete lift equation is:

$$\begin{aligned}
 L &= p_{t_j} \delta \frac{t}{h} (S - S_d) + p_{t_j} \delta \frac{t}{h} S_d \left[\frac{1}{\eta_p} + \left(\frac{S_x}{S_d} c \right)^2 (K-1) \right] + 2 p_{t_j} \delta \frac{t}{h} S_d \left(\frac{S_x}{S_d} c \right)^2 \\
 &\quad + 2 p_{t_j} S_j \cos \theta
 \end{aligned}$$

$$Q_w = S_j V_j$$

$$= S_j \sqrt{\frac{2}{\rho_w} p_{t_j}}$$

so that water power becomes

$$P_{T_j} = p_{t_j}^{3/2} S_j \sqrt{\frac{2}{\rho_w}}$$

Air power at the entrance to the base plenum volume (or exit of the diffuser) is

$$P_{T_a} = Q_a p_{t_d}$$

where the air volume flow is taken as before, from the Hughes definition of plenum exit discharge coefficient.

$$P_{T_a} = p_{t_d} S_x C \sqrt{\frac{2}{\rho_a} p_b}$$

Diffuser exit total pressure p_{t_d} may be handled in the same manner as when expanding Component II of the lift equation.

$$p_{t_d} = p_{t_b} + K q_d$$

$$= \frac{p_b}{\eta_p} + K p_b \left(\frac{S_x}{S_d} C \right)^2$$

$$= p_b \left[\frac{1}{\eta_p} + \left(\frac{S_x}{S_d} C \right)^2 K \right]$$

$$L = p_{t_j} \left[\delta \frac{t}{h} \left\{ (S - S_d) + S_d \left[\frac{1}{\eta_p} + \left(\frac{S_x}{S_d} C \right)^2 (K-1) \right] + 2 S_d \left(\frac{S_x}{S_d} C \right)^2 \right\} + 2 S_j \cos \theta \right]$$

$$= p_{t_j} \left[\delta \frac{t}{h} \left\{ S + S_d \left[\frac{1}{\eta_p} - 1 + \left(\frac{S_x}{S_d} C \right)^2 (K+1) \right] \right\} + 2 S_j \cos \theta \right]$$

The power equations will require p_{t_j} . The lift equation will be solved for p_{t_j} and divided by S/S for convenience.

$$p_{t_j} = \frac{L}{S \left[\delta \frac{t}{h} \left\{ \frac{S}{S} + \frac{S_d}{S} \left[\frac{1}{\eta_p} - 1 + \left(\frac{S_x/S}{S_d/S} C \right)^2 (K+1) \right] \right\} + 2 \frac{S_j}{S} \cos \theta \right]}$$

The area ratios may be expressed in a more convenient form:

$$\frac{S_x}{S} = \frac{h\ell}{S}$$

$$\frac{S_j}{S} = \frac{\ell t}{S} = \frac{h\ell}{S} \frac{t}{h}$$

$$p_{t_j} = \frac{L/S}{\delta \frac{t}{h} \left\{ 1 + \frac{S_d}{S} \left[\frac{1}{\eta_p} - 1 + \left(\frac{h\ell/S}{S_d/S} C \right)^2 (K+1) \right] \right\} + 2 \frac{h\ell}{S} \frac{t}{h} \cos \theta}$$

Water power and air power equations may now be written and combined into total power required. Water power required at the jet efflux is

$$P_{T_j} = Q_w p_{t_j}$$

Where the water volume flow is

Air power becomes

$$P_{T_a} = P_b^{3/2} S_x C \sqrt{\frac{2}{\rho_a}} \left[\frac{1}{\eta_p} + \left(\frac{S_x}{S_d} C \right)^2 K \right]$$

Writing base pressure in terms of the jet turning parameter δ gives

$$P_{T_a} = P_{t_j}^{3/2} \left(\delta \frac{t}{h} \right)^{3/2} S_x C \sqrt{\frac{2}{\rho_a}} \left[\frac{1}{\eta_p} + \left(\frac{S_x}{S_d} C \right)^2 K \right]$$

The combined power equation is

$$\begin{aligned} P_T &= P_{T_j} + P_{T_a} \\ &= P_{t_j}^{3/2} \left\{ S_j \sqrt{\frac{2}{\rho_w}} + \left(\delta \frac{t}{h} \right)^{3/2} S_x C \sqrt{\frac{2}{\rho_a}} \left[\frac{1}{\eta_p} + \left(\frac{S_x}{S_d} C \right)^2 K \right] \right\} \end{aligned}$$

Combining terms and multiplying by S/S ,

$$P_T = P_{t_j}^{3/2} S \sqrt{\frac{2}{\rho_a}} \left\{ \frac{S_j}{S} \sqrt{\frac{\rho_a}{\rho_w}} + \frac{S_x}{S} \left(\delta \frac{t}{h} \right)^{3/2} C \left[\frac{1}{\eta_p} + \left(\frac{S_x/S}{S_d/S} C \right)^2 K \right] \right\}$$

The area ratios S_j/S and S_x/S were expanded previously.

$$\begin{aligned} P_T &= P_{t_j}^{3/2} S \sqrt{\frac{2}{\rho_a}} \left\{ \frac{h\ell}{S} \frac{t}{h} \sqrt{\frac{\rho_a}{\rho_w}} + \frac{h\ell}{S} \left(\delta \frac{t}{h} \right)^{3/2} C \left[\frac{1}{\eta_p} + \left(\frac{h\ell/S}{S_d/S} C \right)^2 K \right] \right\} \\ &= P_{t_j}^{3/2} S \frac{h\ell}{S} \sqrt{\frac{2}{\rho_a}} \left\{ \frac{t}{h} \sqrt{\frac{\rho_a}{\rho_w}} + \left(\delta \frac{t}{h} \right)^{3/2} C \left[\frac{1}{\eta_p} + \left(\frac{h\ell/S}{S_d/S} C \right)^2 K \right] \right\} \end{aligned}$$

The power equation will be completely in terms of vehicle and jet geometry (and C) when the jet total pressure equation is substituted. Substituting and simplifying,

$$P_T = \frac{\frac{L}{2\sqrt{\rho_a}} \sqrt{\frac{L}{S}} \left\{ \frac{h\ell}{S} \sqrt{\frac{2}{\rho_a}} \left\{ \frac{t}{h} \sqrt{\frac{\rho_a}{\rho_w}} + \left(\delta \frac{t}{h} \right)^{3/2} c \left[\frac{1}{\eta_p} + \left(\frac{h\ell/S}{S_d/S} c \right)^2 K \right] \right\} \right\}^{\frac{2}{2}}}{\left[\delta \frac{t}{h} \left\{ 1 + \frac{S_d}{S} \left[\frac{1}{\eta_p} - 1 + \left(\frac{h\ell/S}{S_d/S} c \right)^2 (K+1) \right] + 2 \frac{h\ell}{S} \frac{t}{h} \cos \theta \right\} \right]^{\frac{3}{2}}}$$

$$= \frac{\frac{L}{2\sqrt{\rho_a}} \sqrt{\frac{L}{S}} \left\{ 2\sqrt{2} \frac{h\ell}{S} \left\{ \frac{t}{h} \sqrt{\frac{\rho_a}{\rho_w}} + \left(\delta \frac{t}{h} \right)^{3/2} c \left[\frac{1}{\eta_p} + \left(\frac{h\ell/S}{S_d/S} c \right)^2 K \right] \right\} \right\}}{\left[\delta \frac{t}{h} \left\{ 1 + \frac{S_d}{S} \left[\frac{1}{\eta_p} - 1 + \left(\frac{h\ell/S}{S_d/S} c \right)^2 (K+1) \right] + 2 \frac{h\ell}{S} \frac{t}{h} \cos \theta \right\} \right]^{\frac{3}{2}}}$$

This is the same basic form that was utilized with other configurations; that is,

$$P_T = P_{i\infty} G$$

Where

$$P_{i\infty} = \frac{L}{2\sqrt{\rho_a}} \sqrt{\frac{L}{S}} \underbrace{\left\{ \frac{h\ell}{S} \sqrt{\frac{2}{\rho_a}} \left\{ \frac{t}{h} \sqrt{\frac{\rho_a}{\rho_w}} + \left(\delta \frac{t}{h} \right)^{3/2} c \left[\frac{1}{\eta_p} + \left(\frac{h\ell/S}{S_d/S} c \right)^2 K \right] \right\} \right\}^{\frac{2}{2}}}_{\text{water power}} \underbrace{\left\{ \frac{h\ell}{S} \sqrt{\frac{2}{\rho_a}} \left\{ \frac{t}{h} \sqrt{\frac{\rho_a}{\rho_w}} + \left(\delta \frac{t}{h} \right)^{3/2} c \left[\frac{1}{\eta_p} + \left(\frac{h\ell/S}{S_d/S} c \right)^2 K \right] \right\} \right\}^{\frac{2}{2}}}_{\text{air power}}$$

$$G = \frac{1}{\left[\delta \frac{t}{h} \left\{ 1 + \frac{S_d}{S} \left[\frac{1}{\eta_p} - 1 + \left(\frac{h\ell/S}{S_d/S} c \right)^2 (K+1) \right] + 2 \frac{h\ell}{S} \frac{t}{h} \cos \theta \right\} \right]^{\frac{3}{2}}}$$

Note that the water power and air power components still occur as individually identifiable terms. This is an essential feature when installation losses are to be included. This will be discussed further in Section 10.3.

Since the power required equation so unwieldy, a simplified form will be written based upon the following assumptions:

a. Velocities under the base are negligible, hence $p_{t_b} = p_b$

b. Pressure lift is due entirely to base pressure; i.e.,

$$V_d = 0$$

$$p_d = p_b$$

Under these assumptions, the basic water power equation remains the same and air power becomes

$$\begin{aligned} P_{T_a} &= p_b^{3/2} S_x C \sqrt{\frac{2}{\rho_a}} \\ &= p_{t_j}^{3/2} \left(\delta \frac{t}{h} \right)^{3/2} C S \frac{h\ell}{S} \sqrt{\frac{2}{\rho_a}} \end{aligned}$$

Lift becomes:

$$\begin{aligned} L &= p_{t_j} \delta \frac{t}{h} S + 2 p_{t_j} S_j \cos \theta \\ &= p_{t_j} S \left[\delta \frac{t}{h} + 2 \frac{S_j}{S} \cos \theta \right] \end{aligned}$$

and jet total pressure is

$$P_{t_j} = \frac{L/S}{\delta \frac{t}{h} + 2 \frac{h\ell}{S} \frac{t}{h} \cos \theta}$$

The combined power equation becomes

$$P_T = p_{t_j}^{3/2} \left[S \frac{S_j}{S} \sqrt{\frac{2}{\rho_w}} + \left(\delta \frac{t}{h} \right)^{3/2} S \frac{h\ell}{S} C \sqrt{\frac{2}{\rho_a}} \right]$$

$$P_t = \frac{\frac{2}{2} \frac{L}{S} \sqrt{\frac{L}{S}} \frac{h\ell}{S} \sqrt{\frac{2}{\rho_a}} \left[\frac{t}{h} \sqrt{\frac{\rho_a}{\rho_w}} + \left(\delta \frac{t}{h} \right)^{3/2} C \right]}{\left[\delta \frac{t}{h} + 2 \frac{h\ell}{S} \frac{t}{h} \cos \theta \right]^{3/2}}$$

$$= \frac{P_{\text{too}} 2\sqrt{2} \frac{h\ell}{S} \left[\overbrace{\frac{t}{h} \sqrt{\frac{\rho_a}{\rho_w}}}^{\text{water power}} + \overbrace{\left(\delta \frac{t}{h} \right)^{3/2} C}^{\text{air power}} \right]}{\left[\delta \frac{t}{h} + 2 \frac{h\ell}{S} \frac{t}{h} \cos \theta \right]^{3/2}}$$

Again, the water and air power components are individually identifiable, hence easily adjusted for installation losses.

For any given δ and θ (hence a given C), minimizing hovering power requires that t/h become infinite. Since large t/h values lead to large water ducts in the vehicle, hence high vehicle weight, a compromise must be reached between theoretical hovering power and the amount of water that must be carried in the water ducting.

It is apparent that any comparison between the water wall and air wall hovering power requirements will be strongly influenced by the specific geometry of the water wall vehicle. A realistic comparison must be based upon a specific set of vehicle requirements.

Because of the indeterminate nature of the minimum theoretical hovering power, no attempt has been made to fully optimize the water jet geometry. However, a comparison is presented of the optimum theoretical air jet hovering power with a partially optimized water jet. The partial optimization follows.

- The hovering power factor G was plotted as a function of δ and $h\ell/S$ for several values of t/h . θ was held constant at 33° for simplicity. The more complete power equation was used. Figure 10-2 shows a typical curve ($t/h = 0.003$).
- The two-parameter graph in Figure 10-3 was drawn by combining the "minimum G " lines from each graph discussed in (a).
- The partially optimized G of Figure 10-4 was plotted from lowest G values shown in Figure 10-3 for each value of $h\ell/S$. These points correspond to the highest t/h line shown, $t/h = 0.011$.

The partially optimized G is compared, on Figure 10-4, to the minimum theoretical G from the Convair theory for peripheral air jet vehicles.

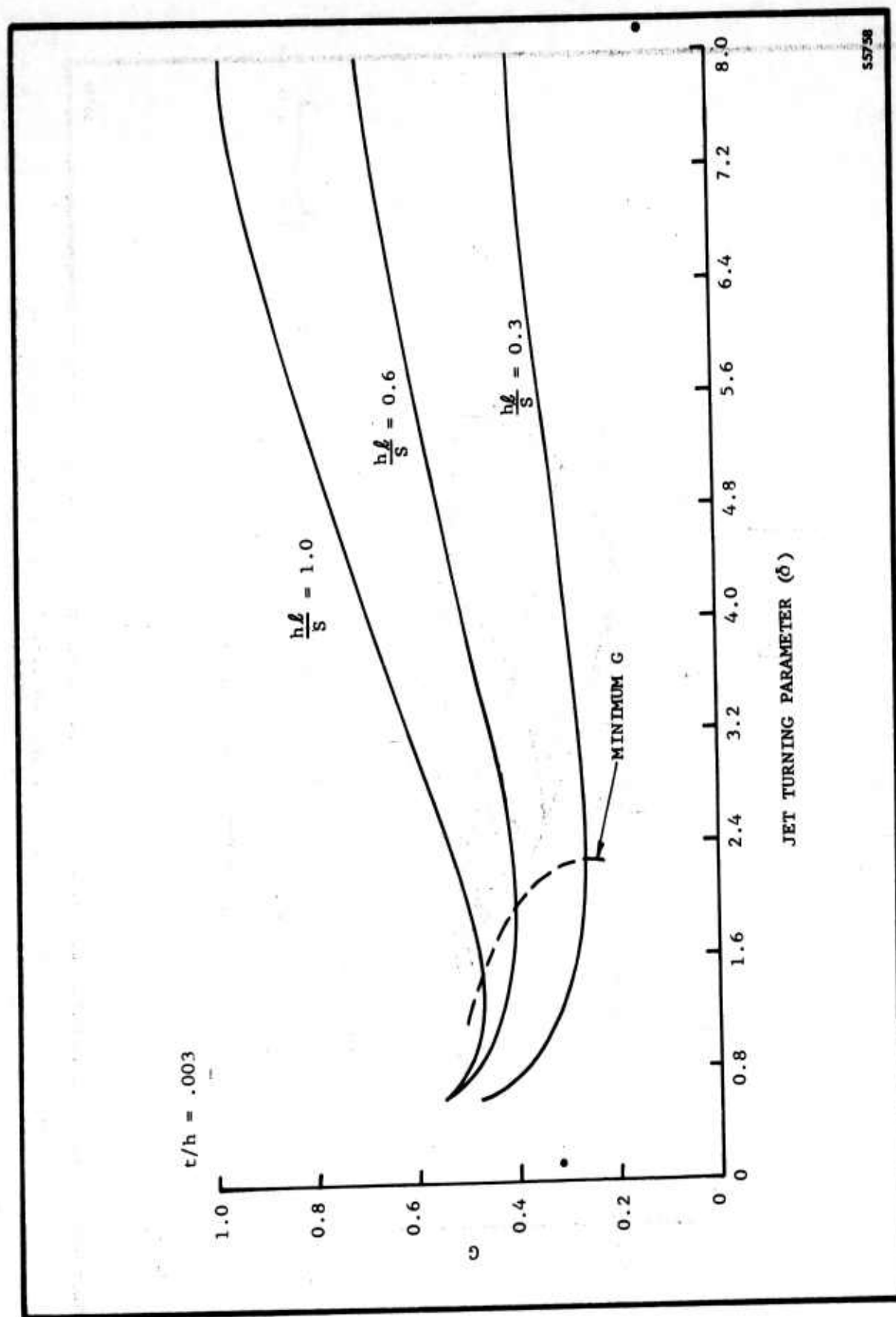
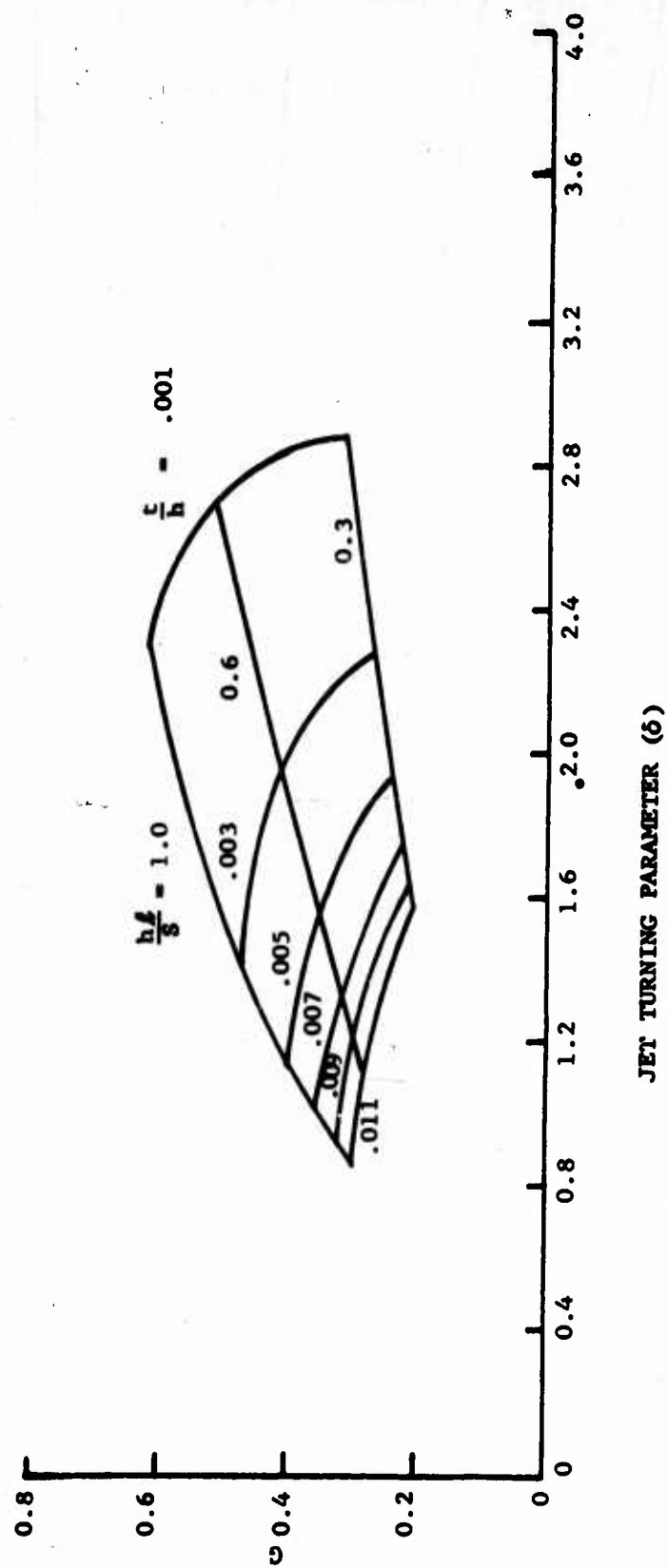


FIGURE 10-2. HOVERING GROUND EFFECT POWER FACTOR - $\theta = 33$ DEGREES



55739

FIGURE 10-3. MINIMUM HOVERING GROUND EFFECT POWER FACTOR - EFFECT OF JET THICKNESS AND JET TURNING PARAMETER - $\theta = 33$ DEGREES

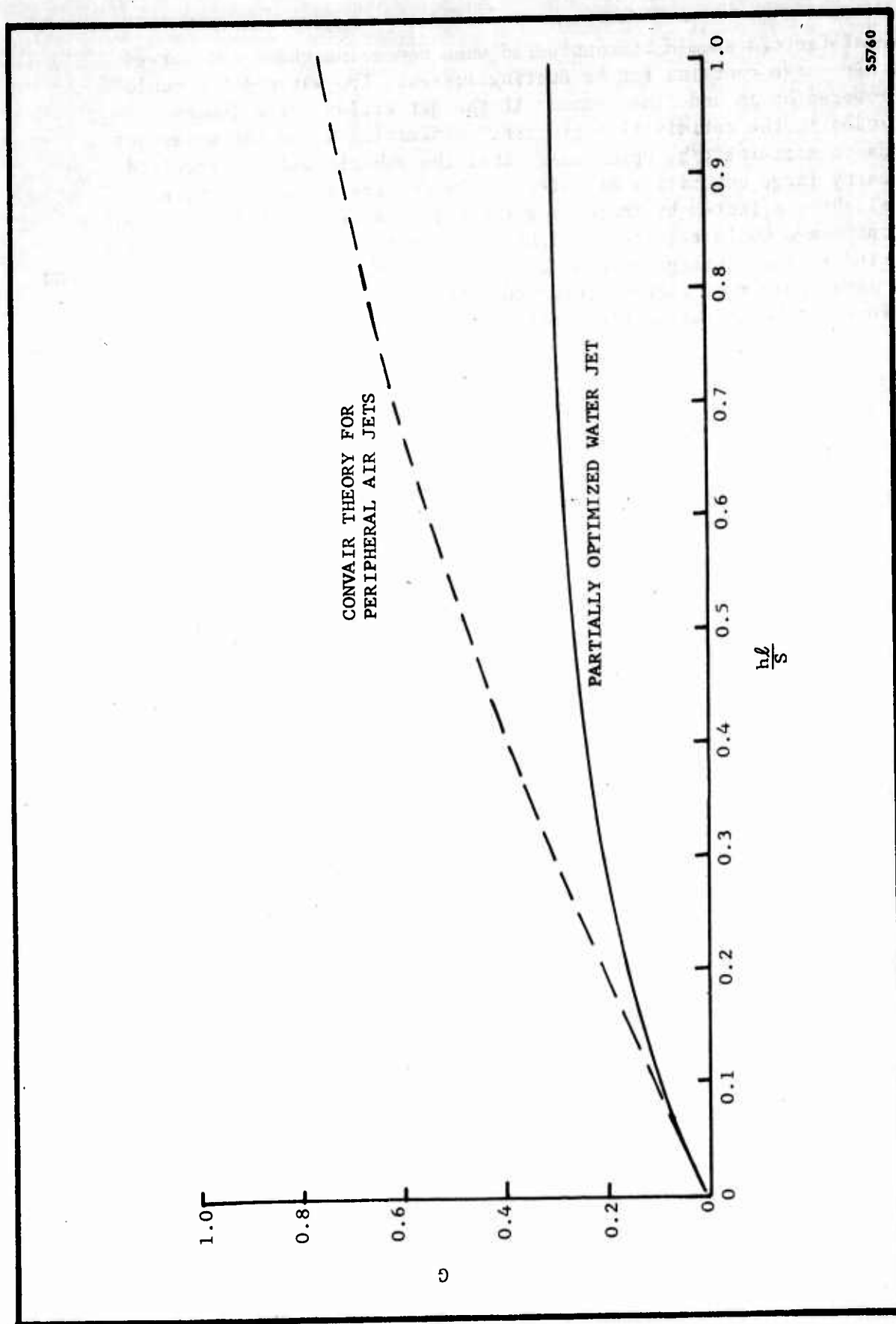


FIGURE 10-4. MINIMUM HOVERING GROUND EFFECT POWER FACTOR - $\theta = 33$ DEGREES

Several factors should be considered when comparing these two curves. Neither curve contains fan or ducting losses. The water jet G could be lowered by an undefined amount if the jet efflux angle θ were included in the optimization process. Minimizing G for the water jet tends to maximize t/h , which means that the vehicle will be required to carry large quantities of water in the ducting system. However, G is slightly affected by increasing t/h beyond a certain point. Probably an optimum G would require a slightly higher t/h if the weight of water carried in the ducting could be brought into the optimization. Considering the large number of factors involved, the comparison of Figure 10-4 is believed to be as reasonable a comparison as is practical at this time.

10.2 TEST DATA

10.2.1 Two-Dimensional Water Wall

Two-dimensional water wall performance has been extensively investigated, according to Reference 37. The results of these tests are presented in Reference 38, which is classified. Test data published in Reference 37 indicate that water wall performance may be generalized in terms of an air discharge coefficient C , a jet turning parameter δ , and the discharge angle θ . C and δ are discussed in detail in Section 10.1. An Aeronutronic fairing of Hughes C data from Reference 37 is presented on Figure 10-1a as a function of δ . The effect of θ on C is shown on Figure 10-1b, and is taken directly from Reference 37.

10.2.2 Full-Scale Vehicles

Two full-scale vehicles described in Reference 36 are presently being tested. Performance and stability are discussed qualitatively in Reference 36 because (a) the vehicles were designed with performance as a secondary consideration and (b) stability tests have not yet been completed. Vehicle stability comments from Reference 36 are summarized in Section 10.5.

10.3 INSTALLED POWER REQUIREMENTS

Installed power may be estimated from the hovering power by correcting G for internal ducting and fan losses. These losses are discussed in Sections 2.3 and 3.3 of Publication U-926 and in Section 2.3 of this report. Care must be taken when estimating water ducting losses to keep the velocities in the ducting low. Low water velocities, however, lead to large ducts, hence a heavy load of water inside the vehicle. It may be necessary to sacrifice some ducting efficiency in order to keep vehicle weight down.

Installed power, or shaft power required (S.P.) may be written in terms of the ducting and fan (or pump) efficiencies and the combined power equation.

$$S.P. = P_{i\infty} \left(\frac{G_w}{\eta_{i_w} \eta_{f_w}} + \frac{G_a}{\eta_{i_a} \eta_{f_a}} \right)$$

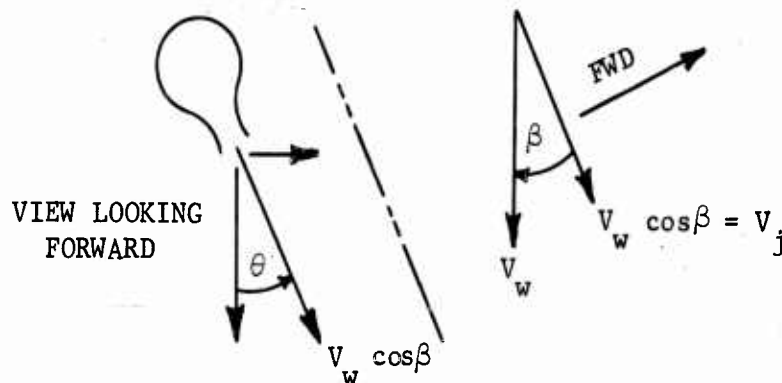
When referred to the power equations presented in Section 10.1, the efficiencies may be applied to the proper portion of G by noting which of the bracketed numerator terms applies to air and which applies to water. G from the simplified power equation of Section 10.1 is written below with the ducting and fan (or pump) efficiencies included.

$$G = \frac{\begin{array}{c} \text{water} \\ \text{power} \end{array} \quad \begin{array}{c} \text{air} \\ \text{power} \end{array}}{\delta \frac{t}{h} + 2 \frac{h\ell}{S} \frac{t}{h} \cos \theta} \cdot \frac{\frac{t}{h} \frac{\rho_a}{\rho_w} \frac{1}{\eta_{i_w} \eta_{f_w}} + \frac{\delta \frac{t}{h}}{\eta_{i_a} \eta_{f_a}}}{3/2}$$

10.4 FORWARD MOTION

The primary factor in extending the water jet hovering power to forward flight is the addition of momentum drag. For a rigorous analysis, however, ram-recovery factors for fan and water scoop inlets and for static pressure variations around the vehicle must be considered. Furthermore, particular attention must be given to optimization of the water-jet parameters if momentum drag is to be kept to a reasonable value.

In forward flight, it is desirable to direct both the fore and aft water-jets in a more rearward direction than at hover. In addition, it is desirable to give the side water jets a rearward velocity component. Consider the following sketch where the slant is defined by the angle β . β will normally be other than zero only for a side jet.



When the wall is slanted in this manner, momentum balance is written using the velocity component normal to the jet exit, and the jet turning parameter becomes

$$\begin{aligned}\delta &= \frac{p_b h}{(V_w \cos \beta)^2 t} \\ &= \frac{p_b h}{p_{tj} t \cos^2 \beta}\end{aligned}$$

if the density of water is assumed to be 2.0. In forward flight it may be assumed that the static pressure on the outside of the jet is not atmospheric, but some p_o (gage pressure). This changes the reference to which the pressure differential across the jet is referred, and the base pressure may be replaced by the pressure differential. The modified turning parameter now becomes

$$\delta = \frac{(p_b - p_o) h}{p_{tj} t \cos^2 \beta}$$

After making the above assumption, this new definition of δ may be applied to a forward, side, or rear jet of a rectangular vehicle at hover or in forward flight, and the corresponding δ applied to the experimental data to find the discharge coefficient C . For a forward or rear wall, β will normally be equal to zero, and for a side jet, p_o may generally be assumed to be zero. Both β and p_o are equal to zero at hover.

With the slant-jet definition, the water jet lift becomes

$$J \cos \theta = \rho_w Q_w V_w \cos \beta \cos \theta$$

where the water volume flow is

$$Q_w = b t V_w \cos \beta$$

where b is the water jet length. Substituting, the jet lift becomes

$$\begin{aligned} J \cos \theta &= b \rho_w t V_w^2 \cos^2 \beta \cos \theta \\ &= b \rho_w (p_b - p_o) \frac{h}{\delta} \cos \theta \end{aligned}$$

where

$$t V_w^2 \cos^2 \beta = (p_b - p_o) \frac{h}{\delta}$$

To simplify the notation when discussing a rectangular vehicle, consider a subscript notation where the subscripts $i=1, 2$, and 3 refer to the forward, side, and aft jets, respectively. Define the length of each jet as b_i . Neglecting jet lift of the air diffuser and air velocities under the vehicle base, the total lift becomes

$$\begin{aligned} L &= p_b S + (J \cos \theta)_{\text{tot}} \\ &= p_b S + \rho_w \sum_{i=1}^3 b_i (p_b - p_{oi}) \frac{h_i}{\delta_i} \cos \theta_i \end{aligned}$$

Solving for base pressure gives

$$p_b = \frac{L + \rho_w \sum_{i=1}^3 b_i p_{oi} \frac{h_i}{\delta_i} \cos \theta_i}{S + \rho_w \sum_{i=1}^3 b_i \frac{h_i}{\delta_i} \cos \theta_i}$$

With the base pressure known, consider the power required for a side jet. Define the water system efficiencies so that water pumping power is given by

$$P_P = \frac{Q_w}{\eta_w} (p_{t_j} - \eta_w V_v^2)$$

The net water momentum drag for the side jet is given by

$$D_{mom} = \rho_w Q_w V_v - \rho_w Q_w V_w \sin \beta$$

and total water power for the side jet becomes

$$P_w = V_v Q_w \left(\frac{V_w^2}{V_v \eta_w} - V_v + \frac{\rho_w V_v}{\eta_p} - \frac{\rho_w V_w \sin \beta}{\eta_p} \right)$$

Substitution of the previously given expression

$$Q_w = b_2 t V_w \cos \beta$$

$$= \frac{(p_b - p_o) h b_2}{\delta V_w \cos \beta}$$

and rearrangement gives

$$P_w = \frac{(p_b - p_o) h b_2}{\delta \cos \beta} \left[\frac{\rho_w V_v \sin \beta}{\eta_p} + \frac{V_w}{\eta_w} - \frac{V_v^2}{V_w} \left(1 - \frac{\rho_w}{\eta_p} \right) \right]$$

This expression will be minimized with respect to V_w and β . All other parameters ($p_b, p_o, \delta, V_v, h b_2, \rho_w, \rho_w, \eta_p$ and η_w) will be assumed constant. This infers that V_w and β will be optimized for a single "design" speed and weight. Other speeds and weights must be investigated in a similar manner. Set

$$\frac{\partial P_w}{\partial V_w} = 0, \quad \frac{\partial P_w}{\partial \beta} = 0$$

and solve simultaneously.

$$\frac{\partial P_w}{\partial V_w} = \frac{(p_b - p_o) h b_2}{\delta \cos \beta} \left[\frac{1}{\eta_w} + \left(\frac{V_v}{V_w} \right)^2 \left(1 - \frac{\rho_w}{\eta_p} \right) \right] = 0$$

$$\frac{\partial P_w}{\partial \beta} = \frac{(p_b - p_o) h b_2}{\delta} \left\{ \frac{\rho_w V_v}{\eta_p \cos^2 \beta} - \frac{\sin \beta}{\cos^2 \beta} \left[\frac{V_w}{\eta_w} - \frac{V_v^2}{V_w} \left(1 - \frac{\rho_w}{\eta_p} \right) \right] \right\} = 0$$

From $\partial P_w / \partial \beta$,

$$\sin \beta = \frac{\frac{\rho_w V_w}{\eta_p}}{\frac{V_w}{\eta_w} - \frac{V_v^2}{V_w} \left(1 - \frac{\rho_w}{\eta_p}\right)}$$

$$= \frac{\rho_w V_w \eta_w V_w}{V_w^2 \eta_p - V_v^2 \eta_w \eta_p + \rho_w V_v^2 \eta_w}$$

From $\partial P_w / \partial V_w$,

$$V_w^2 = V_v^2 \eta_w \left(\frac{\rho_w}{\eta_p} - 1 \right)$$

Combining the last two equations,

$$\sin \beta = \frac{\rho_w V_w \eta_w V_w \sqrt{\eta_w \left(\frac{\rho_w}{\eta_p} - 1 \right)}}{V_v^2 \eta_w \rho_w - V_v^2 \eta_p \eta_w - V_v^2 \eta_w \eta_p + \rho_w V_v^2 \eta_w}$$

$$= \frac{\rho_w \sqrt{\eta_w \left(\frac{\rho_w}{\eta_p} - 1 \right)}}{2 \rho_w - 2 \eta_p}$$

$$\sin \beta = \sqrt{\frac{\eta_w}{\eta_p (2 - \eta_p)}} \quad \text{if } \rho_w = 2.0.$$

If pumping power is set equal to zero,

$$V_w^2 = V_v^2 \eta_w.$$

This results in total power being nearly optimum and the β equation simplifies to

$$\sin \beta = \frac{\rho_w V_w V_v \eta_w}{V_w^2 \eta_p - V_v^2 \eta_p \eta_w + \rho_w V_v^2 \eta_w}$$

$$= \frac{\rho_w \eta_w V_v^2 \sqrt{\eta_w}}{V_v^2 \eta_p \eta_w - V_v^2 \eta_p \eta_w + \rho_w V_v^2 \eta_w}$$

$$= \sqrt{\eta_w}$$

If these nearly optimum expressions for V_w and β are substituted into the water power equation,

$$P_w = \frac{\rho_w (p_b - p_o) h b_2 V_v \sqrt{1 - \eta_w}}{\delta \sqrt{\eta_w} (1 - \eta_w)}$$

$$= \frac{\rho_w (p_b - p_o) h b_2 V_v}{\delta} \sqrt{\frac{1}{\eta_w} - 1}$$

Since in this case

$$V_w^2 = V_v^2 \eta_w,$$

the water power is all momentum drag. The propulsive efficiency may be re-inserted, giving

$$(P_w)_{opt} = \frac{2 V_v (p_b - p_o) h b_2}{\eta_p \delta} \sqrt{\frac{1}{\eta_w} - 1}$$

If it is assumed that the air escaping from the side of the vehicle leaves the base in a lateral direction, the air develops no jet thrust in the direction of vehicle motion, and the air momentum drag is simply

$$D_{mom} = \rho_a Q_a V_v.$$

The fan power is as discussed in the hover section except that it is decreased by ram recovery in the fan inlet. If the fan inlet efficiency, fan efficiency, and diffuser losses can be defined, the air power may be found from the base pressure and air flow. The air flow is

$$Q_a = h b_2 C_2 \sqrt{\frac{2}{\rho_a}} (p_b - p_{o_2})$$

where

$$C_2 = f(\delta_2, \theta_2)$$

and may be determined from Figure 10-1.

For a given vehicle geometry and forward speed the side jet geometry (δ and θ) may be optimized by finding p_b for typical jet parameters for all jets, and using this p_b throughout the optimization. Changes in lift due to changes in jet reaction should be small enough to neglect. Note that if a δ is selected for a calculation of side-jet power, the water power is not affected by θ , and the air power is minimized at the minimum C for that δ . The jet may be optimized by calculating water power plus air power for several values of δ . A θ should be selected which gives the minimum C for each δ . The δ which gives the lowest total power is optimum.

The forward and aft jets may be treated in an analogous manner with $\beta = 0$. In this case, however, both the air power and water power (water momentum drag) are affected by θ . The optimum δ and θ must be found by plotting curves of total power as a function of δ and θ , and finding the minimum power condition. The optimum V_w may be shown to be the same as for the side jet.

The air momentum drag for the fore and aft walls is generally somewhat less than $\rho_a Q_a V_v$, since more air tends to escape through the rear wall than through the front, producing a net jet thrust. Generally, this may be neglected and the total air momentum drag may be taken as $D_{mom} = \rho_a Q_a V_v$.

Neglecting the change in lift due to changes in water jet lift allows each water jet to be optimized independently of the others with only a slight sacrifice in accuracy. These combined to define the jet geometry for a vehicle of specific configuration. The parameters which must be considered fixed to perform the optimization are base pressure, forward speed, and efficiencies. However, when any other vehicle parameters are changed the jet must be re-optimized if power is to be kept to a minimum.

10.5 STABILITY

The peripheral water jet vehicle should be similar to the plenum chamber or peripheral air jet vehicles as far as stability is concerned. If this is the case, the vehicle would be stable and damped in both pitch and heave, at least at low heights.

The only test result available for this type vehicle is the general discussion in Reference 36 of the two full-scale test vehicles that are being operated by Hughes. The discussion is summarized below.

Sidewall Test Vehicle

According to Reference 36, solid side walls provide bouyant stability in pitch and roll. The vehicle is very stable in heave, pitch, and roll at the normal operating height of two feet (height to base ratio h/b of 0.111).

Dynamic Test Vehicle

This vehicle has a peripheral water jet and water cross walls that divide the octagonal base into four compartments. When hovering this vehicle tended to wobble, indicating some instability in pitch and roll at small angles. Hughes believes that the air leakage across the compartmenting water walls is so great that a restoring force cannot build up during small angular fluctuations. The vehicle became stable when in forward motion, possibly, according to Hughes, because of hydrodynamic forces on the water scoops and propulsion system. Heave stability is not discussed. Normal operating height-to-base equivalent diameter ratio h/b is 0.053 to 0.080.

It is noted in Reference 36 that another means of stabilization (besides base compartmentation or bouyant side walls) would be to use small hydrodynamic surfaces. These offer the advantage of relatively high damping, but add hydrodynamic drag. Drag of the hydrodynamic surfaces would be less of sidewalls, but sidewalls have the additional advantage of reducing air leakage.

10.6 OPERATIONAL PROBLEMS

The primary operational problem is a fundamental limitation of the water jet vehicle; the inability to operate over land except at very low heights as a plenum.

Photographs of the Hughes test vehicles indicate that vehicle signature is a minor problem compared to pure air air-cushion vehicles. Foreign-matter ingestion will be confined to spray ingestion. Since spray is inherently less of a problem than with other air-cushion vehicles, spray damage to fans should be reduced and crew visibility improved.

10.8 CONCLUSIONS

10.8.1 Power Required-Hovering

A semi-optimization of water curtain hovering power requirements indicated that the water curtain vehicle may require about half the hovering power of a comparable air curtain vehicle. This advantage is negated to an unknown extent by the weight of the water required to fill the water curtain ducting.

10.8.2 Power Required-Forward Motion

A method is shown for minimizing power during forward flight. The method is dependent upon specific vehicle geometry.

Power minimization is of great importance in forward motion because of the potentially high momentum drag of the water wall. Above a certain speed a water wall vehicle will require more power in forward motion than an equivalent air-wall vehicle. This cross-over speed is a function of specific vehicle geometry and cannot be estimated without analyzing the particular vehicle.

10.8.3 Stability

Little is known about vehicle stability yet. Apparently there is little difference between the water curtain and air curtain vehicles.

10.8.4 Operational Problems

The water curtain cannot operate over land except for a few feet (until the water in the ducting is exhausted). Signature is less of a problem than with any pure air-type vehicle.

11.0 REFERENCES

1. Stanton-Jones, R., "The Development of the Saunders-Roe Hovercraft SRN1", Saunders-Roe Ltd., Publication No. TP. 414, October, 1959.
2. Carmichael, B.H., "Hovering Two-Dimensional Annular Jet Performance Experiments", Aeronutronic, Division of Ford Motor Company, Publication No. U-1053, November, 1960.
3. Gates, M. F., and Cochran, C. L., "Evaluation of Annular Nozzle Ejector", Hiller Aircraft Corporation Report No. ARD-280, November, 1960.
4. Perrone, G., "Progress Report of Navy Contract NONr 3232 Design and Fabrication of a GEM Fan/Duct System", AiResearch Manufacturing Division, the Garrett Corporation. Report No. AP-5026-R. November 11, 1960.
5. Schumpert, P. K., "Steady Flow Ejector Research Program", Lockheed Aircraft Corporation, Georgia Division. Progress Report for Contract NONr-3067 (00) ER-4671, November, 1960.
6. Norman, L. W., "Ground Effect Machine Propulsion System Design Consideration", presented at the IAS 29th Annual Meeting at New York, N. Y., 23 to 25 January, 1961.
7. Kelly, A. P., and Norman, L. W., "The Application of the Gas Turbine to Ground Cushion Vehicles", presented at the ASME Aviation Conference in Los Angeles, California, 12 to 16 March, 1961.
8. Strand, T., and Fujita, T., "Interim Report on GEM Internal Flow", presented at the ONR GEM Contractors Meeting at Washington, D.C., 23 and 24 June, 1960.
9. Stanton-Jones, R., "Hovering - Some Design Problems", Aerospace Engineering Vol. 20, No. 2, February, 1961, p. 16.
10. Johnson, A. E., "Interim Data from Wind Tunnel Tests of DTMB GEM Model 448", David Taylor Model Basin, Washington, D.C., June, 1960.
11. Chaplin, H. R., "Preliminary Correlation with Theory of Data from Wind Tunnel Tests of DTMB GEM Model 448", David Taylor Model Basin, Washington, D. C., June, 1960.

12. Chaplin, H. R., "Ground Cushion Research at the David Taylor Model Basin - A Brief Summary of Progress to Date and a Preliminary Design Technique for Annular Jet GEM's", presented at the Princeton Symposium on Ground Effect Phenomena, Princeton University, 21 to 23 October, 1959.
13. Dobson, F. A., "Preliminary Design of a General-Purpose Air-Cushion Vehicle", Aeronutronic, Division of Ford Motor Company, Publication No. U-927, July, 1960.
14. Carmichael, B. H., "Hovering Annular Jet Stability Experiments", Aeronutronic Publication U-1057, November, 1960.
15. Frost, J. C. M., and Earl, T. D., "Flow Phenomena of the Focused Annular Jet", presented at the Symposium on Ground Effect Phenomena, Princeton University, 21 to 23 October, 1959.
16. Higgins, H. C., and Martin, L. W., "Effects of Surface Geometry and Vehicle Motion on Forces Produced by a Ground Pressure Element", presented at the Symposium of Ground Effect Phenomena, Princeton University, 21 to 23 October, 1959.
17. Kuhn, R. E., and Carter, A. W., "Research Related to Ground Effect Machines", presented at the Symposium of Ground Effect Phenomena, Princeton University, 21 to 23 October, 1959.
18. Nixon, W. B., and Sweeney, T. E., "A Review of the Princeton Ground Effect Program", presented at the Symposium on Ground Effect Phenomena, Princeton University, 21 to 23 October, 1959.
19. Stanton-Jones, R., "The Development of the Saunders-Roe Hovercraft SRN1", presented at the Symposium on Ground Effect Phenomena, Princeton University, 21 to 23 October, 1959.
20. Eames, M. C., "Fundamentals of the Stability of Peripheral Jet Vehicles", Vols. 1-3, Pneumodynamics Corp., a Subsidiary of Cleveland Pneumatic Industries, Inc., November, 1960.
21. Eames, M. C., "Basic Principles of the Stability of Peripheral Jet Ground Effect Machines", presented at the IAS 29th Annual Meeting, New York, N. Y., 23 to 25 January, 1961.
22. Anderson, B. W., "Second Progress Report of Navy Contract NONr 3173 GEM Stability and Control Study", AiResearch Manufacturing Division, the Garrett Corp., November, 1960.

23. Helgesen, J. O., "Some Dynamic Stability Characteristics of a Hovering Peripheral Jet Ground Environment Machine - Motion in Heave Only", Grumman Aircraft Engineering Corporation Research Memorandum RM-184, February, 1961.
24. Unpublished data, David Taylor Model Basin.
25. Walker, N. K., "Preliminary Stability Control and Handling Criteria for Ground Effect Machines (GEMs)", presented at the IAS 29th Annual Meeting, N. Y., BB-1467, November, 1960.
26. White, R. P., Jr., and Vidal, R. J., "Study of the VTOL Downwash Impingement Problem", Cornell Aeronautical Laboratory, Inc. Report No. BB-1467-S-1, 23 to 25 January, 1961.
27. Zajac, F., "Historical Summary of the Development of Nickel Plating", Hamilton Standard Division of United Aircraft Corporation, 12 May, 1960.
28. "Final Report-Ground Effect Machine Structures Study", Ryan Aeronautical Co., Report No. G-42-62, 10 November, 1960.
29. Carmichael, B. H., "Hovering Two-Dimensional Plenum Chamber Experiments", Aeronutronic, Division of Ford Motor Company, Publication No. U-941, July, 1960.
30. Gates, M. F., and Cockran, C. L., "Investigation of Special Ground Effect Machine Configuration", Hiller Aircraft Corporation Report No. ARD-278, November, 1960.
31. Weiland, C., "Labyrinth Seals", presented at the Symposium on Ground Effect Phenomena, Princeton University, 21 to 23 October, 1959.
32. Schneider, A. J., and Rosenbery, M. H., "Tests of Power Seal Configurations for Ground Effect Machines", Grumman Aircraft Engineering Corporation Research Memorandum RM-186, March, 1961.
33. Strand, T., "Interim Report on VRC Channel GEM Concept", presented at GEM Contractors Meeting, Washington, D. C., 16 to 18 November, 1960.
34. Royce, W. W., and Rethorst, S., "Translational Characteristics of Ground Effect Machines", presented at the IAS 29th Annual Meeting, New York, N. Y., 23 to 25 January, 1961, IAS Paper No. 61-79.

35. Schade, R. O., and Parlett, L. P., "Summary of NASA Research on Aerial Jeeps, Flying Planforms, and Ground Effect Machines", Presented at the National Army Aviation Meeting of the IAS, Washington, D. C., 12 to 14 April, 1961.
36. Bowden, G. E., "Analysis of a Recirculating Ground Effect Machine", Presented at the Joint Army-ONR Meeting on Ground Environment Machines, 16 to 18 November, 1960.
37. Nay, H. O., "The Hughes Hydrostreak", Presented at the Tri-Service Ground Effect Machine Conference, Fort Meyer, Virginia, 16 to 18 November, 1960.
38. Heacock, R. H., "Preliminary Laboratory Investigation of Hydrostreak Water Wall Characteristics", Hughes Tool Company - Aircraft Division Report HTC-60-16 (Confidential Report).

DISTRIBUTION

UNITED STATES CONTINENTAL ARMY COMMAND

Commandant
Army War College
ATTN: Library
Carlisle Barracks, Pennsylvania (1)

Director
Operations Research Office
ATTN: Library
The Johns Hopkins University
6935 Arlington Road
Bethesda, Maryland (1)

Army Research Office
Office of the Chief of Research and Development
ATTN: Research Support Division
ATTN: Physical Sciences Division
Department of the Army
Washington 25, D. C. (2)

Army Research Office
ATTN: Lt Colonel Oliver R. Dinsmore
Box CM Duke Station
Durham, North Carolina (1)

TECHNICAL SERVICES

Corps of Engineers

Director
U. S. Army Engineer Research & Development Laboratories
ATTN: Technical Documents Center
Fort Belvoir, Virginia (1)

Ordnance Corps

Commanding General Ordnance Tank Automotive Command
ATTN: ORDMC-REO
Detroit Arsenal
Center Line, Michigan (1)

Commanding General
Quartermaster Research and Engineering Command, U. S. Army
ATTN: Technical Library
Natick, Massachusetts (1)

Transportation Corps

Chief of Transportation

ATTN: TCDRD

Department of the Army

Washington 25, D. C.

(2)

President

U. S. Army Transportation Board

Fort Eustis, Virginia

(1)

Commanding General

U. S. Army Transportation Materiel Command

ATTN: TCMAC-APU

(16)

ATTN: Deputy for Surface Engineering

(2)

P. O. Box 209, Main Office

St. Louis 66, Missouri

Commanding Officer

U. S. Army Transportation Combat Development Group

Fort Eustis, Virginia

(1)

Commandant

U. S. Army Transportation School

ATTN: Adjutant

Fort Eustis, Virginia

(1)

Commanding Officer

U. S. Army Transportation Research Command

ATTN: Research Reference Center

(6)

ATTN: Deputy Commander for Aviation

(1)

ATTN: Aviation Directorate

(1)

ATTN: Military Liaison and Advisory Office

(4)

ATTN: Research Directorate

(50)

ATTN: Executive for Programs

(1)

ATTN: Long Range Technical Forecast Office

(1)

Fort Eustis, Virginia

Transportation Corps Liaison Officer

U. S. Army Engineer Research and Development Laboratories

Building 314, Room A-216

Fort Belvoir, Virginia

(1)

U. S. Army Research and Development Liaison Group (9851 DU)

ATTN: USATRECOM Liaison Officer

(3)

APO 757, New York, New York

U. S. Army Transportation Research Command Liaison Officer

ATTN: ORDMX-LT

Detroit Arsenal

Center Line, Michigan

(1)

UNITED STATES AIR FORCE

Commander
Air Research and Development Command
ATTN: RDR-LA
Andrews Air Force Base
Washington 25, D. C. (1)

Commander Aeronautical Research Laboratories
ATTN: RRLA (Library)
Wright-Patterson AFB, Ohio (1)

UNITED STATES NAVY

Chief of Naval Operations
(OP-343)
Department of the Navy
Washington 25, D. C. (1)

Chief of Naval Research
Code 407M, Colonel R. J. Oddy
Washington 25, D. C. (1)

Chief, Bureau of Ships
Department of the Navy
R&D Current Program Planning Branch (Code 333)
Washington 25, D. C. (3)

Chief, Bureau of Naval Weapons (R-38) (1)
Department of the Navy
ATTN: RA-4 (1)
ATTN: RRSY-15 (1)
ATTN: RRSY-2 (1)
ATTN: RRSY-5 (1)
Washington 25, D. C.

Asst. Chief for Research and Development (OW)
Bureau of Supplies and Accounts
Navy Department
Washington 25, D. C. (1)

Officer in Charge
U. S. Naval Supply Research and Development Facility
ATTN: Library
Naval Supply Depot
Bayonne, New Jersey (1)

Library
Technical Reports Section
U. S. Naval Postgraduate School
Monterey, California (1)

Commanding Officer and Director
David Taylor Model Basin
Aerodynamics Laboratory Library
Washington 7, D. C.

(1)

Commanding Officer and Director
David Taylor Model Basin
ATTN: Mr. A. Hirsh
Hydrodynamics Laboratory
Carderock, Maryland

(1)

UNITED STATES MARINE CORPS

Director
MC Educational Center
Marine Corps Schools
Quantico, Virginia

(2)

Commandant of the Marine Corps
Code A04E
Arlington Annex
Washington 25, D. C.

(1)

Marine Corps Development Center
Marine Corps Schools
ATTN: Air Section
Quantico, Virginia

(1)

U. S. GOVERNMENT INDEPENDENT OFFICES

National Aeronautics and Space Administration
ATTN: Bertram A. Mulcahy
Assistant Director for Technical Information
1520 H. Street, N. W.
Washington 25, D. C.

(6)

Librarian
Langley Research Center
National Aeronautics and Space Administration
Langley Field, Virginia

(3)

Ames Research Center
National Aeronautics and Space Agency
ATTN: Library
Moffett Field, California

(1)

U. S. Government Printing Office
Division of Public Documents
ATTN: Library
Washington 25, D. C.

(1)

Maritime Administration
ATTN: Mr. Fixman
Washington 25, D. C.

(1)

Office of the Secretary of Defense
Director of Defense Research
and Engineering
Committee on Aeronautics
ATTN: Mr. T. C. Muse
Washington 25, D. C.

(1)

National Aeronautics and Space Administration
Lewis Research Center
ATTN: Library
21000 Brookpark Road
Cleveland 35, Ohio

(1)

Exchange and Gift Division
Library of Congress
Washington 25, D. C.

(2)

TRIPARTITE MEMBERS

U. S. Army Standardization Group, U. K.
Box 65, U. S. Navy 100
FPO New York, New York

(1)

Office of the Senior Standardization Representative
U. S. Army Standardization Group, Canada
c/o Director of Equipment Policy
Canadian Army Headquarters
Ottawa, Canada

(1)

Canadian Army Liaison Officer
Liaison Group, Room 208
U. S. Army Transportation School
Fort Eustis, Virginia

(1)

British Joint Services Mission (Army Staff)
ATTN: Lt. Colonel R. J. Wade, RE
DAQMG (Mov & Tn)
3100 Massachusetts Avenue. N. W.
Washington 8, D. C.

(2)

MISCELLANEOUS

Commander
Armed Services Technical Information Agency
ATTN: TIPCR
Arlington Hall Station
Arlington 12, Virginia

(10)

Mr. John J. Glennon, Librarian
Institute of Aeronautical Sciences
2 E. 64th Street
New York 21, New York

(1)

UNIVERSITIES

University of Maryland
ATTN: Professor Weske
Professor Shen
Institute of Fluid Dynamics and Applied Mathematics
College Park, Maryland (1)

Mississippi State University
ATTN: Dr. J. J. Cornish
Department of Aerophysics
State College, Mississippi (1)

Princeton University
ATTN: Mr. T. E. Sweeney
Professor D. C. Hazen
Aeronautical Engineering Department
The James Forrestal Research Center
Princeton, New Jersey (2)

University of Wichita
Department of Engineering Research
ATTN: Mr. R. K. Wattson
Wichita 14, Kansas (1)

University of Virginia
ATTN: Dr. G. B. Matthews
Aeronautical Engineering Department
Charlottesville, Virginia (1)

INDUSTRY

Aeronutronic
A Division of Ford Motor Company
ATTN: Mr. M. F. Southcote
Ford Road
Newport Beach, California (10)

Aerophysics Corporation
ATTN: Dr. G. D. Boehler
17 Dupont Circle
Washington 6, D. C. (1)

AiResearch Manufacturing Company of Arizona
ATTN: Mr. L. W. Norman
402 South 36th Street
Phoenix, Arizona (1)

Bell Aircraft Corporation
ATTN: Mr. E. K. Liberatore
P. O. Box Nr 1
Buffalo 5, New York (1)

Bell Helicopter Corporation
ATTN: Mr. R. Lynn
P. O. Box 482
Fort Worth 1, Texas

(1)

Booz-Allen Applied Research, Inc.
ATTN: Mr. P. Fielding
4921 Auburn Avenue
Bethesda 14, Maryland

(1)

Cleveland Pneumatic Industries, Inc.
ATTN: Mr. C. Eames
Systems Engineering Division
1626 L Street, N. W.
Washington 6, D. C.

(1)

Convair
Division of General Dynamics Corporation
ATTN: Mr. J. E. Loos
Mail Zone 6-109
P. O. Box 1950
San Diego 12, California

(1)

Curtiss-Wright Corporation
ATTN: Mr. J. T. Marshall, Jr.
Wright Aeronautical Division
Wood-Ridge, New Jersey

(1)

Grumman Aircraft Engineering Corporation
ATTN: Dr. C. E. Mack, Chief of Research
Bethpage, L. I., New York

(1)

Gyrodyne Corporation of America
Flowerfield
St. James, L. I., New York

(1)

Hiller Aircraft Corporation
ATTN: Mr. M. F. Gates
1350 Willow Road
Palo Alto, California

(1)

Hughes Tool Company
ATTN: Mr. M. H. Nay
Aircraft Division
Culver City, California

(1)

Hydronautics, Incorporated
ATTN: Mr. M. P. Tulin
200 Monroe Street
Rockville, Maryland

(1)

Aeronutronic Division, Ford Motor Company. Newport Beach, California
STATE-OF-THE-ART SUMMARY
AIR-CUSHION VEHICLES - W. L. Rawlings and D. H. Seiveno, Report No. U-926, RV-1, August 1961, (Contract DA 44-177-TC-724) Task 9R99-01-005-14, 148 pp. TCREC Technical Report 61-108.

Unclassified Report

Existing available knowledge, both theoretical and experimental, of the existing concepts making use of the

(over)

Aeronutronic Division, Ford Motor Company, Newport Beach, California
STATE-OF-THE-ART SUMMARY
AIR-CUSHION VEHICLES - W. L. Rawlings and D. H. Seiveno, Report No. U-926, RV-1, August 1961, (Contract DA 44-177-TC-724) Task 9R99-01-005-14, 148 pp. TCREC Technical Report 61-108.

Unclassified Report

Existing available knowledge, both theoretical and experimental, of the existing concepts making use of the

(over)

1. Fluid Dynamics, Aeronutronic Division, Ford Motor Company. Newport Beach, California
Aerodynamics
STATE-OF-THE-ART SUMMARY
AIR-CUSHION VEHICLES - W. L. Rawlings and D. H. Seiveno, Report No. U-926, RV-1, August 1961, (Contract DA 44-177-TC-724) Task 9R99-01-005-14, 148 pp. TCREC Technical Report 61-108.

Unclassified Report

Existing available knowledge, both theoretical and experimental, of the existing concepts making use of the

(over)

1. Fluid Dynamics, Aeronutronic Division, Ford Motor Company, Newport Beach, California
Aerodynamics
STATE-OF-THE-ART SUMMARY
AIR-CUSHION VEHICLES - W. L. Rawlings and D. H. Seiveno, Report No. U-926, RV-1, August 1961, (Contract DA 44-177-TC-724) Task 9R99-01-005-14, 148 pp. TCREC Technical Report 61-108.

Unclassified Report

Existing available knowledge, both theoretical and experimental, of the existing concepts making use of the

(over)

UNCLASSIFIED

UNCLASSIFIED